

Norwegian University  
of Life Sciences

Master's Thesis 2017 30 ECTS

Faculty of Environmental Sciences and Natural Resource Management

# **Cleaning Schedule based on Soiling Effects on Photovoltaics in Kalkbult, South Africa**

Tor Atle Solend

Renewable Energy – Master's Program



## **Preface**

Before you lie the Master's Thesis "Cleaning Schedule based on Soiling effect on Photovoltaics in Kalkbult, South Africa". It has been written to fulfil the graduation requirements of the Renewable Energy Master's program at the Norwegian University of Life Sciences(NMBU). I wrote this thesis from January to May 2017.

The thesis was written in collaboration with the Solar Energy department at Institute for Energy Technology (IFE) in Kjeller, Norway. It is with humility and great respect I would like to express gratitude to my supervisors, Prof. Muiyiwa Samuel Adamarola (NMBU) and Dr. Josefine Helene Selj (IFE) who have been very helpful throughout the writing process.

Very special thanks to Mari Øgaard (IFE/NMBU) and Armand Du Plessis (Stellenbosch University) for sharing their work and helping me whenever I was in trouble. I would also like to thank my fellow students at IFE and NMBU.

This has been an astonishing experience, surrounded by so much specialized knowledge on different aspects of solar photovoltaics at IFE. My learning curve this semester has been steeper than ever before. This is why I do this, to learn something new every single day.

I hope you enjoy your reading

Tor Atle Solend

Oslo, May 14, 2017

## Sammendrag

Scatec Solars solcellepark i Kalkbult, Sør-Afrika, ligger i et område med gode solforhold og er i lite eller ingen konflikt med matjord. Området er betegnet som et semi-tørt ørkenområde med periodevis lite regn, og støv og sand kan akkumulere på solcellepaneler og redusere effekten på solcellene.

Formålet med denne oppgaven er å analysere effekttapet på solcellene i parken på grunn av støv, og lage en modell som bestemmer om, og hvor ofte, panelene bør vaskes ut ifra effekttapet. Effekttapet vil bli undersøkt ved hjelp av strøm- og spenningsdata fra et eksperimentelt testanlegg inne i solcelleparken. Testanlegget består av flere solcellepaneler av henholdsvis multi-krystallinsk silisium og Kadmium-Tellurid tynnfilmpaneler, og en værstasjon med meteorologiske data. Effekttapsanalysen vil sammenfattes med kostnads- og prisdata for å finne den beste vaskeplanen for solcelleparken. I tillegg ble en støvprøve fra området undersøkt i et elektronmikroskop.

Perioden som er analysert i denne oppgaven strekker seg fra november 2016 til og med april 2017. Effekttapsanalysen for denne perioden viste ingen effekttap for silisiumpanelene, mens tynnfilmpanelene hadde et tap på om lag 1% i November 2016. Dette resulterte i at det ikke lønte seg å vaske panelene i denne perioden. Relativt hyppig regn i perioden så ut til å vaske vekk alt støv fra panelene.

Data fra perioden fra mai 2016 til og med oktober 2016 var tilgjengelig, og i juli 2016 var det nok effekttap fra støv til at modellen utløste vasking. Modellen antar at alt støv blir vasket vekk, og forblir vekk for hele måneden. Når det tas i betraktning at vasking av hele solcelleparken tar 47 dager, vil det være grunn til å tro at støv vil akkumulere samtidig som det vaskes, og det økonomiske grunnlaget for å vaske er tynt sådan.

Støvprøven ble analysert ved hjelp av et elektronmikroskop for å bestemme sammensetning, størrelsesfordeling og marginal skyggeeffekt. Analysen viste at støvet i hovedsak var organisk, med noe salter og silikater. Størrelsesfordelingen viste at gjennomsnittsdiameteren var på  $47,5\mu\text{m}$ , mens den mest frekvente hadde diameter på  $6,5\mu\text{m}$ , og medianen  $11,8\mu\text{m}$ .

## **Abstract**

Scatec Solar's solar photovoltaic power plant in Kalkbult, South Africa, is in an area with excellent properties for harvesting solar energy. Vast areas with little or no conflict with agriculture and high irradiance. This semi-arid area has low precipitation and dust and soiling can be a problem when accumulating on solar module surfaces.

The purpose of this thesis is to investigate the power loss from soiling on the solar panels, and to create a model to investigate if, and when, the modules should be cleaned. The soiling analysis will be conducted by analyzing data from a test facility inside the Kalkbult solar plant. The test facility consists of 16 crystalline Silicon modules, and 8 Cadmium-Telluride thin film modules. Current-Voltage data from these modules is used to calculate losses due to soiling by comparing uncleaned reference modules with clean modules. The results from the soiling analysis will be used to calculate a cleaning schedule. In addition, an experimental analysis of a dust sample from the area is analyzed.

The period considered in this thesis is November 2016 to April 2017. The soiling analysis showed no soiling losses of the silicon modules, and just 1% power loss for the thin film modules in early November 2016. This resulted in no cleaning action in this period, as the marginal cost of cleaning per module was much higher than the marginal cost of soiling from the thin film panels. There was quite frequent rainfall in the period, and the cleaning effect of the rain seemed to eliminate power loss from soiling.

Data from May to October 2016 was available, and in July there was enough soiling to trigger the cleaning schedule. However, the model assumes that all soiling is eliminated for a whole month, and the power plant is cleaned over a period of 47 days, there is reason to believe that soiling will occur simultaneously as the cleaning, and the economically viability of cleaning at all is highly questionable.

A dust sample was analyzed in a scanning electron microscope to determine the composition and size distribution of the local dust in Kalkbult. The analysis showed that the dust was mostly organic, accompanied by salts and silica. The size distribution showed the average size of the dust particles to be 47 $\mu\text{m}$  in diameter, the most frequent had a diameter of 6.5 $\mu\text{m}$  and the median 11.8 $\mu\text{m}$ .

## Nomenclature

Symbol	Description	Unit
$I$	Current	Ampere
$\theta$	Angle of incidence with respect to vertical line from ground to top of atmosphere	Degrees
$V$	Voltage	Volt
$R$	Resistance	Ohm
$P$	Power	Watt
$FF$	Fill Factor	-
$\eta$	Efficiency	-
$E$	Irradiation	kWh
$A$	Area	m <sup>2</sup>
$T$	Temperature	°C
$NOCT$	Nominal Operating Cell Temperature	°C
$I_L$	Irradiance	W/m <sup>2</sup>
$I_0$	Reference irradiance	1000 W/m <sup>2</sup>
$\gamma$	Material dependent constant	-
$Y$	Yield	-
$i$	Time of measurement	Time
$STC$	Standard Test Conditions	-
$S$	Soiling Ratio	-
$\alpha$	Size parameter	-
$D$	Diameter	μm, cm or mm
$\lambda$	Radiation wavelength in μm	μm
$Q_e$	Extinction factor	-
$m$	Refractive index of particle	-
$\tau$	Transmittance	-
$N$	Number of particles	-
$r$	Radius	cm
$\phi$	Phi – logarithmic value	-

$Corr(i,j)$	Correlation between i and j	-
$E[x]$	Expected value operator	-
$\mu_i$	Expected value of i	-
$\sigma_i$	Standard deviation of i	-
$C$	Cost	ZAR
$E_{M,i}$	Electricity production of clean module in period i	kWh
$P_{avg}$	Average electricity price	ZAR
$c$	Marginal cost	ZAR/module
<b><i>Subscripts</i></b>		
$MPP$	Maximum Power Point	-
$PH$	Photocurrent ( $I_{ph}$ )	-
$D$	Diode ( $I_D$ )	-
$S$	Saturation current ( $I_S$ )	-
$m$	Ideality factor	-
$Sh$	Shunt ( $I_{Sh}$ )	-
$SC$	Short Circuit	-
$OC$	Open Circuit	-
$c$	cell temperature ( $T_c$ )	°C
$a$	Ambient temperature ( $T_a$ )	°C
$L$	Incident irradiance ( $I_L$ )	W/m <sup>2</sup>
$m$	Module temperature ( $T_m$ )	°C
$*$	Corrected power ( $P^*$ )	
$R_0$	Rated power ratio	-
$R$	Ratio	-

## Table of Contents

Preface .....	I
Sammendrag.....	II
Abstract.....	III
Nomenclature .....	IV
1 Introduction .....	1
1.1 Problem Definition.....	1
2 Theoretical Prerequisites .....	4
2.1 Solar Energy .....	4
2.1.1 The solar spectrum.....	5
2.2 Solar Photovoltaics.....	7
2.2.1 The semiconductor solar cell and the p-n junction .....	8
2.2.2 Crystalline silicon solar cells.....	10
2.3 Characteristics of Solar Cells .....	11
2.3.1 Efficiency of a solar cell or panel.....	14
2.4 Soiling.....	19
2.4.1 Dust deposition .....	19
2.4.2 Dust properties .....	19
2.4.3 Dust mitigation.....	20
2.4.4 Dust composition .....	21
2.4.5 Particle size distribution.....	21
2.5 Management Science.....	22
3 Methodology.....	24
3.1 Description of the Test Facility.....	24
3.1.1 Photovoltaic Modules .....	26
3.1.2 Weather and irradiation data .....	26



3.1.3	Uncertainties of measurements .....	28
3.1.4	Test facility cleaning methods and surface treatment .....	28
3.2	Data Analysis and PV Performance Parameters .....	29
3.2.1	PV data from Kalkbult test facility.....	29
3.2.2	Maximum power point .....	31
3.2.3	Temperature correction.....	32
3.3	Dust Sample Analysis .....	32
3.4	Cleaning Schedule Model.....	33
3.4.1	Cost of Soiling.....	33
3.4.2	Cost of Cleaning .....	33
3.4.3	Electricity Prices .....	35
3.4.4	Model design.....	37
4	Results.....	38
4.1	PV soiling analysis .....	38
4.1.1	Silicon modules .....	38
4.1.2	Thin film modules.....	44
4.1.3	Data analysis .....	47
4.2	Dust Sample Analysis .....	53
4.2.1	Image analysis .....	53
4.2.2	Particle distribution.....	56
4.2.3	Soil composition.....	58
4.3	Cleaning schedule .....	61
4.3.1	Model inputs .....	61
4.3.2	Without Feed-in-Tariff .....	61
4.3.3	With Feed-in-Tariff.....	65
5	Discussion.....	70

5.1	Soiling analysis of the I-V data from the PV modules .....	70
5.1.1	Data corrections.....	70
5.1.2	Irradiance effects on temperature corrections and efficiency.....	73
5.2	Dust sample analysis .....	74
5.3	Cleaning Schedule .....	74
6	Conclusions .....	76
7	Further inquiries.....	77
8	References .....	78
Appendix A.....		i
Appendix B .....		v
Appendix C .....		vii



# 1 Introduction

Today, most of the world's electricity is generated by fossil fuels, and the emissions that follow the production contributes to the warming climate, as well as local air pollution. Electricity production accounts for 25% of the global CO<sub>2</sub>-emissions. (Intergovernmental Panel on Climate Change. Working Group III & Edenhofer 2014). To accomplish the climate goal from the Paris agreement, it is vital to transform the energy sector completely. Accompanied by wind power, solar energy has emerged as the most important energy technology to mitigate climate change.

Solar photovoltaic (PV) technology is developing fast, becoming more and more efficient, and the price per watt is dropping fast. In many countries, PV is now competitive with the cheapest fossil power source; coal power. In 2016, the total installed PV capacity exceeded 300 GW globally (Bellini 2017).

All existing PV plants producing power today, will not benefit from better efficiencies of tomorrow's technology. Thus, the already installed capacity will want to keep the efficiency as high as possible to ensure that the gap between old and new cost effectiveness does not become too large. To keep the efficiency as high as possible means maintaining the panels, and with maintenance there are costs.

Soiling is a problem that most PV systems are influenced by, as dust and residue on the surface attenuates the incident irradiance and thus the power output and efficiency. In deserts and arid locations, soiling can be a significant problem when the rate of dust deposition can be much higher than in other climates. Most studies of soiling in dry climates have been conducted in the middle east, India and United States. Only a handful studies have been conducted on the southern hemisphere.

Scatec Solar's PV park in Kalkbult, located in the Northern Cape region of South Africa, is the scope of this thesis. The location is in a semi-arid area south of the Namib Desert, with excellent properties for solar PV. The average daily insolation of Kalkbult is 6.8 kWh/m<sup>2</sup> and 2480 kWh/m<sup>2</sup> per year (Appendix B). Inside the PV park there is an experimental test facility with several polycrystalline silicon and Cadmium Telluride thin film modules.

## 1.1 Problem Definition

The experimental test facility analyzed in this thesis is part of Scatec Solar's 75MW solar PV plant in Kalkbult, South Africa. Kalkbult, 30.16° south and 24.14° east, is the name of a farm in the Northern Cape region, 60km north of the town De Aar (Figure 1-1) The solar plant started operating in September 2013. (ScatecSolar 2017) The test facility was built through the research project SANCOOP, a bilateral

research project funded by the Research Council of Norway. The project is a collaboration between IFE, Stellenbosch University and Scatec Solar, running from 2014-2017. The test facility was built in 2015 and has been operational for approximately 1.5 years.

From the data made available from the test facility, this thesis will seek to investigate and answer the following:

- How much soiling losses are there during the summer period in Kalkbult from November 2016 to April 2017?
- What is the composition of the dust particles in the area and their marginal attenuation?
- Based on the soiling losses, how often should the solar panels be cleaned?

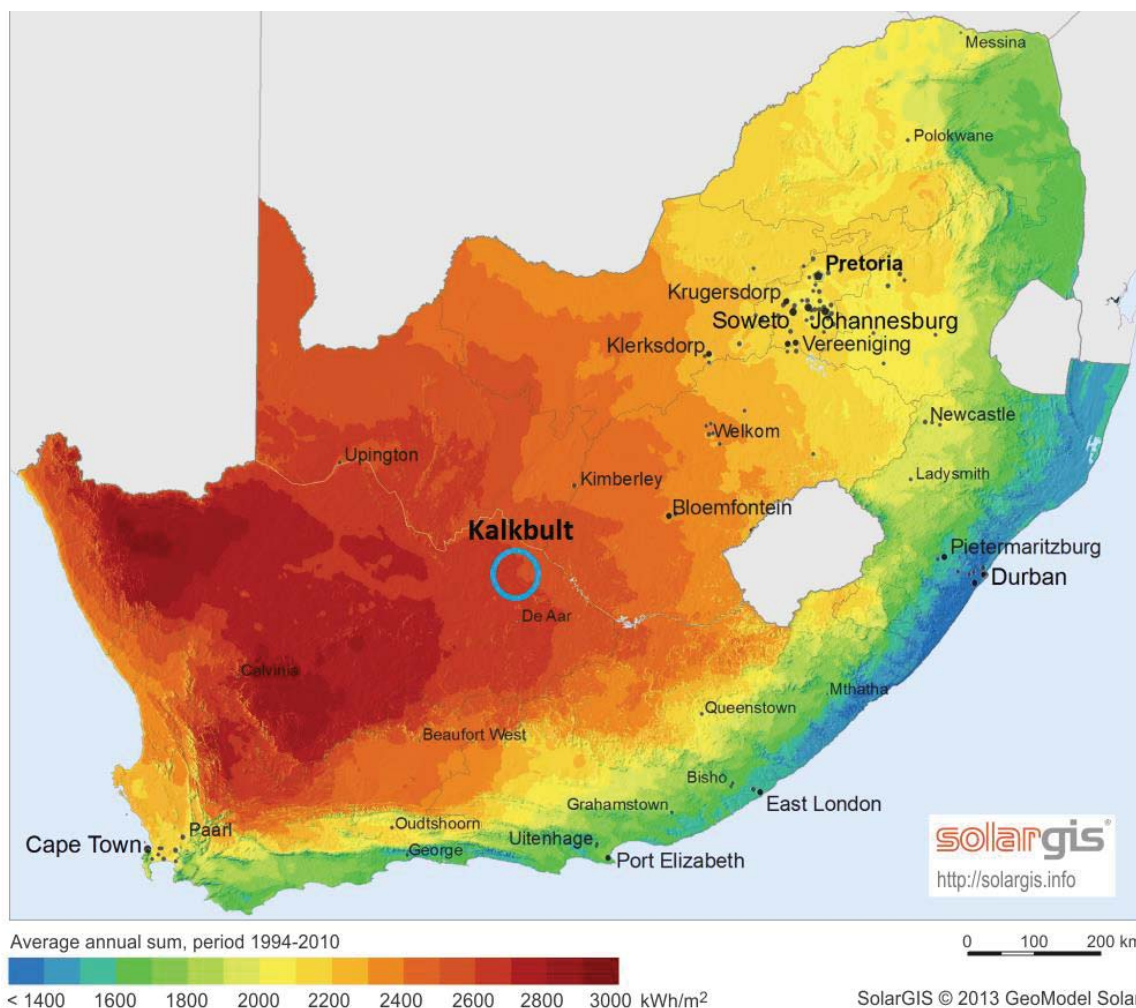


Figure 1-1: This map shows the location of the Solar PV plant in Kalkbult. The color indicates irradiation. Image is copied with courtesy of SolarGIS GeoModel Solar: <http://geosun.co.za/wp-content/uploads/2014/10/DNI-Solar-map-South-Africa.png>



## 2 Theoretical Prerequisites

The theory chapter on solar photovoltaics (chapter 2.1-2.3) is for the most part based on the book *“Photovoltaics - Fundamentals, Technology and Practice”* (Mertens 2013). Other sources are specified.

### 2.1 Solar Energy

The sun is the thermonuclear fusion reactor that feeds the solar system with energy. On average, the sun emits  $3.84 \cdot 10^{26} W$  of power from nuclear fusion in the core. This number is called the solar luminosity. At the top of earth's atmosphere (TOA) solar power is measured as irradiance, or electromagnetic energy flux. Flux is energy per unit area and time ( $W/m^2$ ). The flux density decreases with increased distance from the sun, and the irradiance at TOA is  $1366 W/m^2$  on average. This is called the solar constant. However, the solar constant is not actually constant, but varies by around  $\pm 3 W/m^2$  over the year due to changes in solar activity and the effect of earth's elliptic orbit around the sun.

From TOA and down to the surface, some of the irradiance is absorbed by gasses, reflected by clouds or scattered by collisions with gas molecules. The irradiance is thus reduced additionally until it hits the surface. The surface irradiance can be divided in two; direct irradiance and direct normalized irradiance. The difference between the two is that the direct irradiance is measured on a horizontal surface with respect to the earth, meaning that the surface has a non-normal angle to the sun. The direct normalized irradiance is thus measured with a normal surface to the sun. Unless the sun is perpendicular to the horizontal surface, the normalized surface would always receive more power per surface area.

Due to the tilted axis of the earth the surface irradiance varies throughout the year. This causes the maximum solar altitude during the day to change with the seasons. Solar altitude is the angle the sun forms with respect to the surface from the observer's point of view. Thus, during winter the sunlight travels through a bigger portion of the atmosphere and receives less solar energy than during summer.

On the ground, the direct radiation from the sun is complemented by diffuse radiation caused by scattered light from the atmospheric particles, and reflected radiation (figure 2-1). The total amount of radiation that hits a surface is the sum of direct, diffuse and reflected radiation, called global radiation.

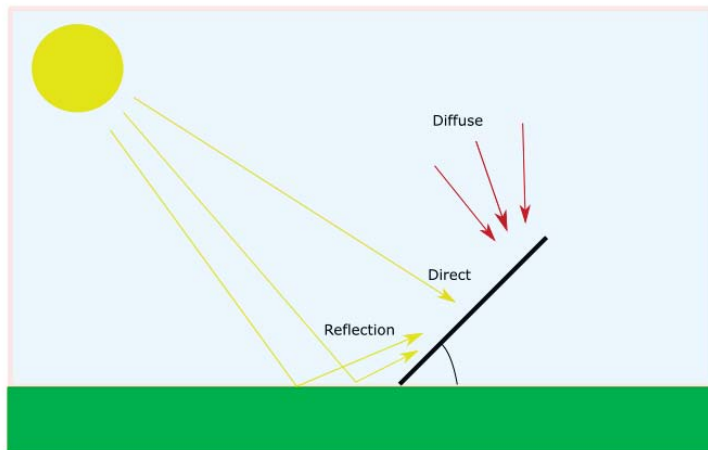


*Figure 2-1: Components of incident radiation on a tilted plane.*

### **2.1.1 The solar spectrum**

The sun's radiation spectrum can be described as a blackbody radiator with the same temperature as the sun. As sunlight travels through the atmosphere, some of the light is absorbed or scattered by the gases. In space, the spectrum closely follows the blackbody radiation, illustrated in Figure 2-2. At ground level, some of the intensity is lost due to absorption and scattering of gases and molecules in the atmosphere. The radiation spectrum at ground level limits the energy that can be harnessed for solar energy purposes on terrestrial solar devices.



## Spectrum of Solar Radiation (Earth)

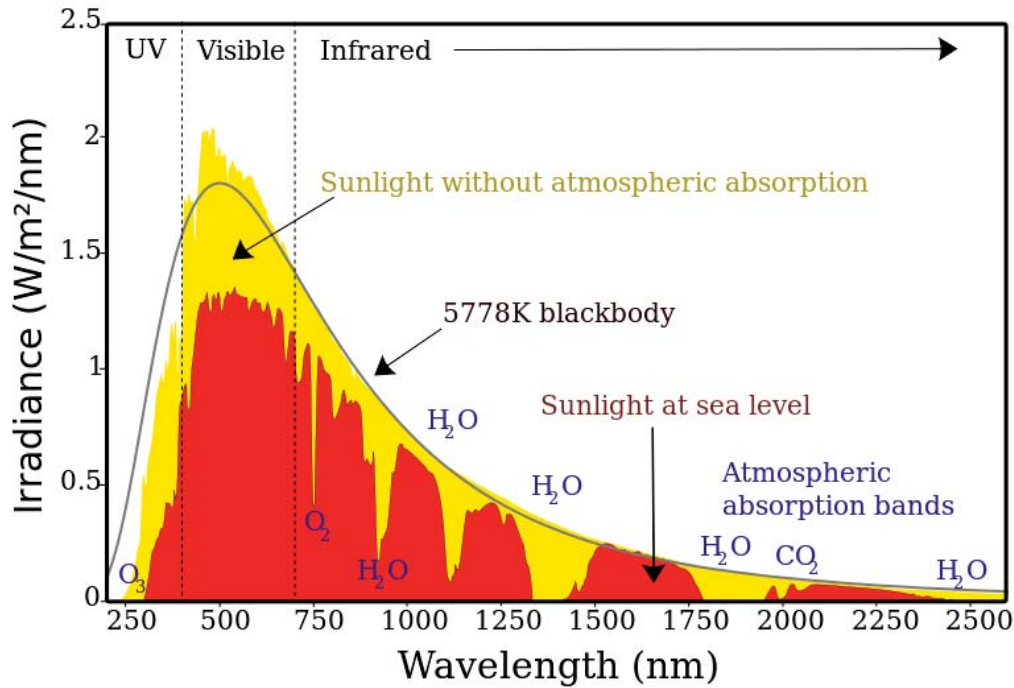


Figure 2-2: The spectrum of solar radiation. The yellow part is the radiation that hits the outer boundary of earth's atmosphere, and the red part is what is left of the light after going through the atmosphere. Image is copied with courtesy of CC BY-SA 3.0, <https://commons.wikimedia.org/w/index.php?curid=2623187>

One usually refers to the irradiance in space and on sea level as the AM0 and AM1 respectively, where AM0 is sunlight unhindered by the atmosphere, and AM1 stands for 1 times the vertical distance from sea level to TOA. Thus, at sea level, the air mass volume can never be smaller than 1 (Figure 2-3). Since AM1 only occurs in the region around equator, AM1.5 was chosen as a standard value for characterization and testing. Air mass volume is calculated by a simple equation:

$$AM(X_{\theta}) = \frac{1}{\cos(\theta)} \quad (1)$$

Where  $\theta$  = Angle of incidence with respect the ground normal

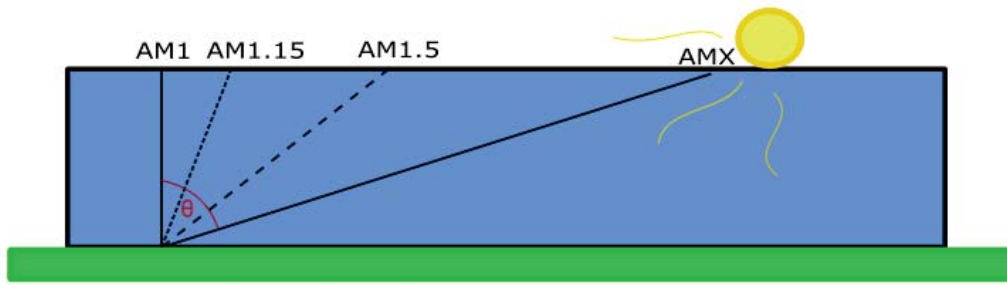


Figure 2-3: Representation of Air Mass Volume.

## 2.2 Solar Photovoltaics

The solar cell industry has seen a remarkable growth and price reduction rate during its lifetime in the market. The module price trend versus the cumulative production has dropped 23% for every doubling of production during the last 35 years. (Phillips & Warmuth 2016)

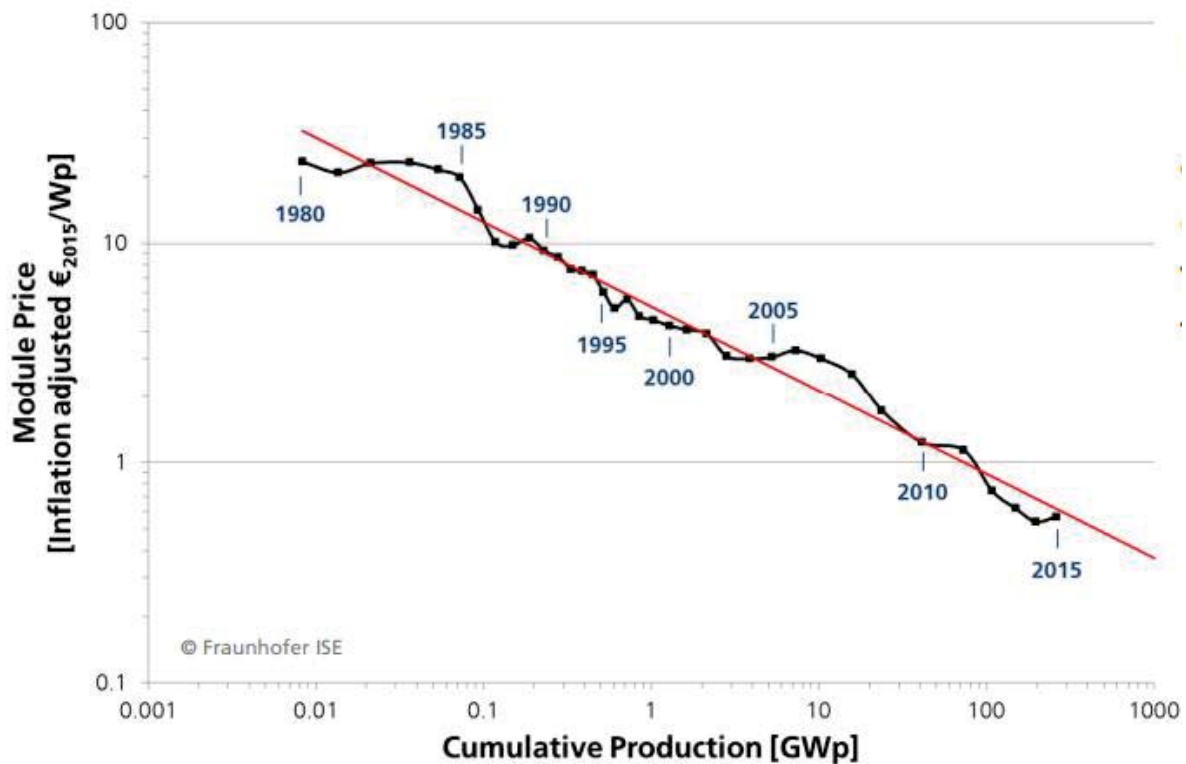


Figure 2-4: A Log-Log representation, or learning curve, of the cost development of solar PV modules from 1980-2015. This plot is copied with courtesy of Fraunhofer ISE from their publication "Photovoltaics Report"

The efficiency of the modules has naturally evolved in the same period. Multi junction solar cells are the most efficient today, but they are in the laboratory stage of development, and the most common silicon based modules have reached about 25%. In recent years, the most impressive efficiency growth rates are within perovskite and quantum dot cells (Figure 2-5), but their efficiencies are still far inferior to conventional silicon solar cells which dominates the market.

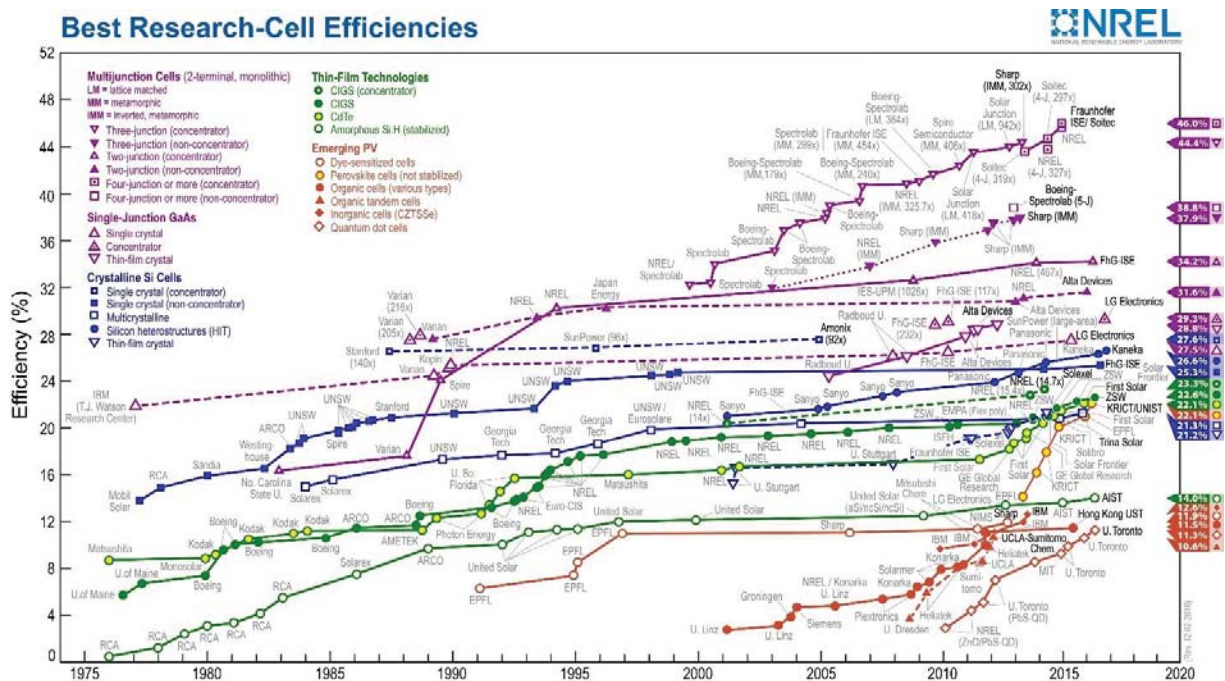


Figure 2-5: Efficiencies of different solar cell technologies. This plot is copied with courtesy of the National Renewable Energy Laboratory, Golden, CO [https://www.nrel.gov/pv/assets/images/efficiency\\_chart.jpg](https://www.nrel.gov/pv/assets/images/efficiency_chart.jpg)

### 2.2.1 The semiconductor solar cell and the p-n junction

Silicon has the atomic number 14, which means that the two inner shells (K and L band) of the atom are full (2+8 electrons), and four electrons are in the valence band (Figure 2-6). The silicon atom seeks to bond with four other electrons to fill the outer band, and can thus form a pure silicon crystal structure.

## 14: Silicon

2,8,4

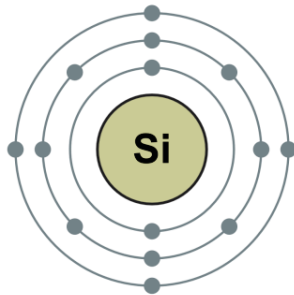


*Figure 2-6: Representation of the silicon atom. Image is copied with courtesy of Pumbaa (original work by Greg Robson) (Wikimedia commons) <https://commons.wikimedia.org/w/index.php?curid=715360>*

Semiconductor solar cells are solid-state devices that convert incident solar irradiance into electric power. A basic solar cell consists of two layers of semiconductor material, i.e. silicon, and a metal grid to conduct electricity. One layer needs to have a surplus of free electrons (n-layer), and the other needs surplus of electron holes (p-layer). The free electrons are attracted by the electron holes in the other layer. In the boundary between the layers, electrons will cross over to fill the electron holes, creating a negative charge in the p-layer, and a positive charge in the n-layer. This boundary region is called a p-n junction or depletion zone, where the opposite charges of the two layers create an electric field. When this p-n junction is illuminated by sunlight, the free electrons on the n-layer will seek to get past the p-n junction to fill the electron holes, and vice versa.

To achieve the excess of free electrons in the n-layer, and excess of holes in the p-layer, the silicon is doped by a material with one more or one less electron in its valence band respectively. Phosphorous and Boron are examples of such materials. In Figure 2-7, a phosphorus atom is connected to the crystalline silicon structure and provides a free electron.

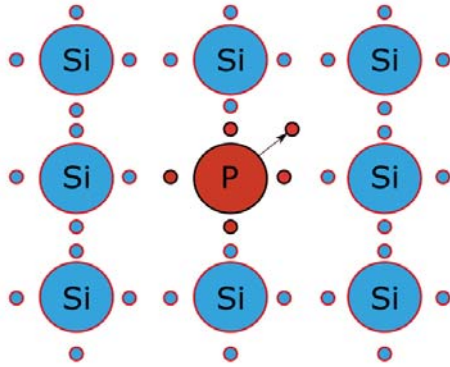


Figure 2-7: Adding phosphorous to the crystalline structure of silicon provides a free electron.

When the p-n junction is illuminated by sunlight, photons with the right wavelength and energy will excite electrons from the valence band to the conduction band, creating current. The gap between the valence and conduction band is called the band gap and this gap coincides with the energy needed to excite electrons Figure 2-8.

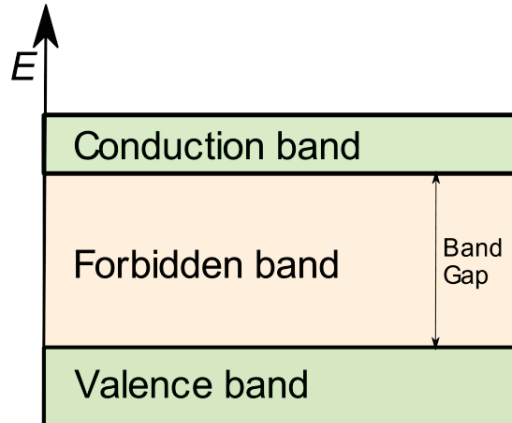


Figure 2-8: Band gap of a semi-conductor. The energy needed to excite an electron to the conduction band equals the band gap energy.

### 2.2.2 Crystalline silicon solar cells

The dominating photovoltaic technology on the market today is the silicon crystalline solar cells with a market share of over 90%. The remaining 10% of installed capacity mainly consists of thin film technologies like Cadmium-Telluride (CdTe) modules (Schmela 2016).

The crystalline solar cells can be divided into mono- and multi-crystalline. Mono-crystalline solar cells are the most efficient, but the cheaper multi-crystalline are not far behind. The basic difference between the two is the purity of the crystalline structure in the wafers. The difference between mono- and multi-crystalline cells lies in the manufacturing process, where the monocrystalline cell is made of one single crystalline ingot that is grown in a centrifuge around a crystalline seed, and the multi-crystalline cell is made by melting silicon in a mold around a crystalline seed. The molding process creates several crystal structures in the wafer instead of one, resulting in a little lower efficiency per area than the monocrystalline. (Luque & Hegedus 2011)

## 2.3 Characteristics of Solar Cells

The electrical behavior of a solar cell can be described as current as a function of voltage, and can be expressed as a photodiode (one-diode) equation by a simplified or standard model:

$$I = I_{Ph} - I_D = I_{Ph} - I_S * \left( e^{\frac{V}{m * V_T}} - 1 \right) \quad [Simplified\ model] \quad (2)$$

OR

$$I = I_{Ph} - I_D = I_{Ph} - I_S * \left( e^{\frac{V + I * R_S}{m * V_T}} - 1 \right) - \frac{V + I * R_S}{R_{Sh}} \quad [Standard\ model] \quad (3)$$

Where:

$I_{Ph}$  = photocurrent

$I_D$  = current through a photodiode

$I_S$  = the saturation current

$V$  = voltage

$V_T$  = thermal voltage

$m$  = the ideality factor

$R_S$  = Series resistance

$R_{SH}$  = Shunt resistance

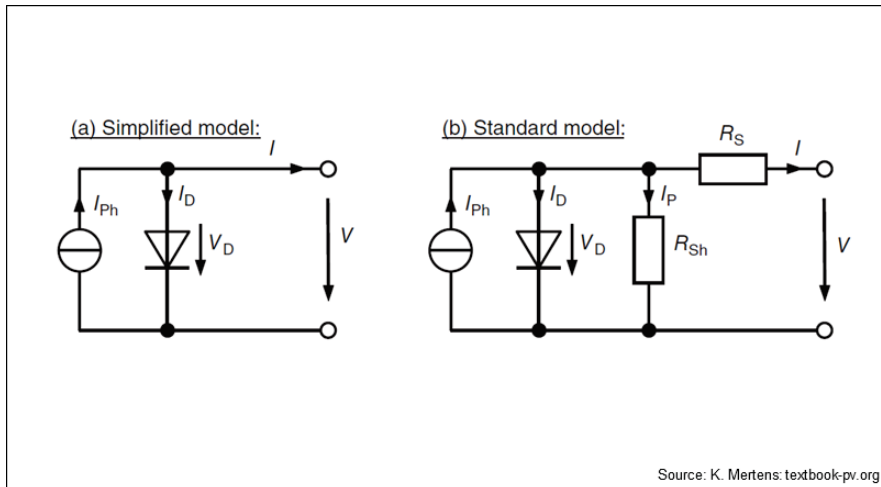


Figure 2-9: The simplified and standard model of a photodiode. Source: courtesy of K. Mertens: textbook-pv.org

These equations (2 and 3) work well on a theoretical level, but real life solar cells are better represented by the two-diode model:

$$I = I_{Ph} - I_{S1} * \left( e^{\frac{V+I*R_S}{V_T}} - 1 \right) - I_{S2} * \left( e^{\frac{V+I*R_S}{2*V_T}} - 1 \right) - \frac{V + I * R_S}{R_{Sh}} \quad (4)$$

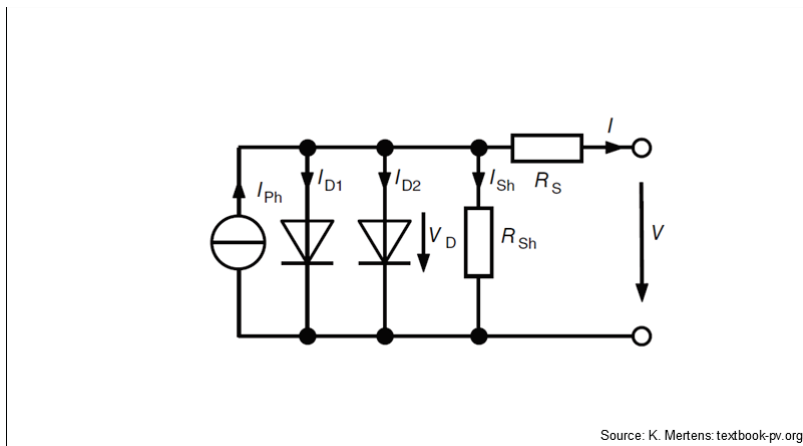


Figure 2-10: The two-diode model is a better representation of a real solar cell. Source: courtesy of K. Mertens: textbook-pv.org

Graphically, the two-diode model can represent current as a function of voltage (I-V curve) (Figure 2-11). The I-V curve has several important components used to evaluate the performance of a solar cell.

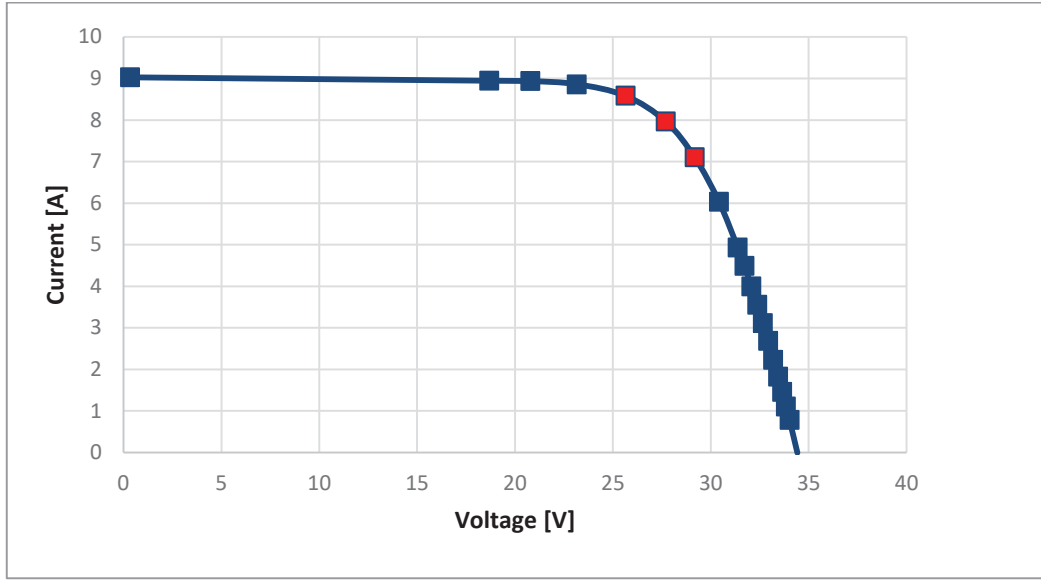


Figure 2-11: I-V curve extracted from Kalkbult test facility. Here, short circuit current equals approximately 9A, open circuit voltage equals approximately 34,5V. The maximum power point ( $P_{MPP}$ ) can be located somewhere in the region of the red markers.

Short circuit current ( $I_{SC}$ ) is the current from a solar cell when it is short circuited. This occurs when voltage is zero, the current equals the photocurrent and is proportional with the irradiance.

$$I_{SC} = I(V = 0) = I_{Ph} - I_S * (e^0 - 1) = I_{Ph} \quad (5)$$

Open circuit voltage ( $V_{OC}$ ) is the voltage when current equals zero:

$$V_{OC} = V(I = 0) = m * V_T * \ln\left(\frac{I_{SC}}{I_S} + 1\right) \quad (6)$$

The maximum power point ( $P_{MPP}$ ) is the point on the I-V curve where the product of current and voltage is at its maximum. The corresponding current is called  $I_{MPP}$  and the voltage  $V_{MPP}$ . From  $P_{MPP}$ :

$$P_{MPP} = I_{MPP} * V_{MPP} \quad (7)$$



From  $P_{MPP}$  one can find the fill factor (FF):

$$FF = \frac{V_{MPP} * I_{MPP}}{V_{OC} * I_{SC}} = \frac{P_{MPP}}{V_{OC} * I_{SC}} \quad (8)$$

FF is an indicator of the quality of a solar cell. For silicon cells, FF usually is in the region of 0.75-0.85, and for thin films 0.6-0.75.

### 2.3.1 Efficiency of a solar cell or panel

A solar cell can never be 100% efficient, by means of converting all incident irradiation into electricity. Silicon, for instance, can only convert certain wavelengths of the solar spectrum. Losses due to incompatible wavelengths of the irradiance with regards to silicon (transmission losses), and photon energy levels incompatible with the band gap energy (thermalizing losses), the usable portion of the irradiance is 49%. (Figure 2-12 and Figure 2-13)

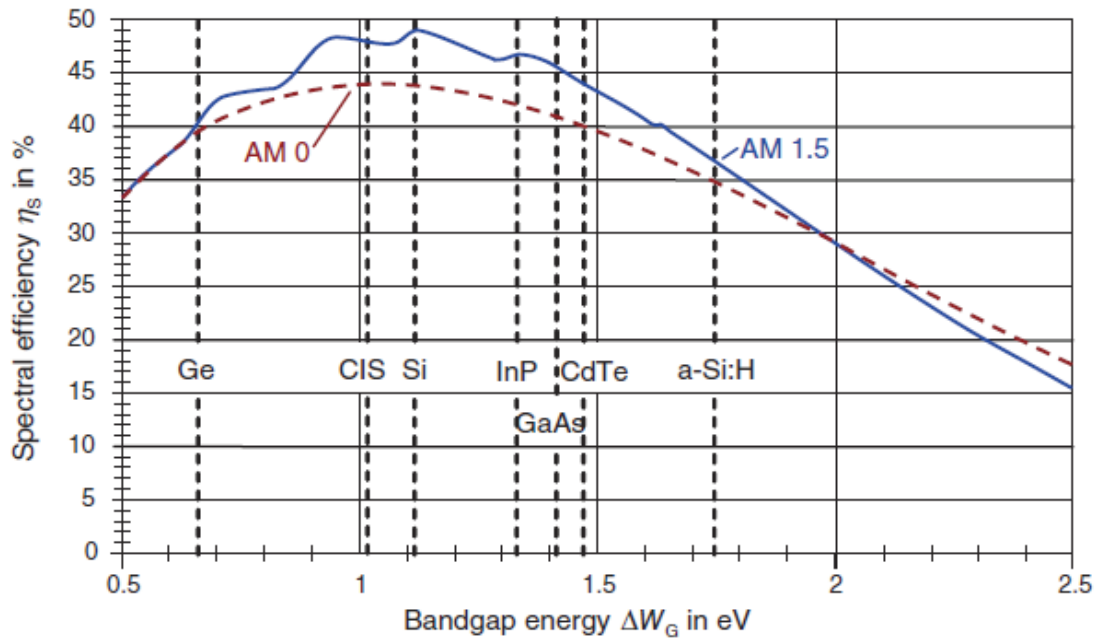


Figure 2-12: Spectral efficiencies of certain materials with their respective bandgap energies (STC values). Source: courtesy of K. Mertens: textbook-pv.org

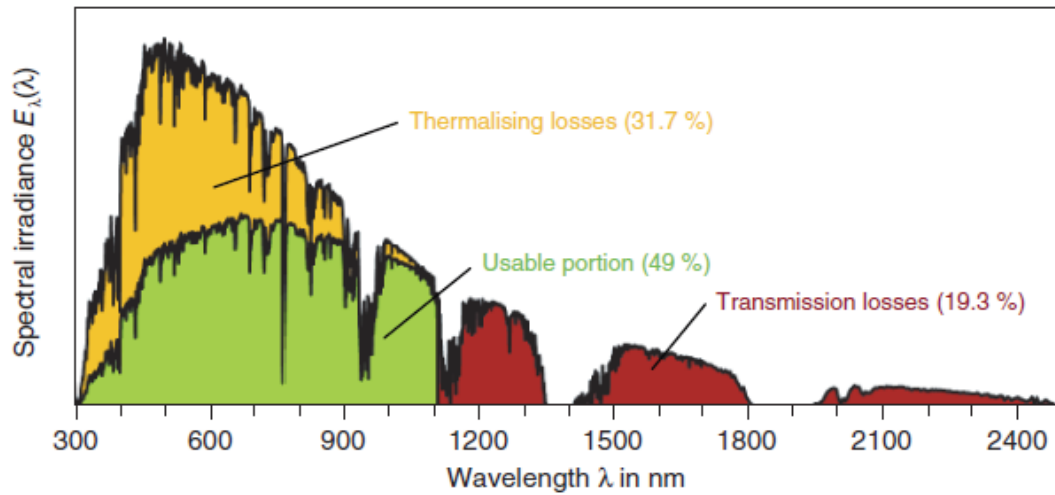


Figure 2-13: Usable and unusable parts of the solar spectrum for a silicon solar cell. Source: courtesy of K. Mertens: textbook-pv.org

In addition to the spectral efficiency, the bandgap energy limits the possible theoretical efficiency for a single p-n junction solar cell to 28.6% at STC, known as the Shockley-Queisser limit, visualized in Figure 2-14. (Shockley & Queisser 1961)

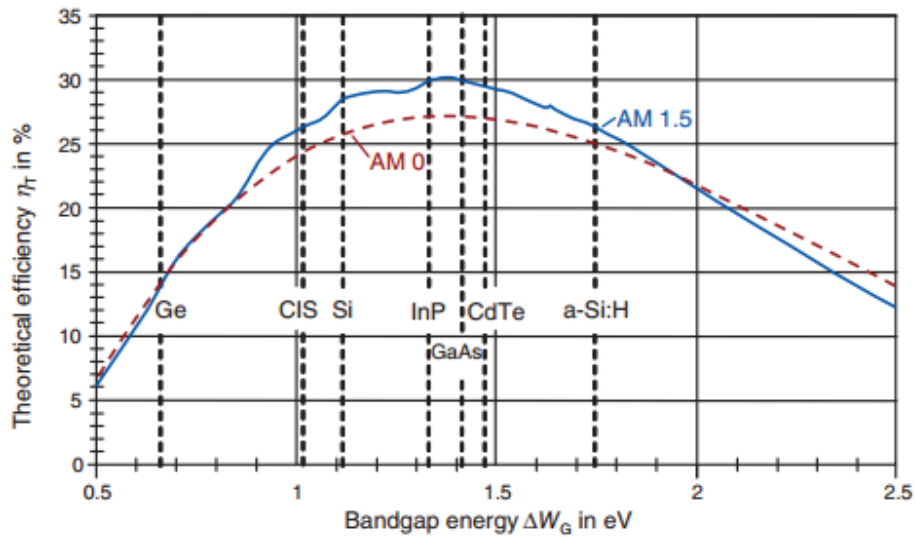


Figure 2-14: Theoretical efficiencies of different solar cell materials according to the Shockley-Queisser limit. Source: courtesy of K. Mertens: textbook-pv.org

The efficiency of a solar cell is its ability to convert incident radiation into electricity.

$$\eta = \frac{\text{Energy out}}{\text{Energy in}} = \frac{P_{MPP}}{E * A} = \frac{FF * V_{OC} * I_{SC}}{E * A} \quad (9)$$

Where:

$E$  = Irradiance

$A$  = Solar cell area

The efficiency reduces when the temperature of the solar cell increases. This happens because with higher temperature, the band gap energy reduces, and thus  $V_{OC}$ . Higher temperature slightly increases  $I_{SC}$ , but the reduction of  $V_{OC}$  far greater (Figure 2-15). This means that the efficiency of a solar panel is temperature dependent, and will increase when the temperature is decreasing.

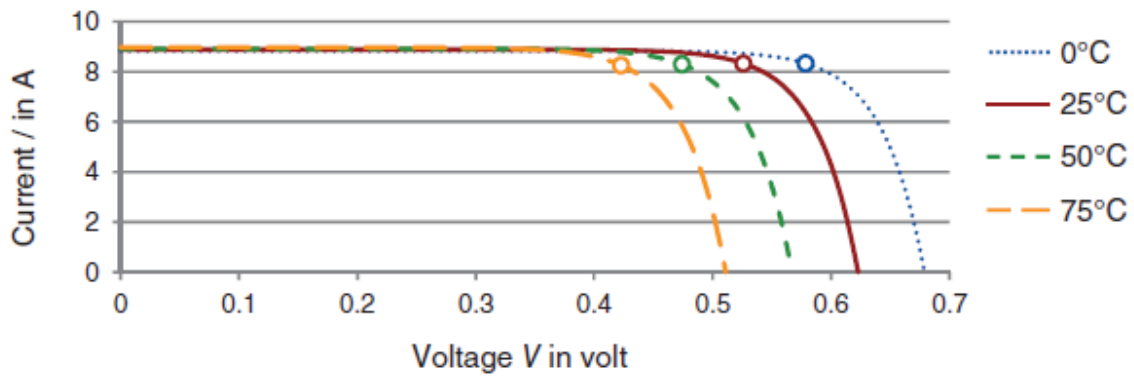


Figure 2-15: Open circuit voltage behavior with solar cell temperature. Source: courtesy of K. Mertens: textbook-pv.org

The loss of power from increased temperature is usually expressed by a temperature coefficient of the maximum power point. The cell temperature is then expressed by equation 10:

$$T_c = T_a + \frac{NOCT - 20^\circ C}{800 \frac{W}{m^2}} * I_L \quad (10)$$

Where:

$T_a$  = ambient temperature

$NOCT$  = Nominal operating cell temperature

$I_L$  = Irradiance

The nominal operating cell temperature is usually found in the specification sheet from the manufacturer of the solar module.

If temperature sensors are mounted on the rear side panel of the modules, the cell temperature can be estimated without ambient and nominal operating cell temperatures (King et al. 2004):

$$T_c = T_m + \frac{I_L}{I_0} * \Delta T \quad (11)$$

Where:

$T_m$  = Back surface temperature

$I_L$  = Irradiance

$I_0$  = Reference irradiance (1000W/m<sup>2</sup>)

$\Delta T$  = 3°C for open rack modules with polymer or glass rear panel.

The power output can be normalized with regards to the cell temperature:

$$P^* = \frac{P_{MPP}}{1 + \gamma(T_c - T_{STC})} \quad (12)$$

Where:

$P_{MPP}$  = Measured maximum power point

$\gamma$  = Material dependent constant

$T_{STC}$  = 25°C

Energy yield is a measure on how much energy is produced compared to the solar module's rated power:

$$Y_{R_0} = \frac{\text{Measured power}}{\text{Rated power (STC)}} \quad (13)$$

A slightly different yield equation can evaluate the performance of a module compared to itself. By comparing the temperature corrected power output over the irradiance at time  $i$  over the same ratio at STC, the module's power output yield is given by equation 14:

$$Y_{RSTC} = \frac{\left(\frac{P_i^*}{I_i}\right)}{\left(\frac{P_{STC}^*}{I_{STC}}\right)} \quad (14)$$

$P^*$  = Temperature corrected power output

$i$  = Time of measurement

$STC = \text{Standard test conditions}$

$\frac{P_{STC}^*}{I_{STC}}$  is obtained by measurement in a controlled environment, preferably by flash testing. If this measurement is not available, the rated power of the module is another option. However, the rated power, available from the spec sheet of the solar module, can have uncertainty ( $\pm 5W$  for the modules analyzed in this thesis) to an extent that makes equation 14 inaccurate for purposes involving high precision measurements. A more accurate reference value can be measured in real life when temperature, irradiance and wind speed is close to STC. Equation 15 has the measurement at time  $i$  divided by a measured reference yield instead of using the rated power.

$$Y_R = \frac{\left(\frac{P_i^*}{I_i}\right)}{\left(\frac{P_0^*}{I_0}\right)} \quad (15)$$

Where:

$P_i^* = \text{Temperature corrected power output at time } i$

$I_i = \text{Irradiance at time } i$

$P_0^* = \text{Temperature corrected power output of the reference measurement}$

$I_0 = \text{Irradiance at reference measurement}$

Assuming all modules are exposed to the same environmental factors, their yield ratios can be compared to identify soiling. Soiling can then be visualized as a soiling ratio where an uncleaned module is compared to a clean module:

$$S_R = \frac{Y_{R_i}}{Y_{R_j}} \quad (16)$$

$Y_{R_i} = \text{Yield ratio of uncleaned module}$

$Y_{R_j} = \text{Yield ratio of regularly cleaned module of same type}$

Uncertainties of calculated soiling ratios can be represented by the statistical measure of standard error (SE), based on the standard deviation (SD) of the population (equation 17).

$$SD = \sigma_x = \sqrt{\frac{1}{N-1} \sum_{i=1}^N (x_i - \bar{x})^2} \quad (17)$$

$$SE = \sigma_{\bar{x}} = \frac{\sigma_x}{\sqrt{N}}$$

## 2.4 Soiling

The definition of soiling is particles with a size less than 500 $\mu\text{m}$  in diameter. This includes pollen, biological matter like hair and cells, textile fibers, but most significantly regarding solar energy is residue from minerals as sand, clay and eroded limestone. These particles cause both shading and scattering of the irradiance and thus reduction of the energy yield. (Sarver et al. 2013)

### 2.4.1 Dust deposition

Tilt angle largely effects dust settlement on the module surface. The larger the angle, the less dust accumulates and settles. Since the typical fixed tilt angle is set at  $\beta = \text{Latitude} \pm 10^\circ$ , dust settlement can be more substantial closer to equator.

Meteorological effects, such as wind, humidity and precipitation influences the deposition. The dust that settles on the modules are, by a considerable extent, carried there by wind, and dust storms can cause large performance loss. Wind can also have a cleaning effect on the solar modules, as the particles are blown off the surface. Large particles are easily removed by wind, but finer particles seem to adhere more to the surface and are less exposed to wind due to their lower profiles. When the particle profile is very low, the force of the wind on the particle will be substantially smaller relative to a higher profile particle, due to the fluid-mechanic no-slip boundary condition close to a surface. Particles with a diameter of less than 50 $\mu\text{m}$  are less affected by wind.

The relative humidity can influence the adhesive properties of the module surface. If the relative humidity approach 100%, dew formation can make dust more adhesive. On the other hand, dew can have a cleaning effect when the dew droplets run off the surface carrying dust particles with them.

The soiling impact on transmittance varies from location to location. For instance, daily cleaned panels in the Thar desert in India shows transmittance losses from 1%-6% with angles 90°, 45° and 0° respectively, while never cleaned panels reported losses from 2%-55% losses. Rainfall greatly inflicts the results of the latter. (Sayyah et al. 2014)

### 2.4.2 Dust properties

The size and composition of the dust particles determine the marginal effect on the transmittance on a solar panel. Particles with high absorption coefficients absorb the incoming radiation, while other fine particles with sizes matching wavelengths of light will reflect and scatter the radiation. This means that a

given mass concentration of finer particles cause greater loss than a same mass of bigger absorbing particles. (Sarver et al. 2013)

The attenuation of incident irradiation from a single particle can be described by scattering and the extinction factor. Scattering is a function of the particles diameter and wavelength of incident radiation, and is called the size parameter:

$$\alpha = \frac{\pi D}{\lambda} \quad (18)$$

$D$  = diameter of the particle's equivalent circle

$\lambda$  = Radiation wavelength in  $\mu m$

The extinction of light is dependent on the particles extinction efficiency. When the size parameter  $\alpha < 3$  the extinction factor  $Q_e$  follows Rayleigh scattering:

$$Q_e = \frac{8\alpha^4}{3} \left[ \frac{m^2 - 1}{m^2 + 2} \right]^2 \quad (19)$$

$m$  = The refractive index of the particle

When particles are bigger than about  $3\mu m$ , the extinction factor saturates to its maximum value, 2, for practically all wavelengths of the solar spectrum used for photovoltaics. This leads to transmittance reduction with a  $90^\circ$  angle of incidence due to number of particles with an average diameter of  $2r$ :

$$\tau_b = \frac{1 - NQ_e\pi r^2}{1} = 1 - NQ_e\pi r^2 = 1 - 2N\pi r^2 \quad (20)$$

$\tau_b$  = Transmittance – attenuation per  $cm^2$

$N$  = Number of particles

$r$  = [cm]

This equation holds until the particles stack on top of each other, which in the experiment by Al-Hasan (1998) happened after the attenuation of incident light reached about 50%. This means that the attenuation increase stays linear until 50% reduction, and non-linear after. (Al-Hasan 1998)

### 2.4.3 Dust mitigation

In principle, there are two ways to mitigate dust settlement on PV modules. Either they are cleaned, or the surface is treated to prevent dust from settling. When cleaning a dirty module, the most usual

method is to use water, either pressurized or with a regular hose. Other common methods involve compressed air, detergents, brushes and cloths.

#### **2.4.4 Dust composition**

To determine the composition of small particles that settles on solar panels, a Scanning Electron Microscope (SEM) is a useful tool. The fundamental principle of a SEM is to direct a focused beam of electrons onto a sample. A detector then analyzes the electrons and signals that bounce off the sample forming a two-dimensional image with a resolution down to 1nm/pixel.

When the electrons interact with the sample, the kinetic energy of the electrons are dissipated as signals. The beamed electrons can either interchange with electrons from the sample, backscatter or excite electrons to a higher energy levels. When electrons in the sample are excited from a lower energy level to a higher, the electron then returns to steady state. In that process, a photon of energy is released, hereby as a characteristic x-ray. Both the interchanged and scattered electrons are caught by a secondary electron detector and converted into an image. The x-ray will be characteristic of the respective substance/molecule and can be used to determine the chemical composition of the sample. (Swapp 2017)

#### **2.4.5 Particle size distribution**

Mineral based particles with sizes in the region of 1000  $\mu\text{m}$  and less are classified as sand, silt and clay by the Krumbein Phi scale. This scale is logarithmic and sorts out the measured particles in intervals suited for presentation. (Qasem et al. 2014)

$$\phi = -\log_2 \left( \frac{D}{D_0} \right) \quad (21)$$

*Where:*

*D = diameter in millimeters*



Table 2-1: Classification of mineral particles by size by the Krumbein-Phi scale

Type	Phi [ $-\log_2(D/1000)$ ]	D [ $\mu\text{m}$ ]
Coarse sand	0-1	1000-500
Medium sand	1-2	500-250
Fine sand	2-3	250-125
Very fine sand	3-4	125-63
Silt	4-5	63-31
	5-6	31-16
	6-7	16-8
	7-8	8-4
Clay/Colloid	<8	<4

## 2.5 Management Science

Management science is a scientific approach of applying mathematics to solve management problems. This methodology is most frequently used in business, but is also applicable to many other purposes where problems can be quantified.

Management science consists of five steps:

1. Observation
2. Problem definition
3. Model construction
4. Model solution
5. Implementation

To identify and define the problem, the system or organization needs to be observed or monitored. The observations or measurements will then be quantified and converted into parameters and variables, i.e. fixed and variable costs. The next step would be to identify the constraints of the problem. Without constraints, the solution could result in no answer, approach infinity or other impractical outcomes which are not suitable for the system or organization. The constraints will decide the area in which the solution will occur. A typical constraint could be a production capacity limit, the maximum or minimum amount of a resource or availability of manpower.

When the problem is defined, the model can be constructed around it to solve for the desired outcome, whether it is minimization of costs, maximization of income or optimization of the system. The quality of

the solution depends on the quality of the input parameters and values. Thus, it is central that the parameters and variables are correctly defined. (Taylor 2013)

### 3 Methodology

#### 3.1 Description of the Test Facility

The test facility consists of 16 polycrystalline silicon modules and 4 Cadmium Telluride (CdTe) thin film modules. In addition, there are two single-axis tracking modules which are not considered in this work.

The layout of the facility is visualized in Figure 3-1. Explanations of the letters and numbers is summarized in table 3-1. Figure 3-2 is a photograph of the test facility.

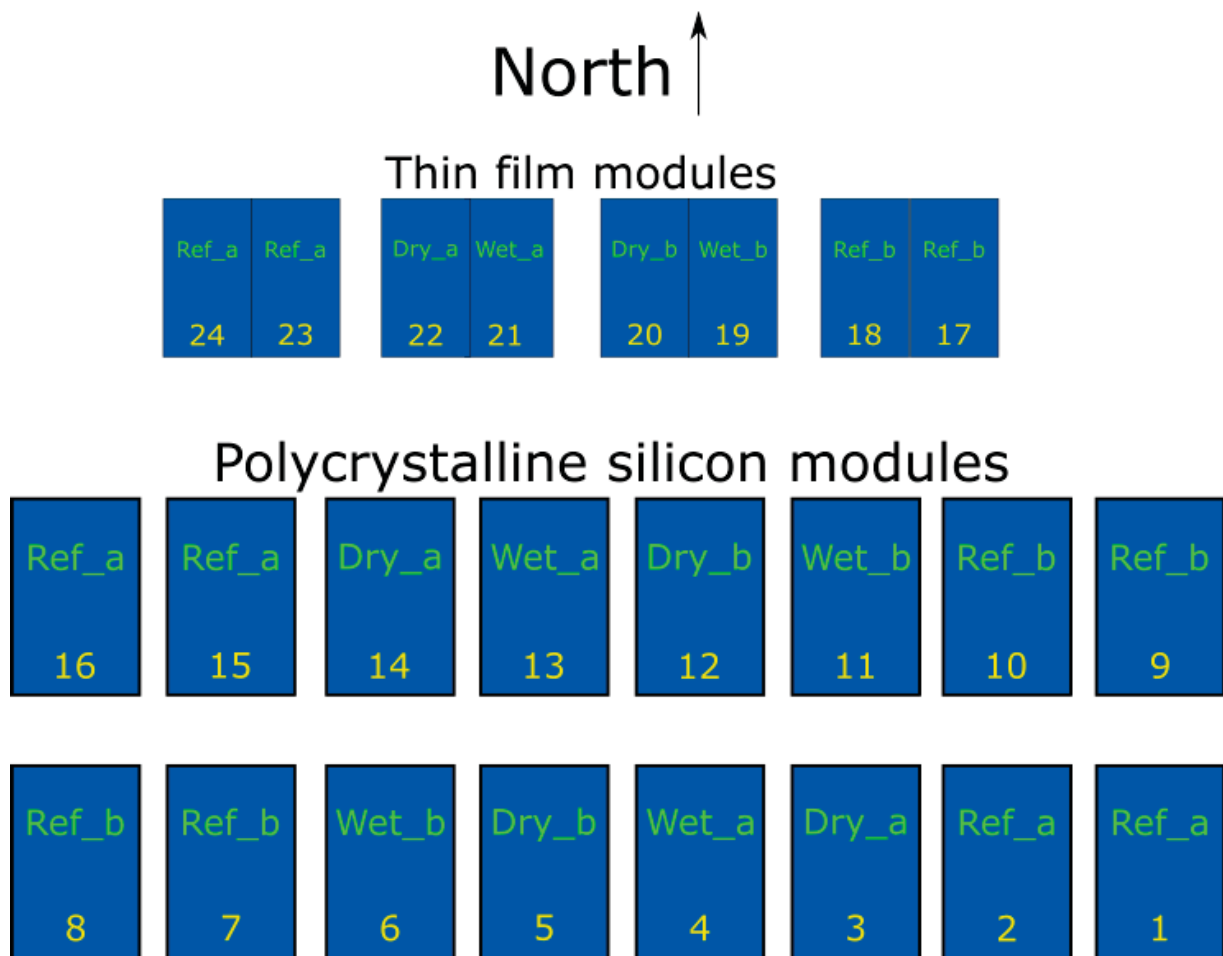


Figure 3-1: Layout of the test facility in Kalkbult (Not to scale). Numbers are identifiers of the respective modules. Ref\_a is anti-soiling treated modules left uncleaned indefinitely. Ref\_b is untreated modules left uncleaned, Wet\_(a/b) is for water cleaned modules, Dry\_(a/b) is dry-cleaned modules. a/b refers to anti-soiling treated (a) and untreated (b) modules respectively.

Table 3-1: Explanation of the cleaning procedures referring to the identifiers in Figure 3-1.

	Treatment	Duration	Module numbers
<b>Ref_a</b>	Hydrophobic coating applied (anti-soiling treatment)	Never cleaned	1,2,15,16 and 23,24
<b>Ref_b</b>	Untreated PV module	Never cleaned	7,8,9,10 and 17,18
<b>Wet_a</b>	Hydrophobic coating applied (anti-soiling treatment). Water cleaned	Cleaned every two weeks	3,14 and 22
<b>Wet_b</b>	Untreated PV module. Water cleaned	Cleaned every two weeks	6,11 and 19
<b>Dry_a</b>	Hydrophobic coating applied (anti-soiling treatment). Dry cleaned	Cleaned every two weeks	4,13 and 21
<b>Dry_b</b>	Untreated PV module. Dry cleaned	Cleaned every two weeks	5,12 and 20



Figure 3-2: Photo of the test facility solar panels, taken from North to South. Thin film modules in front of the silicon modules. In the background to the left is the PV plant. Photo: Mari Øgaard, with permission.

### 3.1.1 Photovoltaic Modules

In Table 3-2, the electrical characteristics for the silicon modules are presented. These values are based on standard test conditions and are found in the specification sheet from the manufacturer.

Table 3-2: Specifications of the Polycrystalline modules.

PV module	$P_{MPP}[W]$	$V_{OC}[V]$	$I_{SC}[A]$	$V_{MPP}[V]$	$I_{MPP}[A]$
JC255M-24/Bb	$255 \pm 5$	37.5	8.86	30.4	8.39
Temperature coefficients	$P_{MPP}[\%/C^{\circ}]$	$V_{OC}[\%/C^{\circ}]$	$I_{SC}[\%/C^{\circ}]$		
	-0.4	-0.3	0.04		

The thin film modules have different properties, and are presented in Table 3-3.

Table 3-3: Specifications of the Thin-Film modules.

PV module	$P_{MPP}[W]$	$V_{OC}[V]$	$I_{SC}[A]$	$V_{MPP}[V]$	$I_{MPP}[A]$
FS-4100/4100A	$100 \pm 5$	87.6	1.57	69.4	1.44
Temperature coefficients	$P_{MPP}[\%/C^{\circ}]$	$V_{OC}[\%/C^{\circ}]$	$I_{SC}[\%/C^{\circ}]$		
	-0.29	-0.28	0.04		

### 3.1.2 Weather and irradiation data

Meteorological data is collected by a weather sensor and rain gauge (WS) by Met One Instruments. WS measures wind speed, wind direction, barometric pressure, ambient temperature, humidity and precipitation at 3 meters above ground level. (MetOne 2013) One-minute interval measurements from the WS are uploaded to an online database.



Figure 3-3: The MetOne weather station.  
Photo: Mari Øgaard, with permission

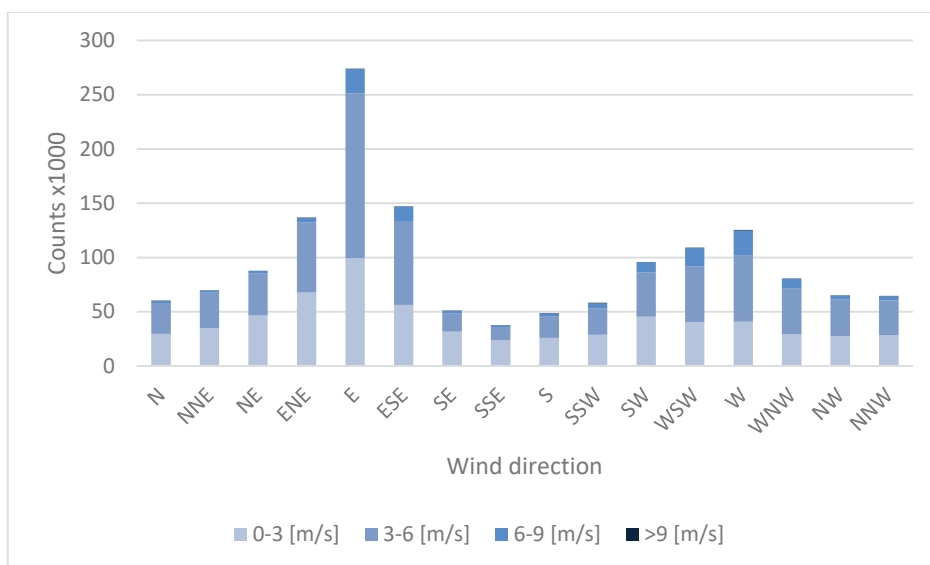


Figure 3-4: Wind directions and wind speeds measured in Kalkbult created from wind data from the weather station in the test facility. The most frequent wind direction is from east, with speeds in the range of 3-6m/s.

### 3.1.3 Uncertainties of measurements

In Table 3-4, the uncertainties for the measurements used in the soiling analysis is summarized.

*Table 3-4: Uncertainties of measurements for the weather station and the I-V data from the modules.*

Weather station accuracy		
Wind speed [m/s]	±	2 %
Wind direction [deg.]	±	5
Ambient temperature [°C]	±	0,4
Module temperature [°C]	±	0,5
Humidity [%]	±	4
Barometric pressure [mbar]	±	2
Rain [mm]	±	1 %
Irradiance [W/m <sup>2</sup> ]	±	3 %
I-V curve [V], [A]	±	1 %

### 3.1.4 Test facility cleaning methods and surface treatment

The modules in the test facility undergo a cleaning regime where some of the modules are cleaned regularly every two weeks. Some modules are left uncleaned to serve as reference to detect soiling. All modules are exposed to the environment; thus rain, wind and humidity can have effects on the soiling levels.

#### 3.1.4.1 Anti-soiling treatment

The modules referred to as “Ref\_a”, “Wet\_a” and “Dry\_a” were coated with a hydrophobic anti-soiling solution. Hydrophobic coatings will make the surface more repellant to water, and the idea behind the anti-soiling function is that when it rains, the soiling particles will be carried by the repelling droplets and thus be washed off.

#### 3.1.4.2 Water cleaning

Approximately 1.5L of distilled water is poured in a clean 20L bucket, two microfiber cloths are soaked in the bucket. One person on a step ladder cleans the module from the top, with downward strokes. About halfway down, the person on the step ladder cannot reach the bottom part of the module, then the person on the ground continues. The cloths are soaked as much as needed, and all visible dust is removed. Precautions are made to ensure no water is spilled or splashed onto the adjacent modules. The modules are dried by downward strokes with super-absorbent cloths. All moisture is removed to

prevent airborne dust from sticking to the surface. This procedure also removes dust that was not cleaned with water.

### 3.1.4.3 Dry-cleaning

The dry-cleaning procedure is conducted by two persons. One person on a step ladder cleans the top part of the module, one person on the ground cleans the bottom part. The modules are cleaned with light downward sweeps, removing all visible dust and avoiding scratches. The cloths are checked to assure they are completely dry before cleaning starts.

## 3.2 Data Analysis and PV Performance Parameters

### 3.2.1 PV data from Kalkbult test facility

The test facility consists of 16 pc-Si modules and 8 CdTe thin film modules. Every ten minutes, a set of 20 current-voltage (I-V) pairs are logged into a database for each module. The IV pairs are generated by a variable resistance device called ActiveLoad. By varying the electric load on the PV power output, the current and voltage change values from short circuit current ( $I_{SC}$ ) and zero voltage, to open circuit voltage ( $V_{OC}$ ) and no current. A basic presentation of the I-V curve can be seen in Figure 3-5.

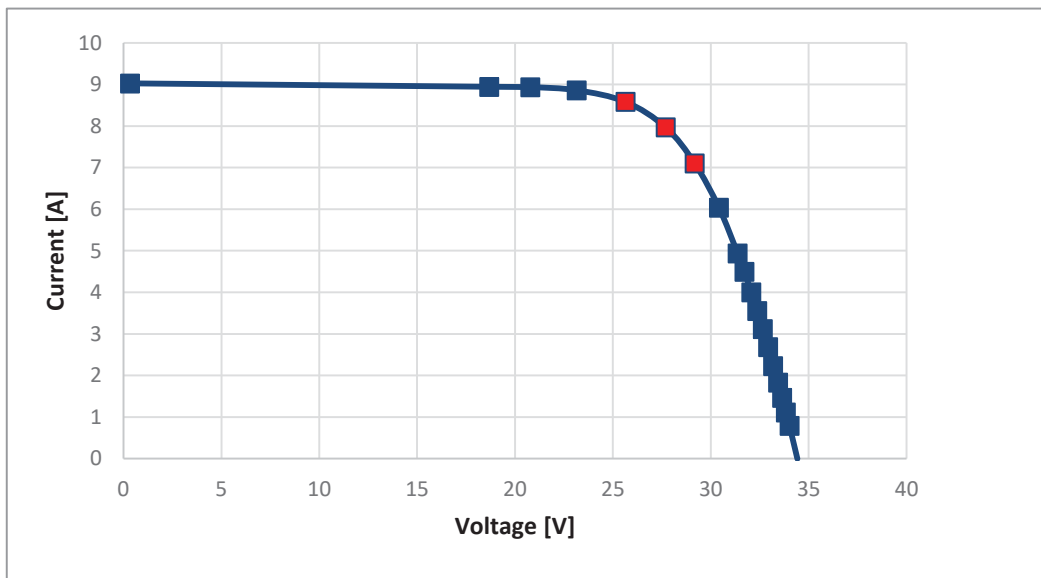


Figure 3-5: I-V curve made from data from one of the silicon modules in Kalkbult.

Maximum power occurs when the product of current and voltage is maximized along the I-V curve. The I-V pairs are logged with a controller device that logs the data to a database, with backup to a SD-card.



The database is accessible online for remote access. Along with the I-V data, a temperature sensor measures the back-plate temperature of the modules.

Daily maximum power usually occurs around midday when the sun is highest in the sky. On a sunny day, the power output stays fairly stable for a couple of hours around noon, with a small peak on *solar* noon (also called high noon), which in Kalkbult is sometime between 12Am and 1PM all year round (NOAA 2017). During the morning and afternoon, low irradiance and low incidence angle will influence the efficiency of the solar panels, and differences in efficiency between modules will be larger. Thus, the solar panels will give more stable outputs around solar noon, and the performance of the modules will be more comparable.

The averaged measurements of power and irradiance over the hour between 12Am and 1PM should thus be quite stable on sunny days. Using an average, and not a single measurement, of one hour (6 measurements) reduces uncertainty due to random errors. The yield and soiling ratios are thus calculated from the midday averages, from 12AM to 1PM.

In addition, only clear days were used to determine soiling losses. The definition of a clear day in this thesis is when the standard deviation of the midday measurements of irradiance is  $\leq 11W/m^2$ . This standard deviation of irradiance is the threshold where the efficiency of the modules' standard deviation stays under 0.1 for the same hour. (This calculation was made by Mari Øgaard (IFE/NMBU), who wrote her Master's thesis from the same dataset, but from an earlier period (Øgaard 2016).)

The difference between a clear and cloudy day can be visualized as difference in correlation between irradiation and power. Two plots (Figure 3-6) from a clouded and clear day respectively, show that the measured irradiance and power output differs more on the cloudy day than the clear day. The correlation coefficient between the power output and irradiance are 0.90 for the cloudy day and 0.99 for the clear day. In case of perfect correlation, the coefficient would equal 1. The calculation was done with equation 22.

$$Corr(P, I) = \frac{E[(P - \mu_P)(I - \mu_I)]}{\sigma_P \sigma_I} \quad (22)$$

$P$  = Power output

$I$  = Irradiance

$\mu_i$  = Expected value of  $i$

$\sigma_i$  = Standard deviations for  $i$

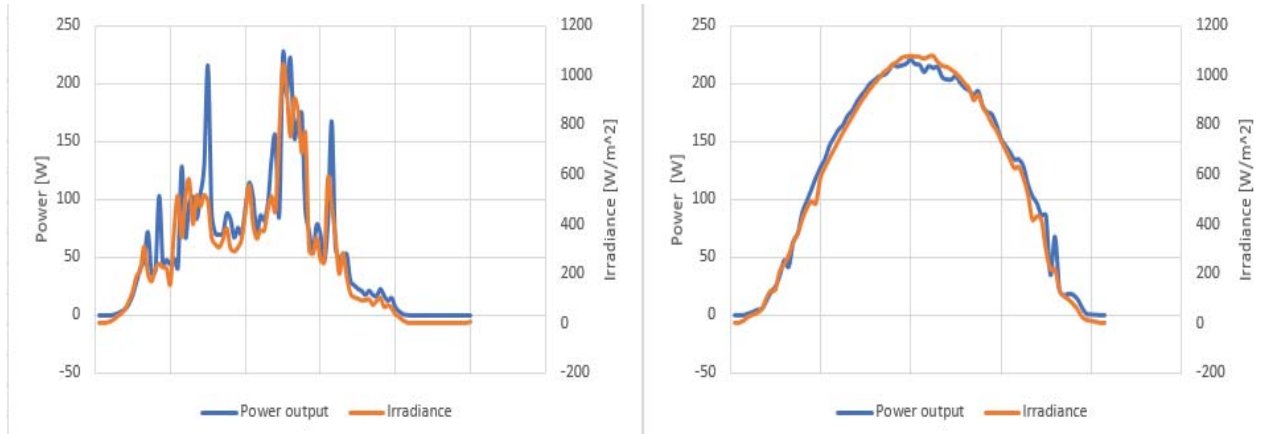


Figure 3-6: A cloudy and a clear day in November. Power output from Polycrystalline module 1 compared to the measured irradiance.

Irradiation is measured by a pyranometer by Kipp&Zonen. The pyranometer is oriented in the same direction and tilt as the PV modules. This orientation outputs the plane of array irradiance ( $G_{POA}$ ). (Kipp & Zonen 2017)

The weather and irradiance data is collected by a master controller which logs the data every minute continuously and uploads to an online database.

### 3.2.2 Maximum power point

To identify the maximum power point, the I-V data from the modules was loaded in MATLAB and run through a software called IVfit, developed by the Energy research Centre of the Netherlands (ECN). This software uses the two-diode model to calculate the maximum power point, described in Figure 2-10. The two diode model is applicable to both polycrystalline and CdTe solar modules (Prorok et al. 2005).

### **3.2.3 Temperature correction**

Since temperature has a substantial effect on the efficiency of solar modules, a correction for temperature is needed to compare the power outputs. The temperature sensors on the rear plates of the modules do not measure the cell temperature directly and must be converted to be used by equation 11. This approach differs from the broadly used method based on NOCT (equation 10), however the latter is based on measurements in a controlled environment which is hard to replicate in nature. (King et al. 2004) The two approaches have been compared in a previous master's thesis (Øgaard 2016) on the same dataset, but for a different period, and the method based on back plate temperature showed to be more accurate. To make results from previous work comparable, same methodology was done in this thesis.

## **3.3 Dust Sample Analysis**

To determine composition and marginal attenuation of the local soiling, a dust sample collected by a dust bucket in the test facility was analyzed. The sample was collected from the site during summer of 2015.

The dust sample was examined by a scanning electron microscope (SEM/EDS) at IFE. The sample was placed on a carbon tab on an aluminum stub and coated with carbon vapor to make the sample conductive. The samples were magnified up to 2200 times, which would make it easy to distinguish between particles and perform size distribution analysis with software.

Grayscale images were produced with a resolution of 512x384 pixels. The grayscale images include a benchmark which was used to determine the approximate diameter of the particles.

Mapping images were made with a resolution of 256 by 192 pixels, with a pixel size of 0.22 $\mu$ m. The mapping was done with respect to Oxygen (O), Sodium (Na), Aluminum (Al), Silicon (Si), Sulfur (S), Chlorine (Cl), Potassium (K), Calcium (Ca), Magnesium (Mg), Phosphorus (P), Iron (Fe) and Copper (Cu).

For each sample, up to 12 point analyses were made by picking out particles from the grayscale images. Each point has its respective graph where spikes show which element is present. The graphs were analyzed to determine the nature of the particles.

For all sample images, a report of mass percentage, atom percentage and respective uncertainties were produced by the SEM/EDS software. Elements with less than 2% mass or atom presence were disregarded. (IFE 2017)

The images of different magnification produced by the SEM were in this thesis regarded as representative for the sample, and for the size distribution of airborne dust for the area at the time of the collection.

ImageJ software was used for size distribution analysis of the sample, adjusted for resolution and magnification. (Schindelin et al. 2012)

The size distribution data was parameterized using Krumbein Phi scale in accordance to the principle of classification of soil from the standard ISO14688-1 “Geotechnical investigation and testing -- Identification and classification of soil” . (ISO 2002)

### 3.4 Cleaning Schedule Model

To establish a cleaning schedule, a model was made in excel. The model is a binary model, which means that decision variables either take value 1 or 0. Hereby 1 means “clean”, and 0 means “do not clean”. The model solves for when the accumulated cost of energy loss due to soiling surpasses the marginal cost of cleaning.

#### 3.4.1 Cost of Soiling

The cost of soiling is calculated by equation 23.

$$C_{s,i} = (1 - S_{R,i}) * E_{M,i} * P_{avg,i} \quad (23)$$

Where:

$C_{s,i}$  = Soiling cost for period  $i$

$S_{R,i}$  = Soiling Ratio for period  $i$

$E_{M,i}$  = Electricity production of a clean module for period  $i$

$P_{avg}$  = Average electricity price received

#### 3.4.2 Cost of Cleaning

Marginal cost of cleaning is calculated from cost information from the PV plant in Kalkbult. Total cost of cleaning is divided by the number of modules to get the marginal cost of cleaning one module (equation 24).

$$c_{cleaning} = \frac{C_{cleaning}}{n_{modules}} \quad (24)$$

The cost input data was retrieved from an employee Scatect Solar in South Africa, and is summarized in Table 3-5.

*Table 3-5: This list is used to estimate the total cost of cleaning for the PV plant in Kalkbult. Prices are in ZAR.*

<u>Item</u>	<u>Quantity</u>	<u>Plant Extrapolated</u>
<b>Modules Washed</b>	33,800	315 000
<b>TCS's Washed</b>	9	42
<b>Water Usage L</b>	18600	93000
<b>Cost of water</b>	R12,090.00	R60,450
<b>Time to wash</b>	5 days	47 days
<b>Cost of labor</b>	R8,650.00	R81,216
<b>Transport per day</b>	R3,230.00	R151,810.00
<b>Cleaning Chemical</b>	R734.20	R3,671.02
<b>Total</b>	R53,774.20	N/A
<b>Cost/module</b>	R1.59	<b>N/A</b>

The extrapolated total cost for the whole PV plant in table 3-5 seemed to be incorrect. The number used to calculate the marginal cost per module was the total cost for 5 days, and 33800 modules. The marginal cleaning cost per module was calculated to ZAR 1.59.

The Kalkbult plant reported their cleaning costs per module to be ZAR 0.93 for labor, and ZAR 0.49 for water. The water consumption per module was estimated to 600mL. He also reported an average increase in overall performance after cleaning of 0.56%. This number was not specified by any time frame or details, and is not considered in this work.

The labor costs include two teams of 7 workers plus two supervisors, cleaning approximately 7000 modules per day. The PV plant consists of 315000 panels in total. The materials used are two trailers with water tanks (one for water, one for soap water), mops, squeegees and vehicles to transport trailers and workers around the plant.

Cost of cleaning is usually a component of the operations and maintenance (O&M) costs of a PV plant. In literature, the value of O&M costs is often set as a percentage of investment costs in levelized cost of

energy (LCOE) calculations, or as a price per kW installed capacity. National Renewable Energy Laboratory's (NREL) "Best Practices in Photovoltaic System Operations and Maintenance" report (Whaley 2016) operates with  $\$19 \pm 10$  per kW per year for O&M in total, or recommends a yearly cost of 0.5% of the investment. It is unclear how much of that number points to the specific cleaning cost. From Electric Power Research Institute's (EPRI) best operations report the cost per cleaning amounts to  $\$0.80\text{--}\$1.30/\text{kW}$  (Enbar et al. 2015). For a 250W panel, the marginal cost would be  $\$0.20\text{--}0.325$  per panel from the EPRI report's values. The value of ZAR 1.59 equals USD 0.12 which is not very far from EPRI's lower boundary value, considering differences in wages between the US and South Africa.

### **3.4.3 Electricity Prices**

The Price Purchase Agreement between the PV plant and South African grid operator company Eskom would contain the real prices received for the electricity. However, this information was not available.

The PV plant in Kalkbult was part of the first of three bidding rounds in the then new South African Renewable Energy Independent Power Producers Procurement Program (REIPPP). This program replaced the former initiative to stimulate renewable energy projects. REIPPP included 20-year contracts with feed-in-tariffs (FiT) for wind, solar PV and concentrated solar power. The average FiT for PV in the first REIPPP bidding round was ZAR 276c/kWh which was used in this model (Eberhard 2014).

Hypothetically, if a FiT was not available, an electricity price following the market price was calculated per month. From the government owned energy company Eskom's website, a tariff book from 2016-2017 was used to calculate market prices matching the power output profile of the PV modules.

The market electricity prices vary during the seasons, weekdays and weekends, and during the day. The seasons are divided in two; Low and High season. The two seasons have different peak, standard and off-peak hours during weekdays and weekends. This is represented in Figure 3-7. Low demand season starts in September and ends in May, and high season is from June to August.

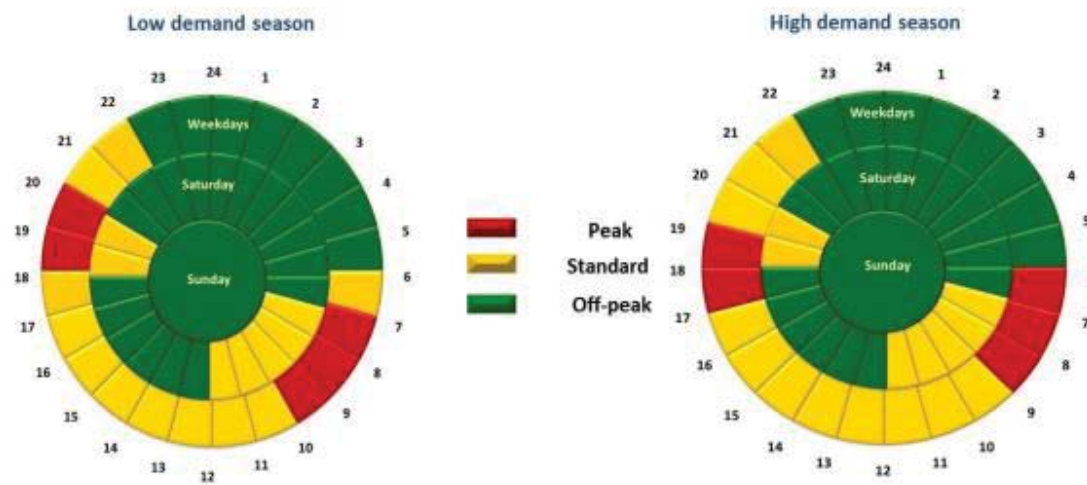


Figure 3-7: Load profiles of the low and high demand seasons in South Africa. Source: courtesy of Eskom, from "Tariffs & Charges Booklet for 2016/17" (ESKOM 2017)

The electricity generators must pay for the grid access, and different zones in the country have different network charges. The Kalkbult plant lies in the Cape Zone, where the network charge is zero. (Eskom 2017)

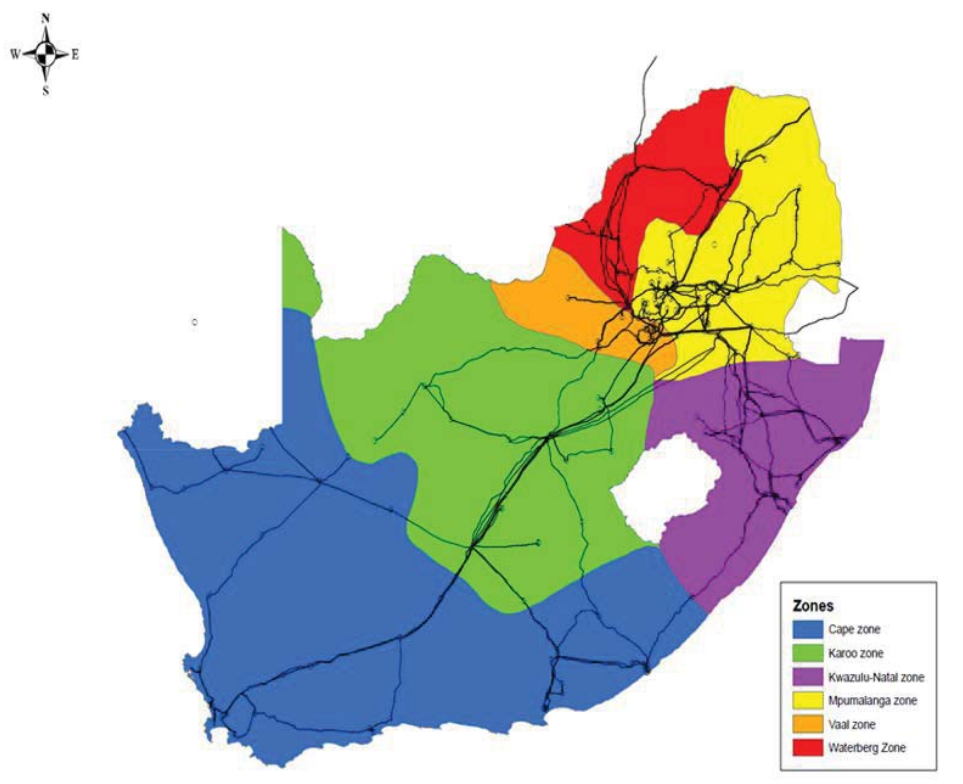


Figure 3-8: Transmission zones are used to calculate transmission fees and distance losses. Source: courtesy of Eskom, from “Tariffs & Charges Booklet for 2016/17” (ESKOM 2017)

The load profile of the PV follows the path of the sun, with low power in the morning and late afternoon, and highest around midday. Since peak hours are in the morning on the weekdays, the high price combined with low production did not influence the average price much. The average price, for both high and low seasons, ended up near equal to the standard price. The results of the price calculations are summarized in Table 3-6.

Table 3-6: Electricity prices in ZAR cents/kWh.

	Peak [c/kWh]	Standard [c/kWh]	Off-peak [c/kWh]	Averaged with PV profile [c/kWh]
High season [June to August]	260	79	43	79
Low season [September to May]	86	59	37	58

### 3.4.4 Model design

The model was made to be as simple as possible to make sure it can be used in other locations. Since the model was designed around the soiling ratio, this value must be calculated for each month to make



the model work. However, if soiling loss is calculated using a different method, the model is easily adaptable. The electricity price must be calculated as an average for each month. In cases of non-flat prices, the average price must be calculated according to the load profile of the solar PV system.

*Table 3-7: The input sheet of the cleaning schedule model. Different input for the two types of modules in the test facility.*

	Silicon		CdTe		Electricity price [ZAR cents/kWh]
	Soiling ratio	Production per Module [kWh]	Soiling ratio	Production per Module [kWh]	
Jan					276
Feb					276
Mar					276
Apr					276
May					276
Jun					276
Jul					276
Aug					276
Sep					276
Oct					276
Nov					276
Dec					276

## 4 Results

This chapter will first present the soiling analysis based on the I-V data from the modules. Second is the results from the experimental analysis of the soil sample. Finally, is the solution to the cleaning schedule model.

### 4.1 PV soiling analysis

#### 4.1.1 Silicon modules

A summary of statistical values for the temperature corrected reference yield day for the silicon modules are presented in Table 4-1. These values are the basis for the Yield Ratios that are calculated with equation 15. The standard deviation and standard error are quite small, indicating stable conditions

and small variations between the modules. If any soiling is left on the surface after the rain the day before, it is assumed to be insignificant.

*Table 4-1: Descriptive statistical values for the averaged midday power output of the silicon modules (15 of 16 modules) at the reference day May 11<sup>th</sup>, 2016.*

<b>Power output [W], temperature corrected</b>	
<b>Average</b>	236,30
<b>Standard Error</b>	0,49
<b>Median</b>	236,13
<b>St. Dev.</b>	1,92
<b>Variance</b>	3,67
<b>Kurtosis</b>	1,94
<b>Skewness</b>	-0,87
<b>Range</b>	7,96
<b>Min</b>	231,46
<b>Max</b>	239,41
<b>Sum</b>	3544,46
<b>Counts</b>	15
<b>Wind [m/s]</b>	1,67
<b>Temp [°C]</b>	16,99
<b>GHI [W/m2]</b>	983,83

Figure 4-1 shows the yield ratios for all groups of modules from November 2016 to April 2017. The heavy fluctuations (spikes and drops) in January and February are probably due to cloudy weather, with fluctuating irradiance.

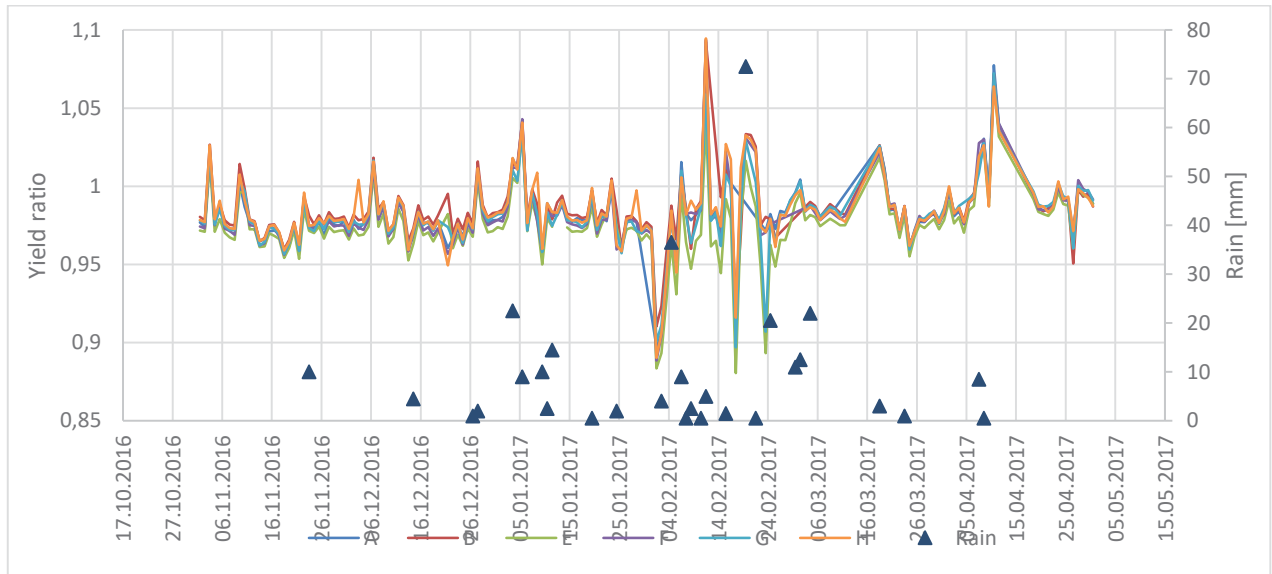


Figure 4-1: Yield ratios (without Polycrystalline module 2) plotted with rain. Ref\_a and Ref\_b are the uncleaned modules, while Wet\_a (anti-soiling) and Wet\_b are wet cleaned, Dry\_a and Dry\_b are dry cleaned.

There is a chance of detecting soiling by looking at trends in the data before and after rain. In Figure 4-2, the yield ratios for the reference (uncleaned) modules were plotted with rain throughout the period. In the first period in November before the first rain day (Nov 23<sup>rd</sup>), the trend appears to be declining slightly, and a slight increase immediately after the rainfall. This period is analyzed closer in chapter 4.1.3.

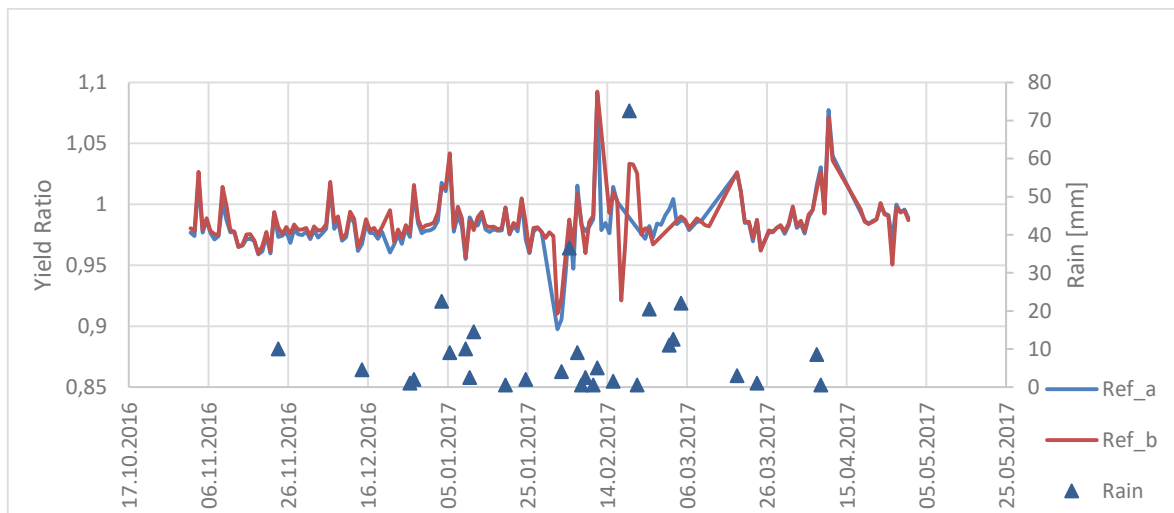


Figure 4-2: Yield ratio of the reference modules with rain. Ref\_a has anti-soiling treatment, Ref\_b has no treatment.

When only clear days are considered, as defined in chapter 3.2.1, irregularities in the measured data due to fluctuations in irradiance is reduced. Figure 4-3 show yield ratio (equation 15) on clear days plotted

with rain. Some days can be characterized as clear, even though rain occurs, but the midday hour (also defined in chapter 3.2.1) is clear. The fluctuations from Figure 4-2 is dampened, which makes this plot easier to interpret with respect to possible soiling. When interpreting yield ratios, the trends are of significance to soiling. A downward trend, preferable between rain days, could indicate accumulation of dust on the module surface. The slight declining trend identified in figure 4-2 is still present here.



Figure 4-3: Yield ratios of the reference modules on clear days plotted with rain.

The soiling ratios, calculated by equation 16, presented in, of the anti-soiling coated modules shows no immediate trends for either the wet or dry cleaned modules (Figure 4-4). The possible trend found in the yield plot (Figure 4-2) does not seem to be present here. No clearly visible differences appear before or after rainfall. When considering the resolution of the scale of the figure, the soiling ratios appear very stable throughout the period.

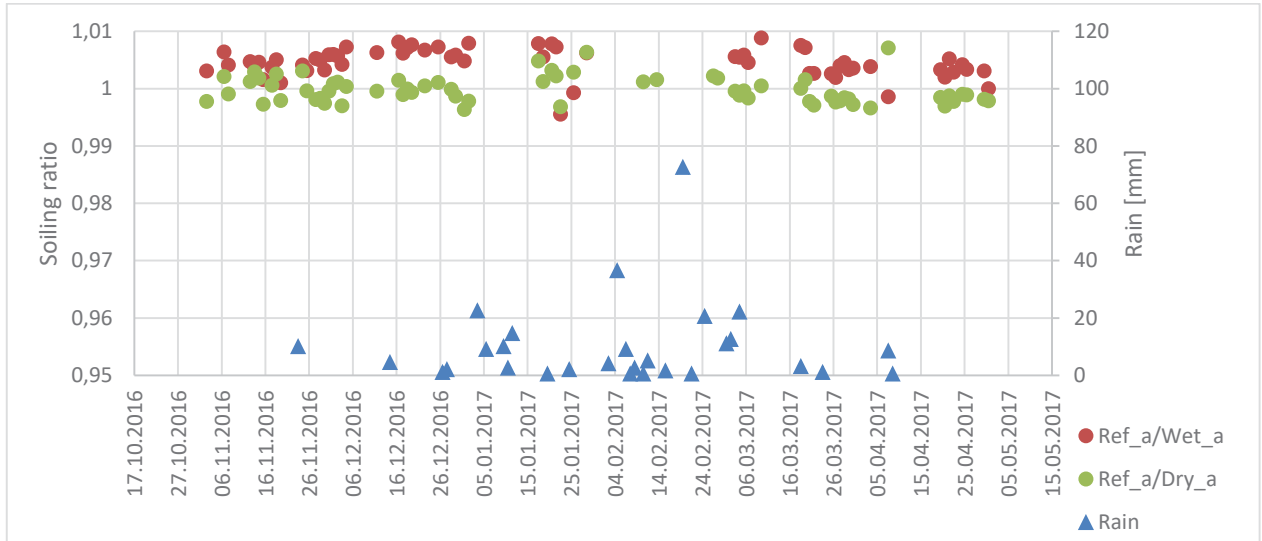


Figure 4-4: Soiling ratio for the Anti-soiling treated Polycrystalline modules. Ref\_a is the reference, Wet\_a is wet cleaned, Dry\_a is dry cleaned.

The soiling ratio of the untreated modules (Figure 4-5) appear to follow the same pattern as the coated modules, with a couple of outliers. The figures do not clearly point out soiling trends by visual inspection, and in chapter 4.1.3 statistical approaches for detecting possible soiling loss of power is investigated.

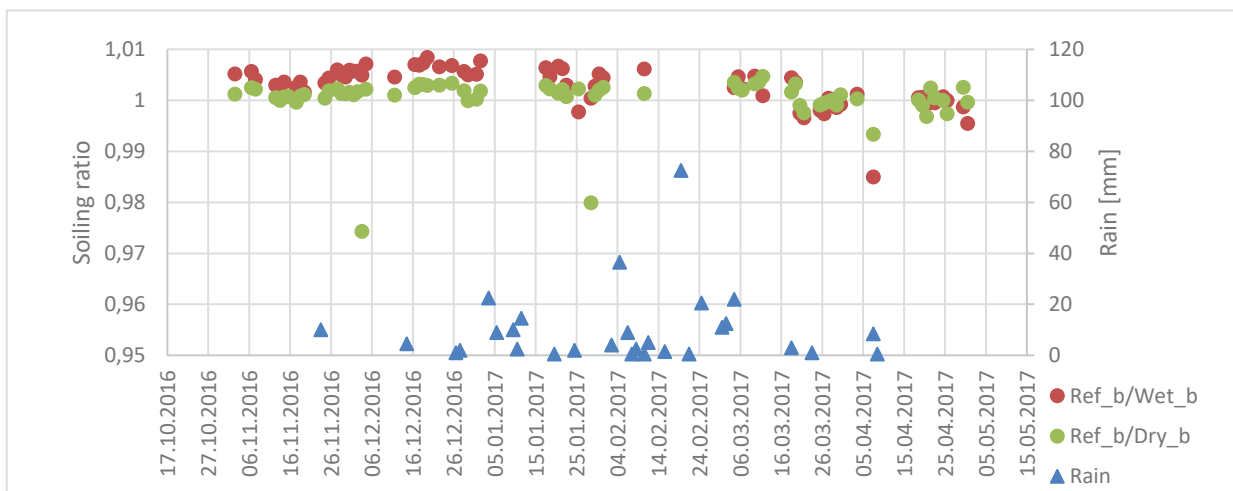


Figure 4-5: Soiling ratios for the untreated Polycrystalline modules. Ref\_b is the reference, Wet\_b is wet cleaned, Dry\_b is dry cleaned.

Ideally, the soiling ratio should take values between 0 and 1, but as seen in both Figure 4-4 and Figure 4-5, several values are higher than 1. If the average soiling ratio of the reference modules are more than one, the uncleaned modules essentially perform better than the cleaned ones.

A possible explanation of the higher than 1 values can be connected to the reference day value for each module (May 11<sup>th</sup>, 2016). If the reference day value is not unbiased with regards to the differences between each module's performance, the soiling ratio will be influenced. Other explanations to these values can be measurement errors, bird droppings or other random errors.

As seen in the figures, rainfall is quite frequent, especially from mid-December. The rainfall compared with the soiling ratios imply that if any soiling occurs, it is cleaned away with rain.

Table 4-2 shows that there is no general soiling for the whole period, and the reference modules seem to perform slightly better than the cleaned ones.

*Table 4-2: The average soiling ratio for anti-soiling treated and untreated modules from November 2016 to April 2017.*

Average soiling ratio	
Anti-soiling treated modules	Untreated modules
1,003	1,002

#### 4.1.2 Thin film modules

The yield ratios for the thin film modules are plotted in Figure 4-6. Because of missing data in May 2016, the reference yield was taken from a different day than the polycrystalline modules. The reference day was chosen to be November 23<sup>rd</sup>, one day after heavy rain, a clear day with hourly averaged midday irradiance level around 1000W/m<sup>2</sup>, low wind speed and ambient temperature close to 25°C. Statistical values of the reference day power output are summarized in Table 4-3.

*Table 4-3: Descriptive statistics for midday average power output of the thin film modules on the reference day, November 23<sup>rd</sup>.*

<b>Power output [W], temperature corrected</b>	
<b>Average</b>	71,30
<b>Standard Error</b>	0,86
<b>Median</b>	71,75
<b>Std. Dev.</b>	2,44
<b>Variance</b>	5,94
<b>Kurtosis</b>	-1,67
<b>Skewness</b>	-0,29
<b>Range</b>	6,54
<b>Min</b>	67,79
<b>Max</b>	74,32
<b>Sum</b>	570,38
<b>Counts</b>	8
<b>Wind [m/s]</b>	2,92
<b>Temp [°C]</b>	26,22
<b>GHI [W/m2]</b>	1086,83

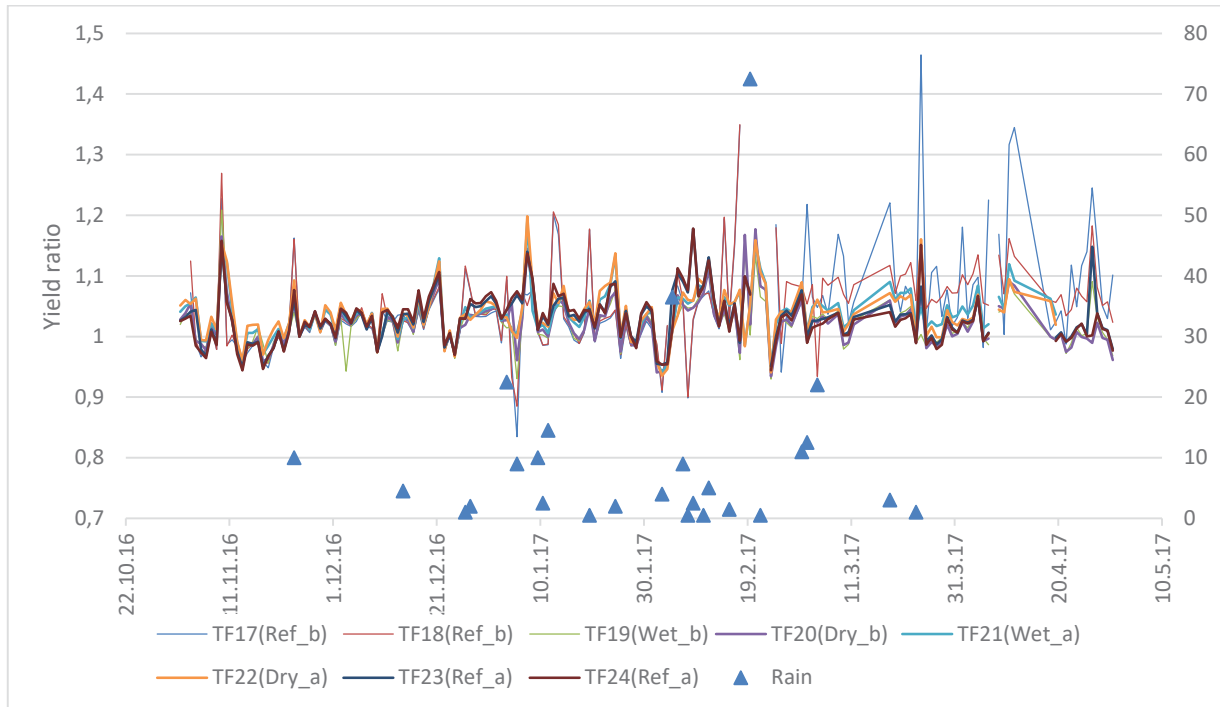


Figure 4-6: Yield ratios for all thin film modules throughout the period of measurement.  $TFx$ =Thin Film module number  $x$ . Calculated by equation 14.

Compared with the silicon modules (Figure 4-1, different scale on Yield ratio axis), the thin film yields fluctuate more. At the end of the measuring period, the yield seems somewhat unstable. The reason behind this is missing data, which made the soiling analysis difficult.

In Figure 4-7, the clear day yields are presented as a scatter plot. When the days with varying irradiance are removed, the fluctuations are significantly reduced (PS! Yield ratio scale is different). This adds to the reasoning behind using only clear midday data (chapter 3.2.1). Towards the end of the period, the spread of the yield ratios increases. TF17(Ref\_b) and TF18(Ref\_b), which are connected to the same ActiveLoad, have quite large fluctuations compared with the other modules.



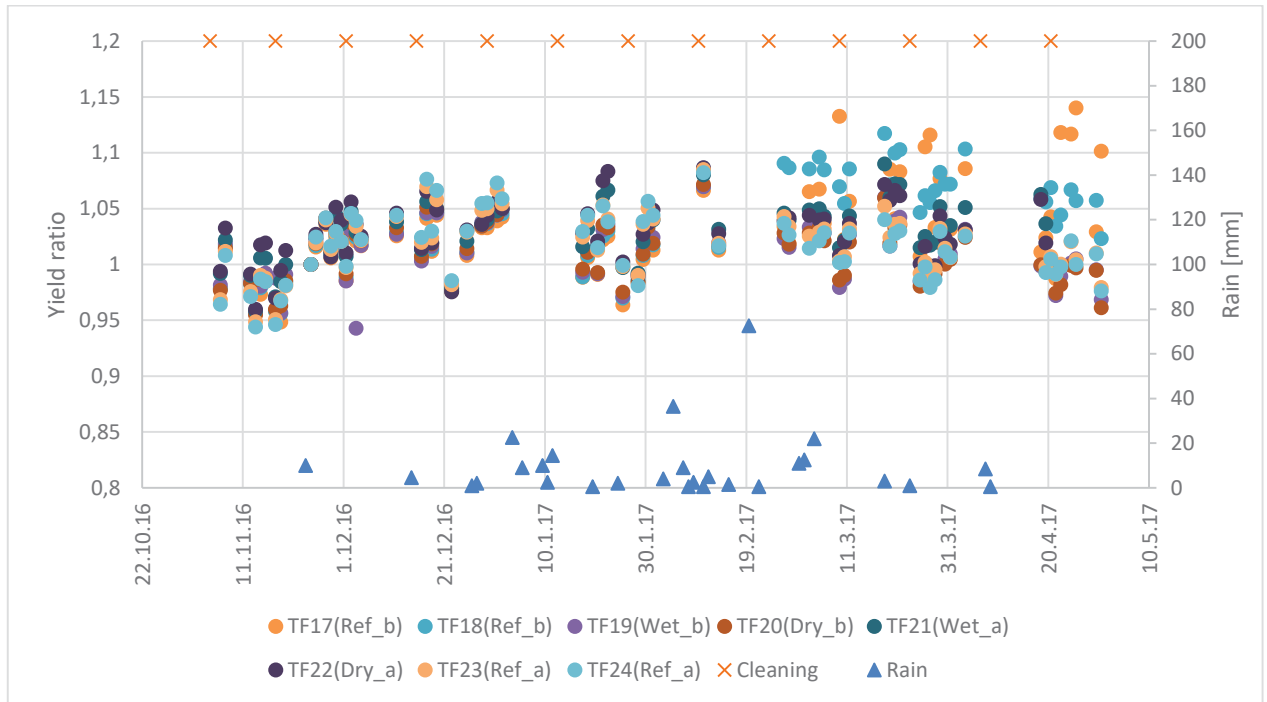


Figure 4-7: Yield ratios of all thin film modules for clear days plotted with rain days and the biweekly cleanings.

The soiling ratios are presented in Figure 4-8, and signs of soiling is seen in group A before the first rain day in November. The soiling seems to only occur on the anti-soiling treated modules (A/E and A/G). The untreated modules seem to lie stable close to 1 until the end of the period where some fluctuations occur. In chapter 4.1.3, the data is analyzed further. Towards the end, both Ref\_b/Wet\_b and Ref\_b/Dry\_b take values well over 1.

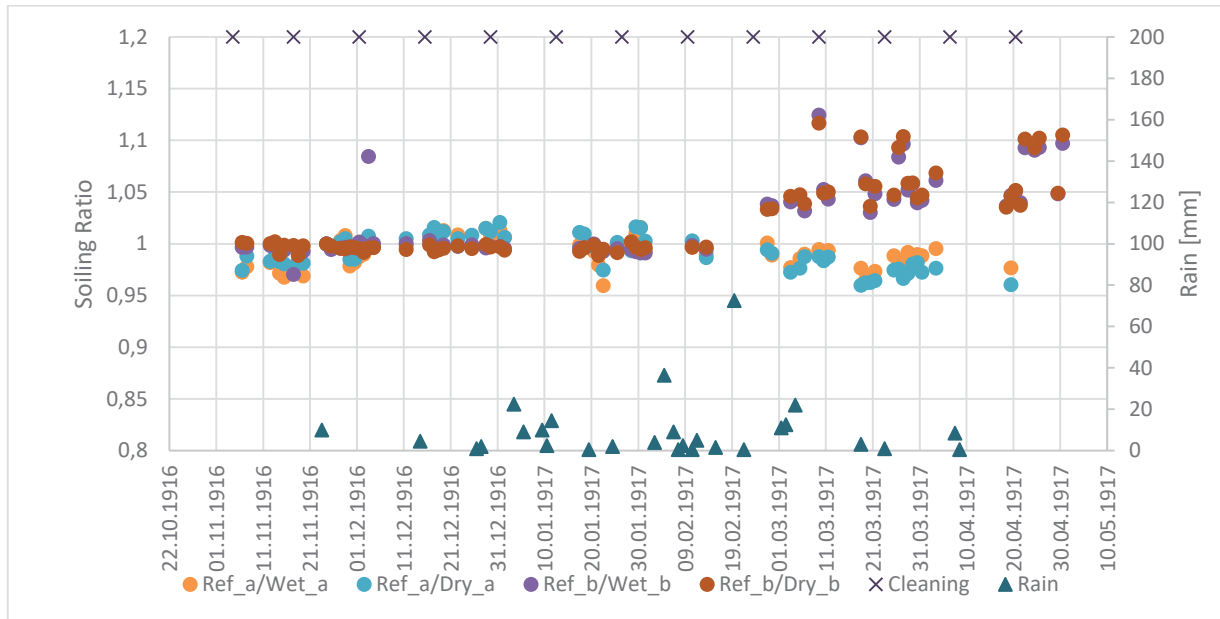


Figure 4-8: Soiling ratios for both anti-soiling treated and untreated thin film modules, plotted with rain days and the biweekly cleanings. Only clear days are used.

### 4.1.3 Data analysis

The periods chosen to investigate further in chapters 4.1.1 and 4.1.2 were analyzed to identify possible soiling. First, the silicon modules are considered, then the thin film modules.

#### 4.1.3.1 Silicon modules

In Figure 4-9 the trends in yield ratios of the modules with anti-soiling treatment are compared to identify soiling as a source of power loss. The equations (see figure) for the trend lines seems approximately identical. When soiling is significantly present, with the assumption that the clean modules (Wet\_a and Dry\_a) are completely clean during the whole period, the expectation would be that the reference module (Ref\_a) would decline relative to the clean modules (Wet\_a and Dry\_a).

The similar trends of both reference and clean modules could mean that soiling is not present, and the slight declination is due to other uncertainties, i.e. irradiance dependency. Another explanation is that the clean modules are in fact not clean, and soiling influences both reference and clean modules alike. During this period, the Wet\_a and Dry\_a are cleaned twice, and soiling could be happening between the cleanings. This can explain the similar trends, however the two clear days (November 18<sup>th</sup> and 19<sup>th</sup>) after

the last cleaning (November 17<sup>th</sup>) do not show increase in yield ratio for the cleaned modules. Thus, this trend analysis could not quantify any soiling or accumulation rate.

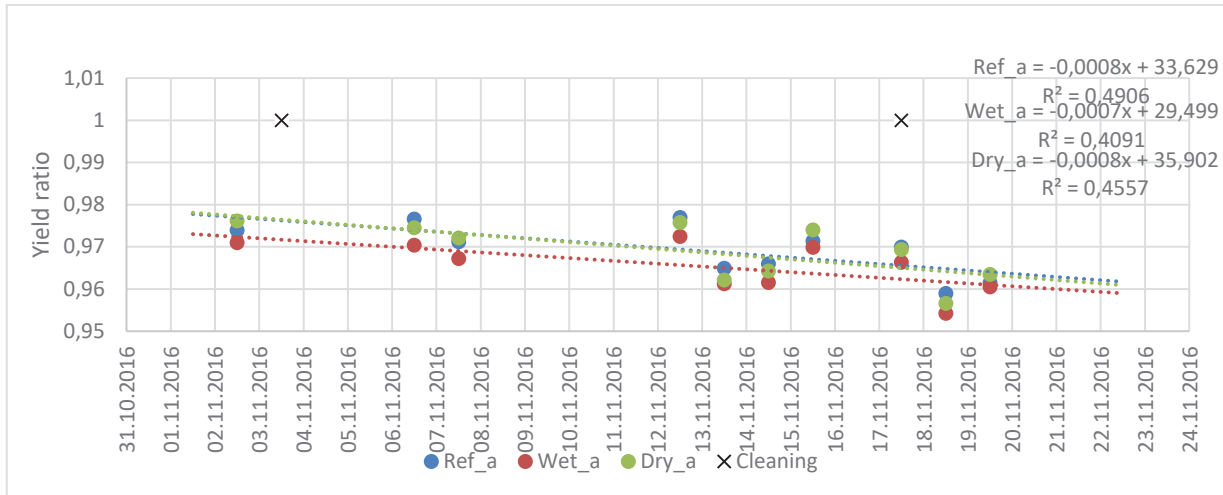


Figure 4-9: Trend lines for anti-soiling treated reference modules compared to clean modules from Nov. 1<sup>st</sup> to Nov. 22<sup>nd</sup>. Only clear days are used.

In Figure 4-10, the untreated modules were analyzed in the same fashion. The results approximately the same as the anti-soiling treated modules.

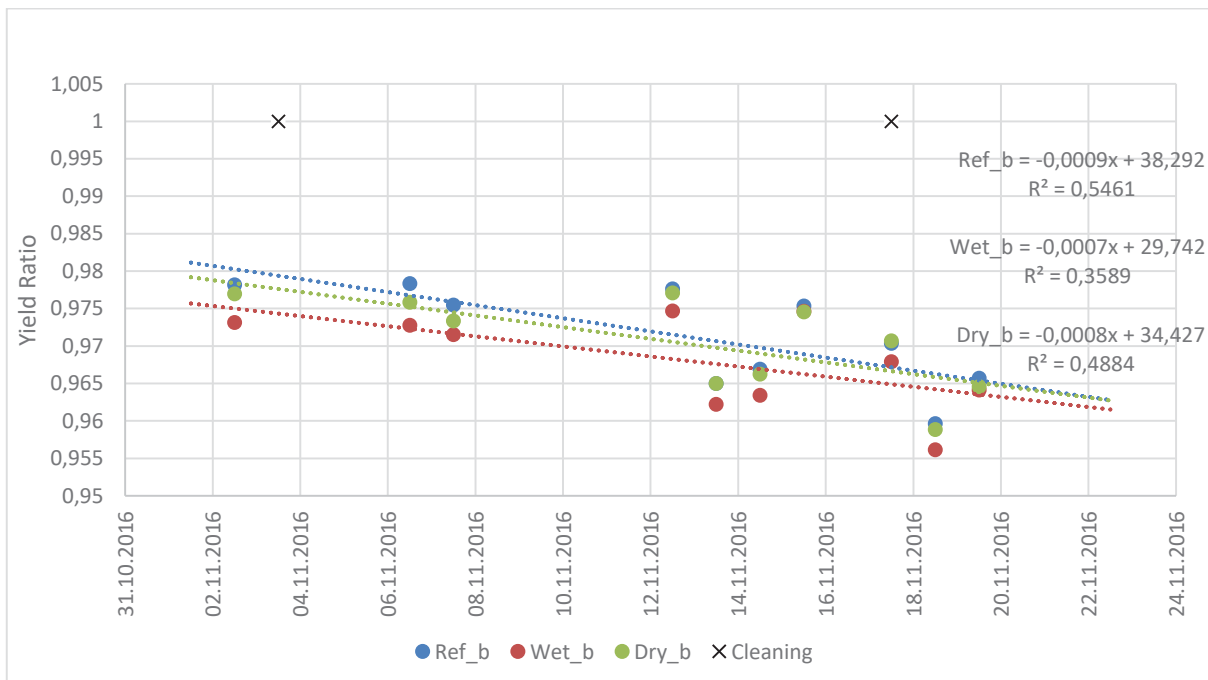


Figure 4-10: Trend lines for the untreated silicon modules. Ref\_b is the uncleaned modules, Wet\_b and Dry\_b are the cleaned modules.

The calculated soiling losses from the soiling ratio method is presented in Table 4-4. All soiling ratios have the value of 1. No soiling was detected during this period.

*Table 4-4: Soiling ratios averaged from Nov 1<sup>st</sup> to 22<sup>nd</sup>.*

	Ref_a/Wet_a	Ref_a/Dry_a	Ref_a/(Wet+Dry)	Ref_b/Wet_b	Ref_b/Dry_b	Ref_b/(Wet+Dry)
<b>Soiling ratio</b>	1,00	1,00	1,00	1,00	1,00	1,00
<b>Loss</b>	0 %	0 %	0 %	0 %	0 %	0 %

In Table 4-5, the average monthly soiling ratios of the reference modules over both wet and dry cleaned modules are displayed along with standard errors indicating the uncertainty. No soiling on the silicon modules was identified during the entire period from November to April.

*Table 4-5: Monthly average soiling ratios for the silicon modules.  
The ratios are of the reference modules over cleaned modules,  
regardless of cleaning method. Ref\_avg is the average of Ref\_a and Ref\_b*

	Ref_a/ (Wet+Dry)_a	Std. Error	Ref_b/ (Wet+Dry)_b	Std. Error	Ref_avg
<b>Nov</b>	1,002	±0,003	1,0025	±0,0005	1,00
<b>Dec</b>	1,003	±0,004	1,003	±0,002	1,00
<b>Jan</b>	1,003	±0,004	1,002	±0,002	1,00
<b>Feb</b>	1,010	±0,009	1,004	±0,001	1,01
<b>Mar</b>	1,002	±0,003	1,0011	±0,0006	1,00
<b>Apr</b>	1,001	±0,003	0,999	±0,001	1,00

#### 4.1.3.2 Thin film modules

The CdTe thin film modules were analyzed over the same period as the silicon modules, from November 1<sup>st</sup> to 22<sup>nd</sup>. In Figure 4-11, the trend line of the uncleaned reference is approximately parallel to the cleaned modules. Only a slight difference with respect to the water cleaned modules was seen. No apparent increase in yield of the cleaned modules was seen after the second cleaning. This analysis could not identify any soiling loss.

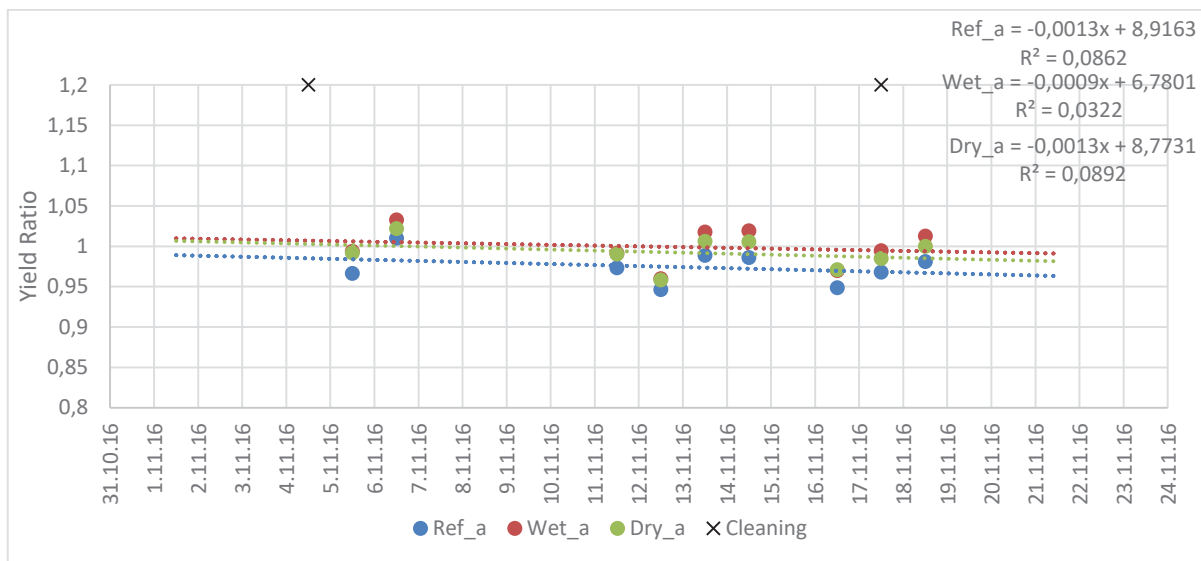


Figure 4-11: Trend lines for the yield ratios of the anti-soiling treated CdTe modules. Ref\_a is the uncleaned, Wet\_a and Dry\_a are wet and dry cleaned respectively.

In Figure 4-12, the untreated modules were analyzed. The trends of the yields are slightly less parallel than the anti-soiling treated modules, and as well a somewhat higher rate of reduction. However, the small number of measurements adds uncertainty, and these results do not stand well on their own.

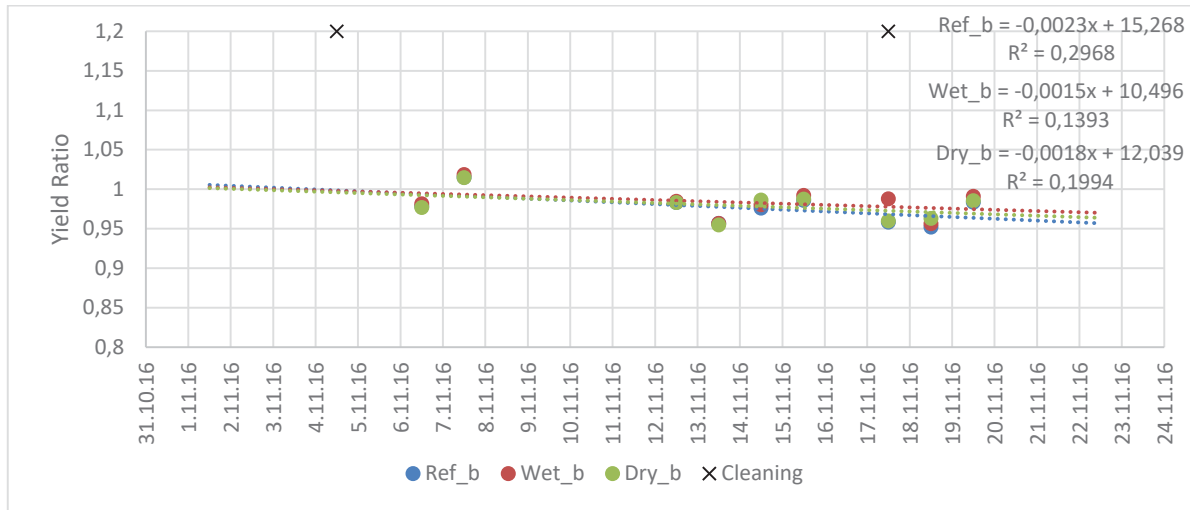


Figure 4-12: Trend lines for the yield ratios of the untreated CdTe modules. Ref\_b is the uncleaned, Wet\_b and Dry\_b are wet and dry cleaned respectively.

In Table 4-6, 1<sup>st</sup> to 22<sup>nd</sup> of November was analyzed by using the average soiling ratio over the period. The soiling on the anti-soiling treated modules were more attenuated than the untreated modules.

Table 4-6: Soiling ratios for the thin film modules averaged over the period from 1<sup>st</sup> to 22<sup>nd</sup> of November 2016.

	Ref_a/Wet_a	Ref_a/Wet_a	Ref_a/(Wet+Dry)	Ref_b/Wet_b	Ref_b/Dry_b	Ref_b/(Wet+Dry)
<b>Soiling ratio</b>	0,98	0,98	0,98	0,99	1,00	1,00
<b>Loss</b>	2 %	2 %	2 %	1 %	0 %	0 %

In table 4-7, the monthly averaged soiling ratios are summarized. From March to April there were some problems with missing data and few clear days. In April, Ref\_a modules (marked with red) had only two days of measurements, and this adds considerable uncertainty to the calculated soiling ratio that month. The standard errors indicate the uncertainty of the calculated soiling ratios. The uncertainty for the Ref\_a soiling ratio in April is 1%, larger by a factor of 2.5 or more compared with the other months. The uncertainties of the Ref\_b soiling ratios were also considerably larger from February to April, than the months before. This corresponds in time with the high values (more than 1) from Figure 4-8.

Table 4-7: Average monthly soiling ratios for the thin film modules. The ratio marked red consists of only two days of measurements because of missing data combined with few clear days. The anti-soiling treated modules have more soiling losses than the untreated modules. Errors represent the uncertainties of the calculations of the average soiling ratios of Ref\_a and Ref\_b respectively. Ref\_avg is the average of Ref\_a and Ref\_b

	Ref_a/ (Wet+Dry)_a	Std. Error	Ref_b/ (Wet+Dry)_b	Std. Error	Ref_avg
<b>Nov</b>	0,985	±0,003	0,996	±0,001	0,99
<b>Dec</b>	1,005	±0,002	1,000	±0,003	1,00
<b>Jan</b>	0,998	±0,004	0,995	±0,001	1,00
<b>Feb</b>	0,994	±0,003	1,02	±0,01	1,01
<b>Mar</b>	0,979	±0,002	1,060	±0,006	1,02
<b>Apr</b>	0,98	±0,01	1,07	±0,01	1,02

## 4.2 Dust Sample Analysis

### 4.2.1 Image analysis

Sample grayscale images 1, 2 and 5 (Figure 4-13) had the same resolution, magnified 30 times, and were analyzed together and parameterized by using the Krumbein Phi-scale  $\phi = -\log_2 \left( \frac{D}{D_0} \right)$ . The most frequent size interval was  $\phi = [6, 7], (8 - 16\mu\text{m})$  (Figure 4-14).

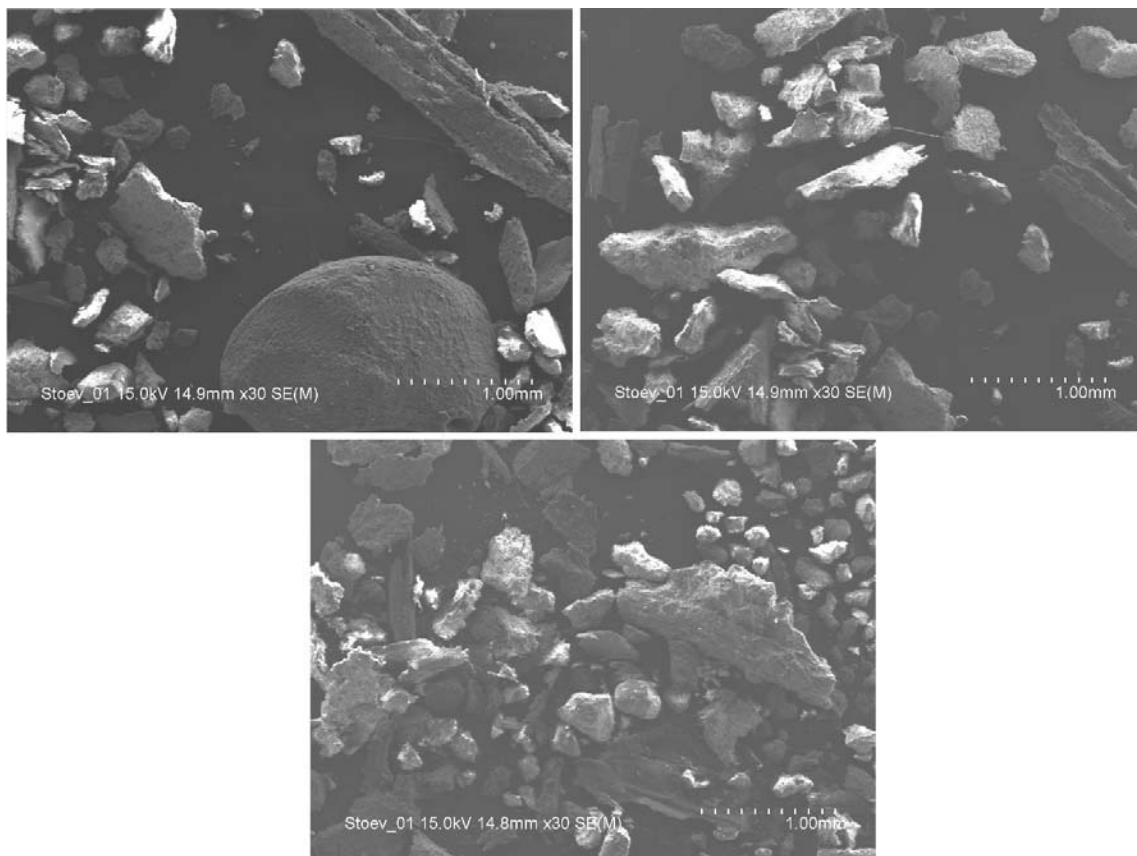


*Figure 4-13: Sample image 1, 2 and 5 magnified 30 times.*

Many of the particles are partially covering other ones, or so close that the ImageJ software may treat two or more particles as one. To overcome this issue, some of the particles had to be separated by outlining the particles manually, by means of altering the image. To reduce the bias risk from such an exercise, only the most obvious cases were altered. Since the number of counts vastly outnumber the altered particles, the bias effect should be minimal.

For each image analysis, a visual inspection of the automatically outlined particles were done to make sure the software calculations were as accurate as possible.



In the gray background area of the images, there were many fine particles which are not clearly visible. These particles were detected by the software when the contrast was enhanced.

Partial particles in the boundary region were not counted.

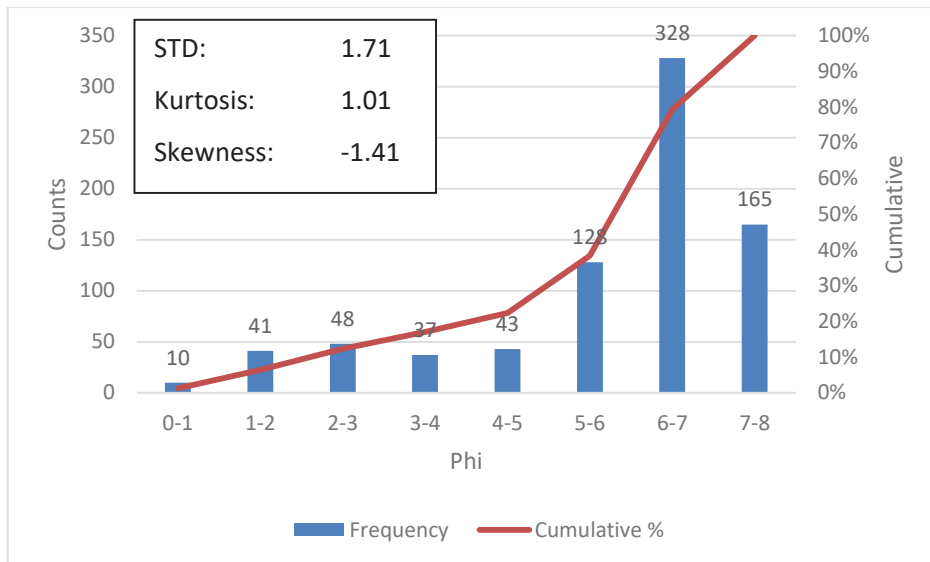


Figure 4-14: Size distribution from the sample images 1, 2 and 5.

Sample image 6 (Figure 4-15 and Figure 4-16) was magnified 250 times and showed the most frequent size in  $\phi = [7, 8]$ , ( $4 - 8\mu\text{m}$ ).

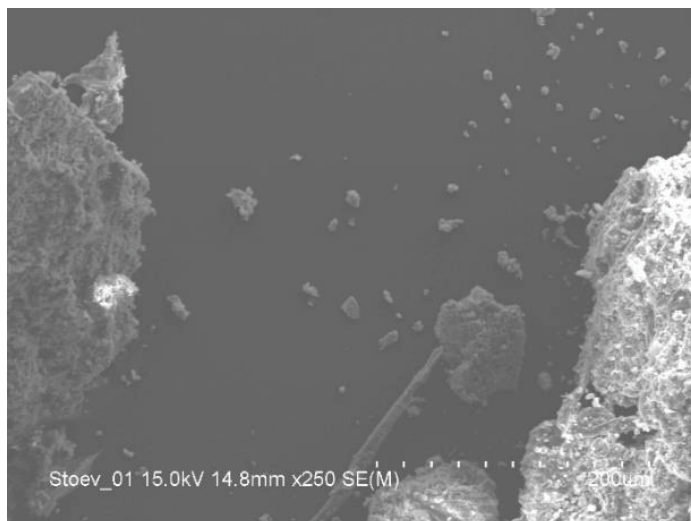


Figure 4-15: Sample image 6, magnified 250 times.

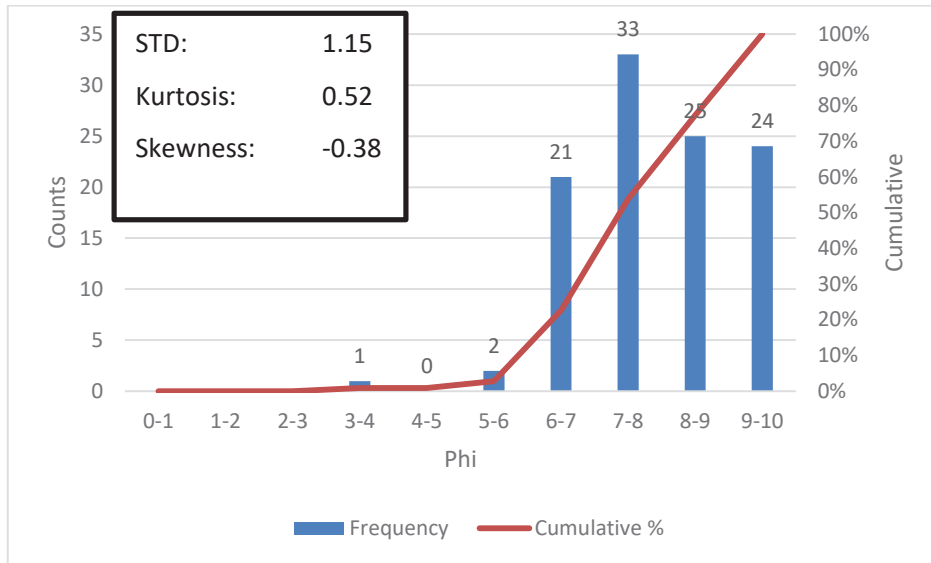


Figure 4-16: Size distribution from sample image 6

Sample image 7 (figure 4-5) was magnified 1500 times, and figure 4-6 shows that the most frequent size was  $\phi = [8, 9]$ , ( $2 - 4\mu\text{m}$ ).

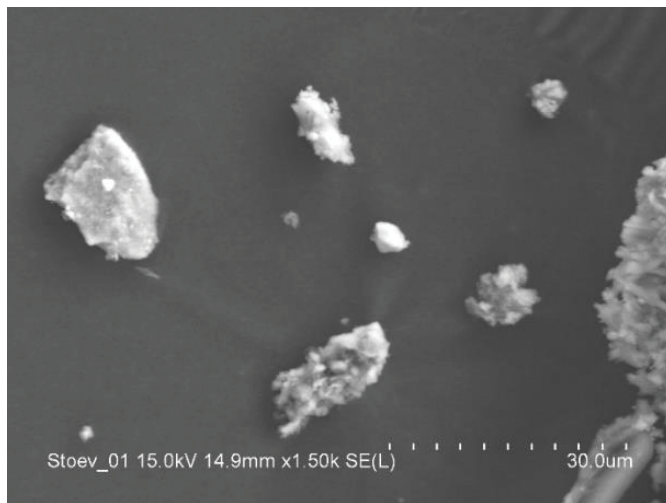


Figure 4-17: Sample image 7 magnified 1500 times.

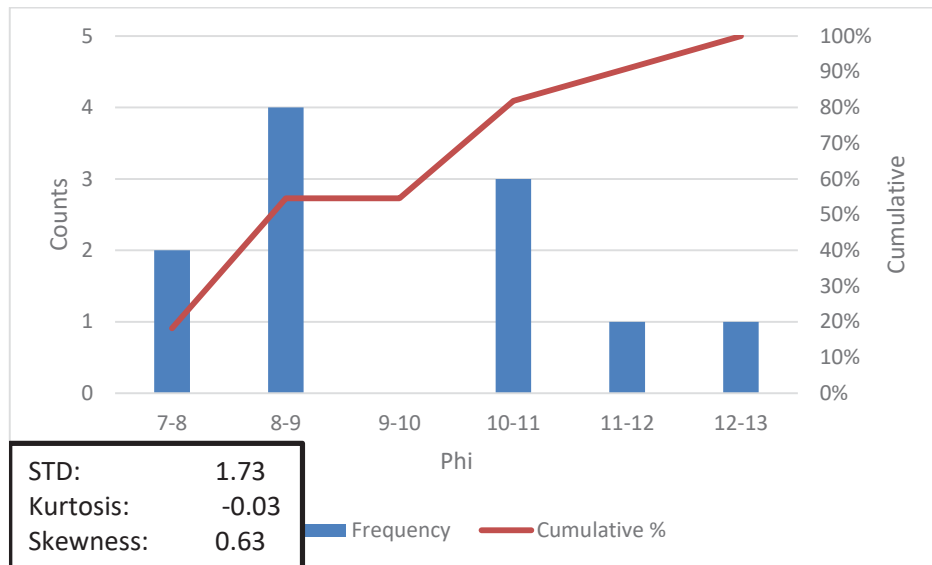


Figure 4-18: Size distribution of sample image 7. (Only 11 counts)

#### 4.2.2 Particle distribution

The entire population of measurements was analyzed to find descriptive statistics. A summary of the analysis is shown in Table 4-8. The mode is the most frequent size, 6.5 $\mu$ m, and is classified as silt according to Table 2-1.

Table 4-8: Descriptive statistics for the population based on the particle diameter.

<b>Descriptive Statistics</b>	
	[ $\mu$ m]
<b>Average</b>	47.5
<b>Standard Error</b>	3.8
<b>Median</b>	11.8
<b>Mode</b>	6.5
<b>St. Dev.</b>	116.2
<b>Variance</b>	13499.9
<b>Kurtosis</b>	61.6
<b>Skewness</b>	6.2
<b>Range</b>	1723.9
<b>Min</b>	0.3
<b>Max</b>	1724.1
<b>Sum</b>	43593.8
<b>Counts</b>	917

The average diameter can say something about the average attenuation from the average particle if this population is representative to the dust particles that settle on the surface. However, it is likely that the larger particles will not settle on the tilted solar panels, and roll or bounce off on impact. While the average diameter is influenced by the extreme values of the measurements, the mode and median is not. The range of the population is quite large compared to both mode and median, and thus is the average greatly influenced by the largest particles. Thus, the mode and median particles should be more representative to the average attenuation from a typical particle that settles on the surface.

The mode is the most frequent particle diameter, found in Table 4-8 to be 6.5μm. For the mode, the marginal attenuation, number of particles that lead to 50% attenuation and the attenuation from 100,000 particles per cm<sup>2</sup> was calculated with equation 20:

$$\tau_{b,mode} = 1 - 2 * N * \pi * \left( \frac{0.00065[cm]}{2} \right)^2 = 1 - N * 6.64 * \frac{10^{-7}}{cm^2}$$

For  $\tau_{b,mode} = 0.5$ :

$$N = \frac{0.5}{6.64 * 10^{-7}} = \frac{753396.2}{cm^2}$$

For  $N = 100,000$ :

$$\tau_{b,mode} = 1 - 100000 * 6.64 * \frac{10^{-7}}{cm^2}$$

$$\tau_{b,mode} = 1 - 0.066/cm^2$$

This amounts to 6.6% attenuation by 100,000 particles per cm<sup>2</sup>.

The median from Table 4-8 represents the middle-sized particle, and the same calculation was made for the median:

$$\tau_{b,median} = 1 - 2 * N * \pi * \left( \frac{0.00118[cm]}{2} \right)^2 = 1 - N * 2.19 * \frac{10^{-6}}{cm^2}$$

For  $\tau_{b,median} = 0.5$ :

$$N = \frac{0.5}{2.19 * 10^{-6}} = \frac{228605.2}{cm^2}$$

For  $N = 100,000$ :

$$\tau_{b,median} = 1 - 100000 * 2.19 * \frac{10^{-6}}{cm^2}$$

$$\tau_{b,median} = 1 - 0.219/cm^2$$

The median particle attenuates 21.9% per 100,000 particles per  $\text{cm}^2$ .

The number of particles until the nonlinearity begins, mentioned in chapter 2.4.2, is when  $\tau_b = 0.5$  (Attenuation = 50%).

The transmittance as a function of number of particles is presented as a graph in Figure 4-19 for the mode and median. When  $\tau_b < 50\%$  the graph will change from linear to exponential ( $e^{-x}$ ) and eventually flat out when  $\tau_b \rightarrow 0$ , according to Al-Hasan (1998).

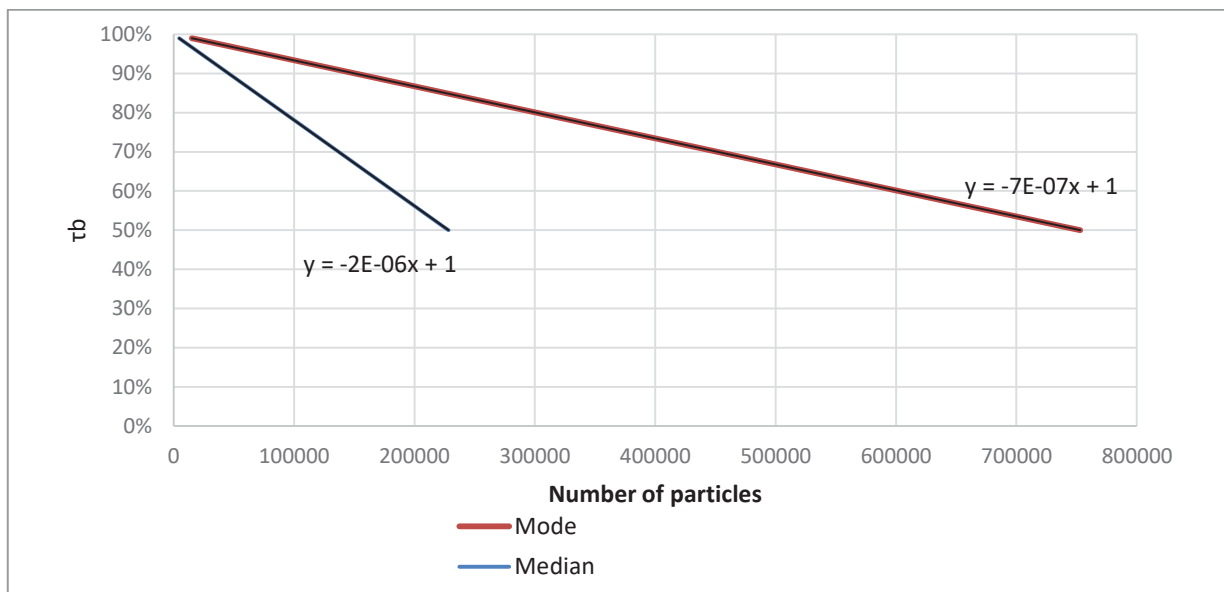


Figure 4-19: Transmittance as a function of number of the mode and median particle size, per  $\text{cm}^2$ .

#### 4.2.3 Soil composition

The point analyses (Figure 4-20) revealed the nature of the particles as carbon based. All measurements had a considerable percentage of Carbon (Figure 4-21), which indicates that the dust is mainly organic. Oxygen, Sodium and Silicon were the other significant elements. The presence of Sodium indicates presence of salts, and Silicon is an important part of silica or quartz ( $\text{SiO}_2$ ) which is commonly found in sand.

Full scale counts: 2487

Stoev-01(2)\_pt1

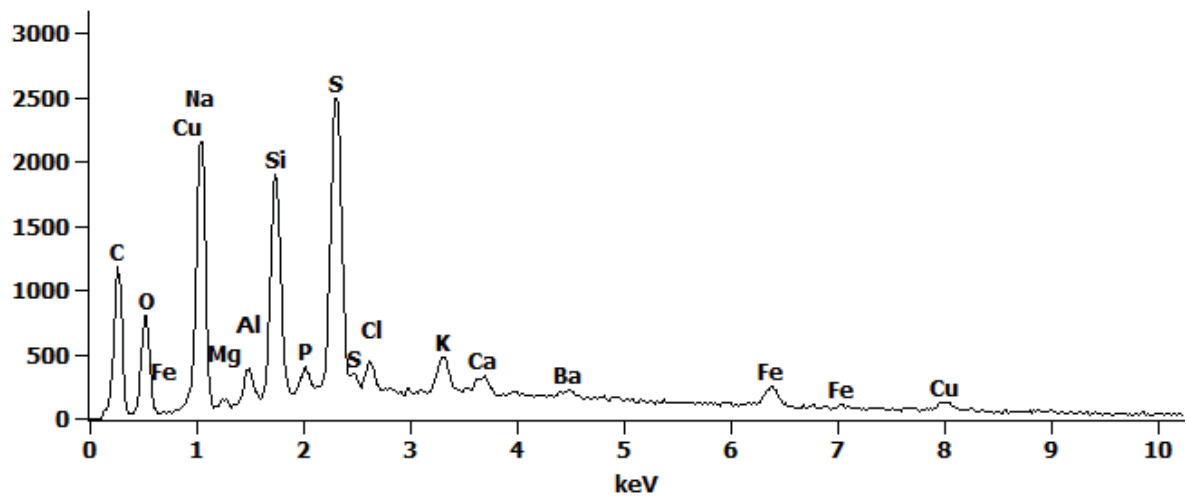


Figure 4-20: Example of one of the point analyses. The vertical size of the spikes does not indicate amount, but presence of the element. The SEM/EDS software calculates the amount.

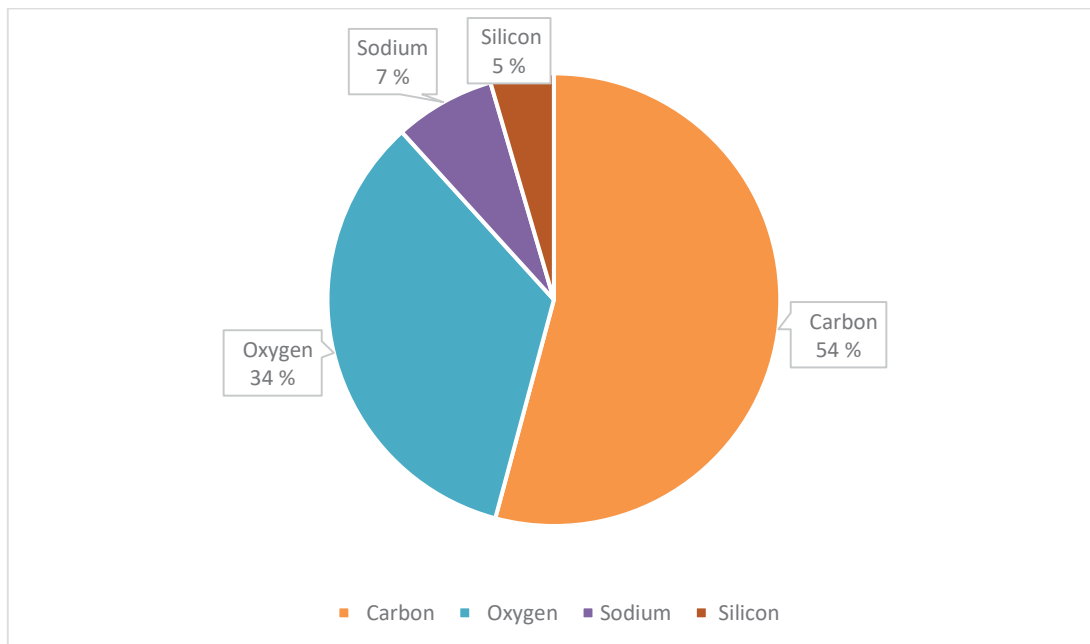
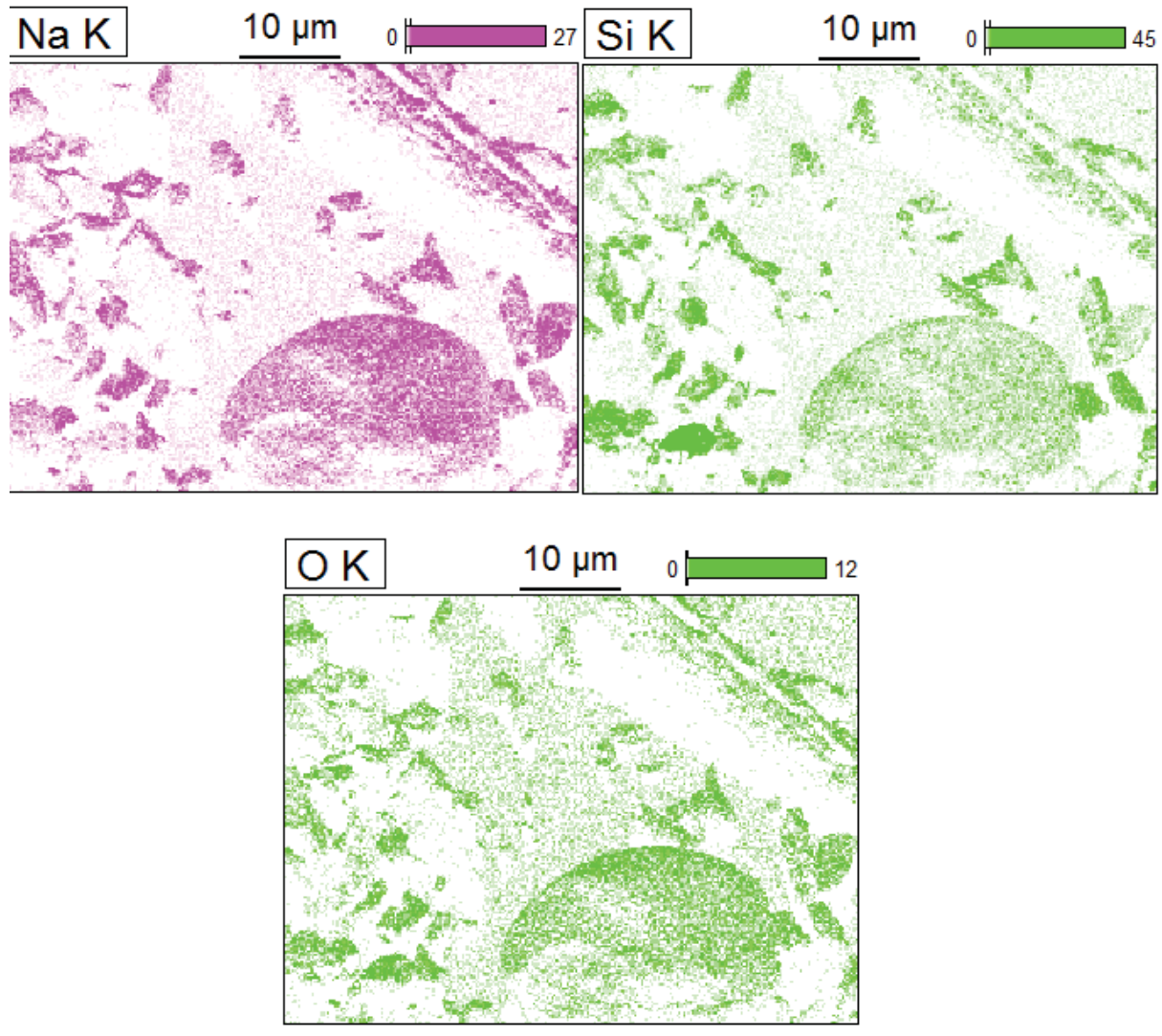


Figure 4-21: The atomic distribution of elements measured in the point analyses of the dust sample. All elements measured with less than 2% presence or less was disregarded. The SEM/EDS cannot detect lighter elements, for instance Hydrogen.

In Figure 4-22, a sample of the mapping images is presented. The parts with higher contrast indicates higher certainty of presence of the respective element. As in the point analyses, Sodium, Silicon and Oxygen is present. Other mapping images were lacking the clear contrasts, and are found in appendix C.



*Figure 4-22: The mapping images highlight the presence of the element (here Sodium, Silicon and Oxygen) with color. Higher contrast means more likely presence. Both Sodium and Silicon have high contrast parts of their respective images.*

## 4.3 Cleaning schedule

### 4.3.1 Model inputs

The monthly electricity production per module was calculated by converting the 10-minute intervallic maximum power points ( $P_{MPP}$ ) into kWh. The  $P_{MPP}$ -values were acquired by using the ivfit-software through MATLAB, using the two-diode method described in chapter 3.2.2. Some missing data, further discussed in chapter 5.1.1, was compensated for by extrapolating from the average daily electricity production in the respective month.

The soiling ratios and production data from the period outside of the of this thesis was given by Mari Øgaard (Øgaard 2016), who wrote her thesis on the previous period.

### 4.3.2 Without Feed-in-Tariff

The electricity prices in this run of the model follow the market prices. Table 4-9 is how the input sheet looks like with the calculated prices from Table 3-6.

*Table 4-9: The input sheet of the cleaning schedule model. Electricity prices are market prices.*

	Silicon modules		CdTe modules		Electricity price [ZARc/kWh]
	Soiling ratio	Production per Module [kWh]	Soiling ratio	Production per Module [kWh]	
Jan	1,000	46,1	1	13,5	58
Feb	1,000	38,1	1	11,3	58
Mar	1,000	48,1	1	14,5	58
Apr	1,000	47,0	1	10,8	58
May	1,000	39,5	1	15,2	58
Jun	0,990	37,7	0,97	14,5	79
Jul	0,985	40,7	0,965	15,6	79
Aug	1,000	46,3	1	18,0	79
Sep	1,000	47,3	1	18,6	58
Oct	1,000	51,0	1	20,5	58
Nov	1,000	47,9	0,99	14,0	58
Dec	1,000	47,6	1	14,3	58

Table 4-10 shows the results for the silicon modules, and Table 4-11 for thin film modules, with market prices. No cleaning action was triggered for either the silicon or thin film modules with these prices.



Table 4-10: Results with market prices on electricity for the silicon modules.

	Silicon modules			
	Soiling loss [%]	Cleaning	Energy loss per module [kWh]	Cost of soiling loss [ZAR]
Jan	0,0 %	0	0,00	0,00
Feb	0,0 %	0	0,00	0,00
Mar	0,0 %	0	0,00	0,00
Apr	0,0 %	0	0,00	0,00
May	0,0 %	0	0,00	0,00
Jun	1,0 %	0	0,38	0,30
Jul	1,5 %	0	0,61	0,48
Aug	0,0 %	0	0,00	0,00
Sep	0,0 %	0	0,00	0,00
Oct	0,0 %	0	0,00	0,00
Nov	0,0 %	0	0,00	0,00
Dec	0,0 %	0	0,00	0,00

Table 4-11: Results for the thin film modules with market prices. No cleaning action is triggered.

	CdTe modules			
Period [Month]	Soiling loss	Cleaning	Energy loss per module	Cost of soiling loss [ZAR]
Jan	0,0 %	0	0,00	0,00
Feb	0,0 %	0	0,00	0,00
Mar	0,0 %	0	0,00	0,00
Apr	0,0 %	0	0,00	0,00
May	0,0 %	0	0,00	0,00
June	3,0 %	0	0,43	0,34
July	3,5 %	0	0,55	0,43
Aug	0,0 %	0	0,00	0,00
Sep	0,0 %	0	0,00	0,00
Oct	0,0 %	0	0,00	0,00
Nov	1,0 %	0	0,14	0,08
Dec	0,0 %	0	0,00	0,00

Table 4-12 shows the calculated soiling ratios needed to trigger cleaning action for the silicon modules in the model with market prices. The values were calculated by the “what if” tool in excel by changing the soiling ratio to equalize the cost of soiling with cost of cleaning. Much more soiling is needed to make cleaning economically viable with these electricity prices.

*Table 4-12: Soiling ratios needed to trigger cleaning action in the model.*

	Soiling ratio	Production per Module [kWh]
Jan	0,940	46,1
Feb	0,928	38,1
Mar	0,943	48,1
Apr	0,942	47,0
May	0,931	39,5
Jun	0,947	37,7
Jul	0,951	40,7
Aug	0,957	46,3
Sep	0,942	47,3
Oct	0,946	51,0
Nov	0,943	47,9
Dec	0,942	47,6

Table 4-13 shows the soiling ratios needed to trigger cleaning action in the model. The low powered thin film modules have a higher marginal cost of cleaning per watt than the silicon modules, thus more soiling is needed to make it economically viable to clean.

*Table 4-13: Soiling ratios for the thin film modules needed to trigger cleaning action in the model.*

	Soiling ratio	Production per Module [kWh]
Jan	0,796	13,5
Feb	0,757	11,3
Mar	0,811	14,5
Apr	0,746	10,8
May	0,819	15,2
June	0,861	14,5
July	0,871	15,6
Aug	0,888	18,0
Sep	0,853	18,6
Oct	0,866	20,5
Nov	0,804	14,0
Dec	0,808	14,3

The “what if” tool was then used to find the electricity prices needed to equalize cost of soiling and cost of cleaning in June and July with (Table 4-14).

*Table 4-14: Electricity prices needed to trigger cleaning action with the actual soiling losses in June and July.*

Period [Month]	Electricity price [ZAR c/kWh]	Soiling loss [%]	Cost of soiling loss [ZAR]
June	421,34	1,0 %	1,59
July	260,50	1,5 %	1,59

#### 4.3.3 With Feed-in-Tariff

The model was then run with the flat FiT for the entire year. The months with highest production will have the highest relative cost of soiling. This means that in the winter months (June-August), where production is at its lowest considering insolation, the soiling ratio must be lower (more soiling) to trigger cleaning in the model. The inputs are summarized in Table 4-15.

*Table 4-15: The input sheet of the cleaning schedule model with inputs. The electricity price is 2.76 ZAR.*

	Silicon modules		CdTe modules		Electricity price [ZARc/kWh]
	Soiling ratio	Production per Module [kWh]	Soiling ratio	Production per Module [kWh]	
Jan	1,000	46,1	1	13,5	276
Feb	1,000	38,1	1	11,3	276
Mar	1,000	48,1	1	14,5	276
Apr	1,000	47,0	1	10,8	276
May	1,000	39,5	1	15,2	276
Jun	0,990	37,7	0,97	14,5	276
Jul	0,985	40,7	0,965	15,6	276
Aug	1,000	46,3	1	18,0	276
Sep	1,000	47,3	1	18,6	276
Oct	1,000	51,0	1	20,5	276
Nov	1,000	47,9	0,99	14,0	276
Dec	1,000	47,6	1	14,3	276

The output of the model for the Silicon modules is presented in Table 4-16. One cleaning, in July, is economically viable according to the input values and the assumption that this cleaning eliminates all soiling loss for that month. The other month with a soiling ratio less than 1, June, was too small loss to overcome the marginal cost of cleaning.

*Table 4-16: Output of the cleaning schedule model given input values from Table 4-15. The threshold for cleaning is a soiling loss between 1 and 2%, and only one cleaning is economically viable.*

	Silicon modules			
	Soiling loss [%]	Cleaning [1=Yes, 0=No]	Energy loss per module [kWh]	Cost of soiling loss [ZAR/module]
Jan	0,0 %	0	0,00	0,00
Feb	0,0 %	0	0,00	0,00
Mar	0,0 %	0	0,00	0,00
Apr	0,0 %	0	0,00	0,00
May	0,0 %	0	0,00	0,00
Jun	1,0 %	0	0,38	1,04
Jul	1,5 %	1	0,61	0,00
Aug	0,0 %	0	0,00	0,00
Sep	0,0 %	0	0,00	0,00
Oct	0,0 %	0	0,00	0,00
Nov	0,0 %	0	0,00	0,00
Dec	0,0 %	0	0,00	0,00
	Sum	1	0,99	1,04

In Table 4-17, the output for the thin film modules are presented. The soiling ratios did not trigger cleaning action in the model. More than 3.5% soiling loss is required in July to trigger cleaning.

*Table 4-17: Output of the cleaning schedule model given input values from Table 4-15 for the thin film modules. The threshold for cleaning is more than 3.5% in July, and no cleaning action is triggered.*

	CdTe thin film modules			
Period [Month]	Soiling loss	Cleaning	Energy loss per module [kWh]	Cost of soiling loss [ZAR]
Jan	0,0 %	0	0,00	0,00
Feb	0,0 %	0	0,00	0,00
Mar	0,0 %	0	0,00	0,00
Apr	0,0 %	0	0,00	0,00
May	0,0 %	0	0,00	0,00
June	3,0 %	0	0,43	1,20
July	3,5 %	0	0,55	1,51
Aug	0,0 %	0	0,00	0,00
Sep	0,0 %	0	0,00	0,00
Oct	0,0 %	0	0,00	0,00
Nov	1,0 %	0	0,17	0,39
Dec	0,0 %	0	0,00	0,00

By using the “What if” tool in excel, the soiling ratios were altered to make cost of soiling equal cost of cleaning. The results for the silicon modules are summarized in Table 4-18. For every month, the boundary soiling ratio is between 0.98-0.99. When production is low, more soiling is required to trigger cleaning action in the model.

*Table 4-18: Soiling ratios needed to trigger cleaning for every month of the year*

Silicon modules		
	Soiling ratio	Production per Module [kWh]
Jan	0,987	46,1
Feb	0,985	38,1
Mar	0,988	48,1
Apr	0,988	47,0
May	0,985	39,5
Jun	0,985	37,7
Jul	0,986	40,7
Aug	0,988	46,3
Sep	0,988	47,3
Oct	0,989	51,0
Nov	0,988	47,9
Dec	0,988	47,6

In Table 4-19, the soiling ratios for the thin film modules were manipulated to match cost of soiling with cost of cleaning. Since the thin film modules have much lower power than the silicon modules, a lot more soiling is needed to make cleaning economically viable.

Table 4-19: Calculated soiling losses for the thin film modules needed to equalize cost of soiling with cost of cleaning.

CdTe thin film modules

	Soiling Ratio	Production per Module [kWh]
Jan	0,957	13,5
Feb	0,949	11,3
Mar	0,960	14,5
Apr	0,947	10,8
May	0,962	15,2
June	0,960	14,5
July	0,963	15,6
Aug	0,968	18,0
Sep	0,969	18,6
Oct	0,972	20,5
Nov	0,959	14,0
Dec	0,960	14,3

The “what if” tool was then used to find the electricity prices needed to equalize cost of soiling and cost of cleaning in June, July and November for the thin film modules (Table 4-20). The calculated price in July is not far from the FiT.

Table 4-20: Electricity prices needed to equalize cost of cleaning and cost of soiling loss.

Month	Electricity price [ZAR c/kWh]	Soiling loss	Cost of soiling [ZAR]
June	366,37	3,0 %	1,59
July	291,44	3,5 %	1,59
Nov	569,53	2,0 %	1,59



## 5 Discussion

This chapter will discuss the results from the previous chapter in the same order. First the soiling analysis based on I-V data, then the soil composition experiment and last the cleaning schedule.

### 5.1 Soiling analysis of the I-V data from the PV modules

In this section, the results of the I-V analysis will be discussed.

#### 5.1.1 Data corrections

When analyzing the I-V data from the modules, one of the reference modules (Poly2) showed different behavior than the other references (poly1, 15 and 16). This is visualized in Figure 5-1 (Orange line) and Figure 5-2 (red and black lines). It was expected that all lines would follow the same pattern, with only slight differences indicating possible soiling. The deviations were too big, and when only one of the reference groups showed this behavior seen in the two figures, there was reason to believe something was wrong with the data. To correct for the discrepancies, all data from module Poly2 was removed. One could argue that only values that contribute to irregularities should be corrected or removed, however this could lead to bias results.

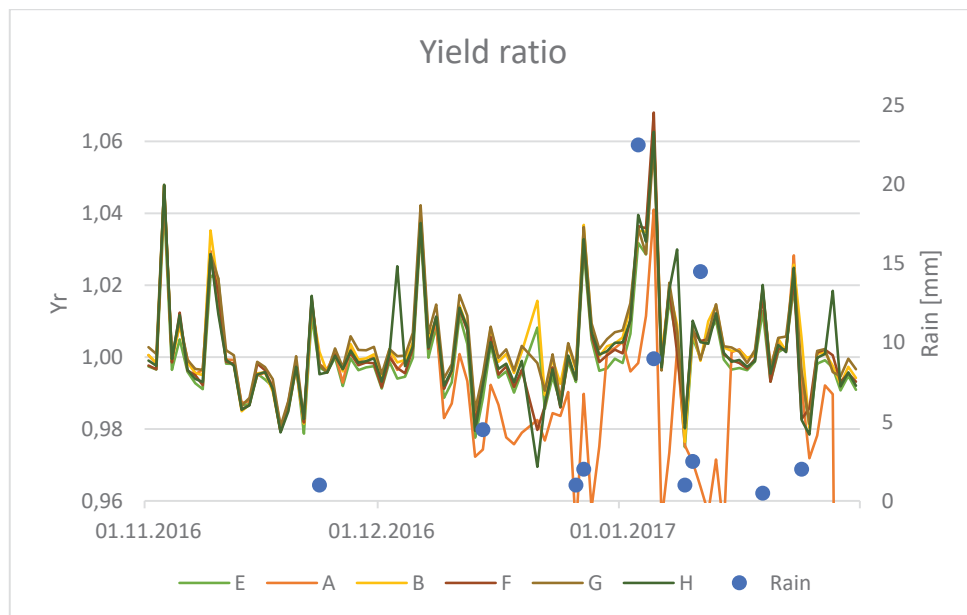


Figure 5-1: Yield ratios of polycrystalline modules from November 2016 to January 2017. A and B are the reference modules, while E and F are wet cleaned and G and H dry cleaned.

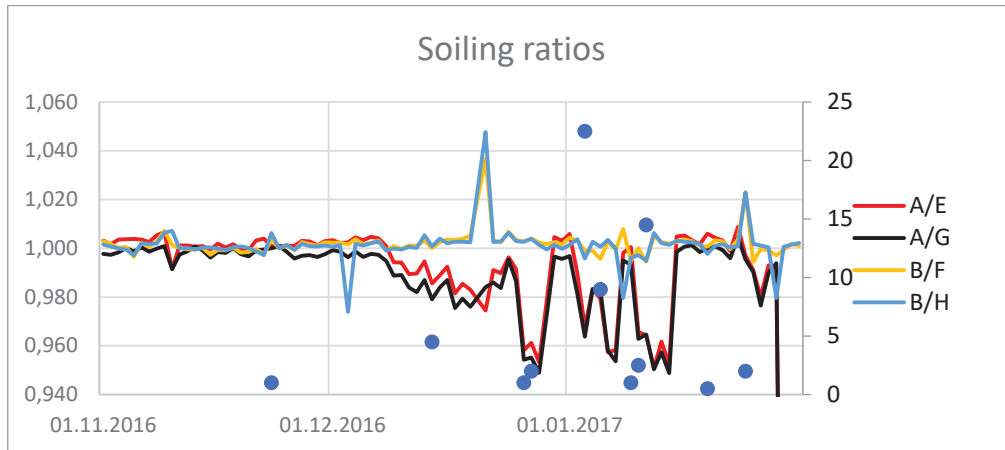


Figure 5-2: Power output ratios visualized as the reference modules (A=Ref\_a, B=Ref\_b, E=Wet\_a, F=Wet\_b, G=Dry\_a, H=Dry\_b) over wet- and dry-cleaned modules respectively in the period from November '16 to January '17.

When the data from Polycrystalline module 2 was removed, all modules seemed to have a similar pattern throughout the period (Figure 4-1 chapter 4.1.1).

To investigate the difference in yield and soiling ratios with and without the second silicon module (Poly2), two correlation tables were made (table 5-1 and 5-2):

Table 5-1: Correlation coefficients between Irradiance and Yield ratios for the polycrystalline modules. Ref\_a show low correlation with the other modules.

	GHI	Ref_a	Ref_b	Wet_a	Wet_b	Dry_a	Dry_b
GHI	1						
Ref_a	-0,24	1					
Ref_b	-0,70	0,30	1				
Wet_a	-0,68	0,30	0,99	1			
Wet_b	-0,71	0,29	0,94	0,96	1		
Dry_a	-0,65	0,30	0,98	0,98	0,97	1	
Dry_b	-0,65	0,30	0,89	0,90	0,95	0,92	1

Table 5-2: Correlation between Irradiance and Yield ratios, corrected for discrepancies from Poly2 module. A correlate much better with the other modules.

	<b>GHI</b>	<b>Ref_a</b>	<b>Ref_b</b>	<b>Wet_a</b>	<b>Wet_b</b>	<b>Dry_a</b>	<b>Dry_b</b>
<b>GHI</b>	1						
<b>Ref_a</b>	-0,69	1					
<b>Ref_b</b>	-0,70	0,95	1				
<b>Wet_a</b>	-0,68	0,96	0,99	1			
<b>Wet_b</b>	-0,71	0,98	0,94	0,96	1		
<b>Dry_a</b>	-0,65	0,97	0,98	0,98	0,97	1	
<b>Dry_b</b>	-0,65	0,94	0,89	0,90	0,95	0,92	1

The data from Poly2 had considerable influence on the calculated power, as seen in the correlations between Ref\_a and the other modules in the second column in table 5-1. When data from Poly2, Ref\_a correlated more with the other modules, as seen in column 2 in table 5-2. The cause of the discrepancy was not identified, but is probably due to defects in the module or problems with the ActiveLoad.

In addition, one other module (Polycrystalline 12) seemed to fail in April. The I-V data ended abruptly, and the deviating measurements were removed from the calculations. The abrupt ending of the I-V data made it easy to identify when the error occurred, thus the bias risk seemed minimal.

Of the Thin film modules, modules 21 and 22 started outputting irregular data from April 20<sup>th</sup>. From that date, the data was not used in any calculations. As mentioned in chapter 4.1.2 to Figure 4-7 and Figure 4-8, thin film modules 17 and 18 showed some fluctuating yield and soiling ratios. These two modules are connected to the same ActiveLoad, and that could be the source of the fluctuations. However, this was not properly identified, and thus not considered here.

The weather station was down two weeks, one in March and one in April. When calculating electricity production (used in the cleaning schedule model) for those months, the production in those periods were extrapolated by taking the daily average of the respective month times number of days the weather station was down. No other extrapolations, i.e. yields or soiling ratios, were made with these two weeks.

### 5.1.2 Irradiance effects on temperature corrections and efficiency

When conducting experiments in a laboratory, the environment can be controlled to eliminate external effects that influence a measurement. This is obviously difficult to achieve outdoors in the real world. The environment will have an impact on every measurement, and the magnitude of the impacts change continuously with the weather.

The yield ratio curves in figures 4-1 and 4-2 are not smooth, with both high and low spikes. In an ideal world, these curves would have been smoother and thus easier to interpret visually. The yield ratios are from calculations corrected for cell temperature (equation 11) effect on the I-V curve (figure 2-13), thus the temperature correction is either slightly inaccurate, or there are other random effects influencing the I-V data. A non-random effect can be due to irradiance dependency of the solar module. According to the data sheet for the poly silicon modules (Appendix A), the coefficient of the efficiency as a linear function of irradiance is  $-0,0005\%/(\text{W}/\text{m}^2)$  in the interval of 600-1000  $\text{W}/\text{m}^2$ . In the interval under 600  $\text{W}/\text{m}^2$ , the function is non-linear. When evaluating this number with real data, the coefficient was four times bigger than the data sheet suggested Figure 5-3.

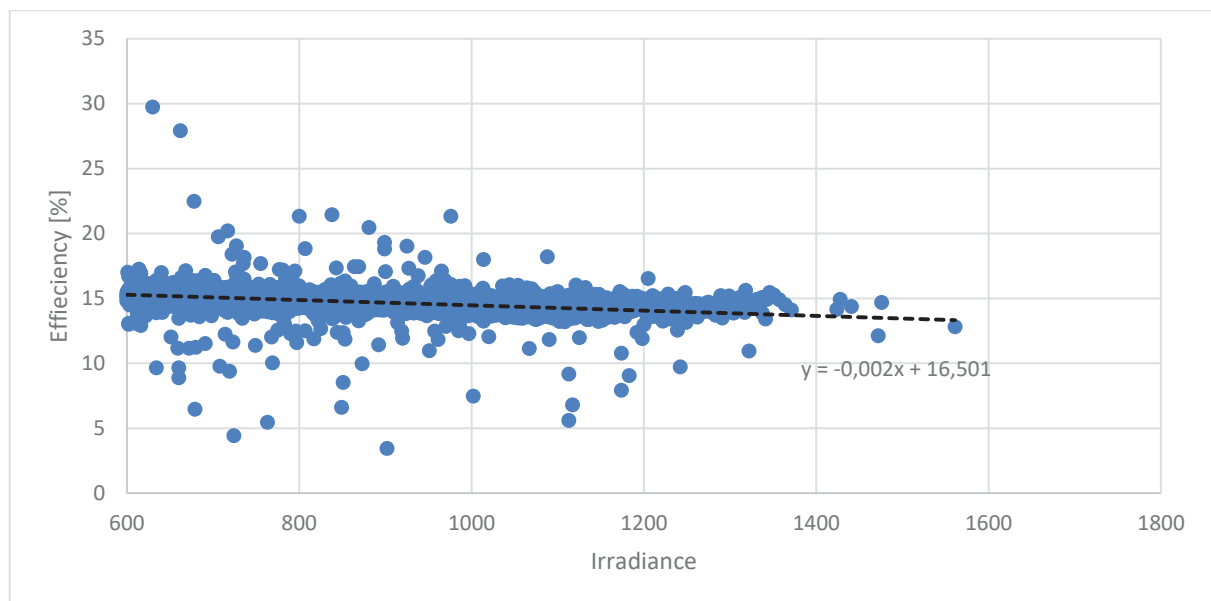


Figure 5-3: Irradiance dependency of Polycrystalline module 3 from November 2016 to April 2017. The equation shows four times steeper slope than what the data sheet suggests.

The pyranometer measures irradiance instantaneous every minute, while the active load measures the I-V values every 10 minutes, also instantaneous. Since one module can be several meters from the

pyranometer, the irradiance at each point can differ. If the irradiance differs much from the pyranometer to the module, the temperature correction (equation 11) will be inaccurate.

The temperature sensor on the back of each module cannot measure the temperature for the whole module, but only at the point of measurement. Cell temperatures of the individual cells are not necessarily the same across the module. This temperature variation can also have an impact of the temperature corrected output.

Thus, the temperature corrected power output is an approximation, and when soiling levels showed to be so small, the power loss from attenuation was difficult to identify when the effect was competing with environmental effects. However, this method is more accurate than using ambient temperature, as the latter is more influenced by the environment.

## **5.2 Dust sample analysis**

When preparing the dust samples, they were coated by the process of carbon evaporation. This process leaves carbon on top of the samples and will interfere with the results of the point analyses. Other uncertainties can also be present in this experiment. Thus, it is important to have this in mind while interpreting the point measurement results. The Kalkbult solar plant is in an arid area, and the dust was expected to consist mostly of mineral, and not organic, compounds. When carbon was present in all point analyses, it raised questions of contamination in either the SEM/EDS measurements or in the sample itself. However, the samples were collected during summer of 2015, and precipitation is not rare, so organic compounds can mix with the mineral sand. The images from the SEM did however not reveal particles with typical resemblance of pollen.

The sample from the dust bucket may not be representative of the dust particles that settles on the module surface. Since the modules are inclined, larger particles will roll off and not adhere to the surface. The sample did however give a general impression of the types of dust present in the area.

## **5.3 Cleaning Schedule**

The cleaning schedule model result with the FiT showed that in July, the marginal cost of soiling loss was larger than the marginal cost of cleaning. This result means that if the cleaning happens before the period starts, and this eliminates all soiling all of July, it is economically viable to clean. The model also assumes that the cleaning is instantaneous for the whole PV plant. This is obviously not a perfect image of the real world, and more assumptions must be made to see if it is economically viable to clean. Since

the whole plant is cleaned over period of 47 days, the first panel to be cleaned will be exposed to soiling for 47 days before it can be cleaned again. Thus, if the soiling level triggers the cleaning schedule model, about one third of the plant will continue to accumulate dust for a whole month before it is cleaned. When considering the average rainfall (Figure 5-4), with 1 day of rain in both June and July, at least one day of rain should statistically occur during the cleaning period. (Veret som var 2017) The economic viability of cleaning is thus questionable when assuming the rain washes most of the soiling away.

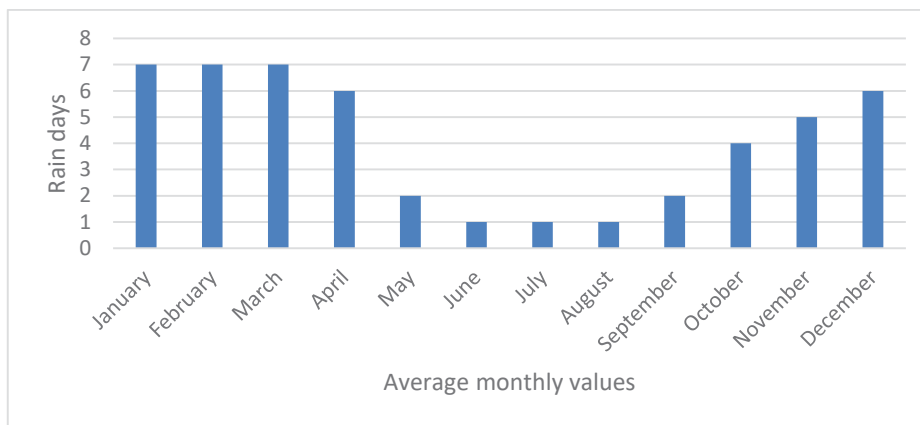


Figure 5-4: 1961-1990 average rain days per month in Kalkbult, South Africa.

If the cleaning is combined with a visual inspection of the modules, the decision to clean or not could be different. An inspection would potentially detect defects like cracks, burn marks from short circuits or other visual defects that could prove to be of value to the power plant operators. The value of inspection would reduce the cleaning cost if the inspection was part of the cleaning procedure. To quantify this value is difficult and would rely on factors specific to the PV plant operator's preferences.

This year of data is not necessarily representative for every year, and in some years soiling can have a bigger impact. However, based on all results and assumptions made in this thesis, it seems unlikely that cleaning becomes economically viable in Kalkbult without adding some form of value to the cleaning process, i.e. inspection.

## 6 Conclusions

Soiling is a serious problem for many solar PV plants, especially in very dry, desert-like environments. The Kalkbult PV plant is in a semi-arid location, with desert like conditions in and around the area. However, the soiling analysis showed very little power loss from soiling in Kalkbult during the summer, here from November to April. The silicon modules had no detectable soiling at all, and the CdTe thin film modules showed only small levels of soiling, where, counterintuitively, the anti-soiling treated modules were more susceptible to soiling than the untreated ones. On average, just 1% soiling loss in November for the thin film modules was observed.

While the expectation regarding the composition of the soil sample was that it would be mineral based, the point analyses showed considerable presence of carbon. In addition, there were Oxygen, Sodium and Silicon present, indicating salts and silica.

The most frequent particle size showed to be  $6.5\mu\text{m}$  in diameter, the attenuation was calculated to be 6.6% for  $N=100,000/\text{cm}^2$ , and 21.9% for the  $11.8\mu\text{m}$  median particle.

Based on the soiling analysis, only July 2016 had enough soiling to match cost of soiling with cost of cleaning. However, since the cleaning procedure lasts for 47 days, soiling will simultaneously occur during cleaning, and the cost effectiveness of cleaning is questionable. Based on the assumptions and calculations in this thesis, cleaning of the panels is not recommended for this site.

## **7 Further inquiries**

- The methods used to detect soiling losses in this thesis were not always able to quantify soiling. A more accurate approach could be to evaluate the solar module parameters in a laboratory by flash testing, both to have a more accurate reference value and to factor in irradiance dependency.
- A more comprehensive soiling analysis considering environmental effects, such as humidity, wind, angle of incidence and dew formation.
- An analysis of glass samples with dust from different periods to get a more representative size distribution of the dust particles, and to evaluate attenuation from different angles of incidence.
- Develop a cleaning schedule model that includes accumulation of soiling while cleaning is taking place. Adding a value to an inspection of the PV plant can reduce the cost of cleaning, and can be considered in a new model.



## 8 References

- Al-Hasan, A. Y. (1998). A new correlation for direct beam solar radiation received by photovoltaic panel with sand dust accumulated on its surface. *Solar Energy*, 63 (5): 323-333.
- Bellini, E. (2017). Global installed PV capacity exceeds 300 GW, IEA PVPS.
- Eberhard, A. (2014). South Africa's Renewable Energy IPP Procurement Program: Success Factors and Lessons: Public-Private Infrastructure Advisory Facility (PPIAF)
- Enbar, N., Weng, D. & Klise, G. T. (2015). Budgeting for Solar PV Plant Operations & Maintenance: Practices and Pricing: Sandia National Laboratories (SNL-NM), Albuquerque, NM (United States).
- Eskom. (2017). *Tariffs & Charges Booklet for 2016/17*. Available at: [http://www.eskom.co.za/CustomerCare/TariffsAndCharges/Documents/2016\\_17%20Draft%20Tariff%20Book%20%20March%202016%20Internet%20ver.pdf](http://www.eskom.co.za/CustomerCare/TariffsAndCharges/Documents/2016_17%20Draft%20Tariff%20Book%20%20March%202016%20Internet%20ver.pdf).
- IFE. (2017). *IFE's Scanning Electron Microscope (SEM)*: Institute for Energy Technology. Available at: [https://www.ife.no/en/ife/departments/materials\\_and\\_corrosion\\_tech/files/sem-specifications](https://www.ife.no/en/ife/departments/materials_and_corrosion_tech/files/sem-specifications) (accessed: 08.03.2017).
- Intergovernmental Panel on Climate Change. Working Group III & Edenhofer, O. (2014). *Climate change 2014 : mitigation of climate change : Working Group III contribution to the Fifth Assessment Report of the Intergovernmental Panel on Climate Change*. New York, NY: Cambridge University Press. xv, 1435 pages pp.
- ISO. (2002). *ISO 14688-1:2002 Geotechnical investigation and testing -- Identification and classification of soil -- Part 1: Identification and description*. <https://www.iso.org/standard/25260.html>.
- King, D. L., Kratochvil, J. A. & Boyson, W. E. (2004). *Photovoltaic array performance model*: United States. Department of Energy.
- Kipp & Zonen. (2017). *SMP10 pyranometer, the smartest way to measure solar radiation - Kipp & Zonen*. Available at: <http://www.kippzonen.com/Product/281/SMP10-Pyranometer#>.
- Luque, A. & Hegedus, S. (2011). *Handbook of photovoltaic science and engineering*. 2nd ed. Chichester, West Sussex, U.K.: Wiley. xxxii, 1132 p. pp.
- Mertens, K. (2013). *Photovoltaics: Fundamentals, Technology and Practice*: John Wiley & Sons.
- MetOne. (2013). *MSO Weather Sensor*: Met One Instruments Inc. Available at: [http://www.metone.com/docs/mso\\_datasheet.pdf](http://www.metone.com/docs/mso_datasheet.pdf).
- NOAA. (2017). *NOAA Solar Calculator*. Available at: <https://www.esrl.noaa.gov/gmd/grad/solcalc/> (accessed: 14.05.2017).
- Phillips, D. S. & Warmuth, W. (2016). ©Fraunhofer ISE: Photovoltaics Report. <http://www.ise.fraunhofer.de/>.
- Prorok, M., Werner, B. & Żdanowicz, T. (2005). Applicability of equivalent diode models to modeling various thin-film photovoltaic (PV) modules in a wide range of temperature and irradiance conditions. *Electron Technology: Internet Journal*, 37 (6): 1-4.
- Qasem, H., Betts, T. R., Mülleijans, H., AlBusairi, H. & Gottschalg, R. (2014). Dust-induced shading on photovoltaic modules. *Progress in Photovoltaics: Research and Applications*, 22 (2): 218-226.
- Sarver, T., Al-Qaraghuli, A. & Kazmerski, L. L. (2013). A comprehensive review of the impact of dust on the use of solar energy: History, investigations, results, literature, and mitigation approaches. *Renewable & Sustainable Energy Reviews*, 22: 698-733.

- Sayyah, A., Horenstein, M. N. & Mazumder, M. K. (2014). Energy yield loss caused by dust deposition on photovoltaic panels. *Solar Energy*, 107: 576-604.
- ScatecSolar. (2017). *Kalkbult, South Africa, 75 MW*. Available at: <http://www.scatecsolar.com/Portfolio/South-Africa/Kalkbult-South-Africa-75-MW>.
- Schindelin, J., Arganda-Carreras, I., Frise, E., Kaynig, V., Longair, M., Pietzsch, T., Preibisch, S., Rueden, C., Saalfeld, S. & Schmid, B. (2012). Fiji: an open-source platform for biological-image analysis. *Nature methods*, 9 (7): 676-682.
- Schmela, M. (2016). *Global Market Outlook: SolarPower Europe*. <http://www.solarpowereurope.org/insights/global-market-outlook/>: SolarPower Europe. Available at: <http://www.solarpowereurope.org/insights/global-market-outlook/>.
- Shockley, W. & Queisser, H. J. (1961). Detailed balance limit of efficiency of p-n junction solar cells. *Journal of applied physics*, 32 (3): 510-519.
- Swapp, S. (2017). *Scanning Electron Microscopy (SEM)*: University of Wyoming. Available at: [http://serc.carleton.edu/research\\_education/geochemsheets/techniques/SEM.html](http://serc.carleton.edu/research_education/geochemsheets/techniques/SEM.html).
- Taylor, B. W. (2013). *Introduction to management science*. 11th ed. Boston: Pearson. xvii, 822 p. pp.
- Veret som var. (2017). Veret som var New Kalkbult, Northern Cape (Sør-Afrika). Available at: [http://www.yr.no/stad/S%C3%B8r-Afrika/Northern\\_Cape/New\\_Kalkbult/statistikk.html](http://www.yr.no/stad/S%C3%B8r-Afrika/Northern_Cape/New_Kalkbult/statistikk.html) (accessed: 09.05.2017).
- Whaley, C. (2016). *Best Practices in Photovoltaic System Operations and Maintenance*: NREL (National Renewable Energy Laboratory (NREL), Golden, CO (United States)).
- Øgaard, M. (2016). *Effect of soiling on Photovoltaic Modules in Kalkbult, South Africa*: Norwegian University of Life Science. Unpublished manuscript.

## Appendix A



### First Solar Series 4™ PV Module

ADVANCED THIN FILM SOLAR TECHNOLOGY



#### INDUSTRY BENCHMARK SOLAR MODULES

As a global leader in PV energy, First Solar's advanced thin film solar modules have set the industry benchmark with over 10 gigawatts (GW) installed worldwide and a proven performance advantage over conventional crystalline silicon solar modules. Generating up to 8% more energy than competing modules with the same power rating, First Solar's Series 4™ and Series 4A™ PV Modules deliver superior performance and reliability to our customers.



#### PROVEN ENERGY YIELD ADVANTAGE

- Up to 8% more energy than conventional crystalline silicon solar modules with the same power
- Superior temperature coefficient (-0.29%/°C) resulting in greater energy yield in typical field operating temperatures
- Superior spectral response resulting in a proven energy yield advantage in humid environments
- Anti-reflective coated glass (Series 4A™) enhances energy production



#### ADVANCED PERFORMANCE & RELIABILITY

- Improved long-term power-output warranted for 25 years
- Compatible with advanced 1500V plant architectures
- Independently tested to pass accelerated life and stress tests beyond industry standards
- Highly predictable energy in all climates and applications
- Independently certified for reliable performance in high temperature, high humidity, extreme desert and coastal environments

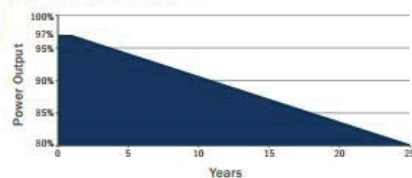


#### CERTIFICATIONS & TESTS

- Thresher Test, Long-Term Sequential Test, and PID-Free
- IEC 61646 1500V, IEC 61730 1500V, CE
- IEC 61701 Salt Mist Corrosion, IEC 60068-2-68 Dust and Sand Resistance
- ISO 9001:2008 and ISO 14001:2004
- UL 1703 and ULC 1703 Listed Class B Fire Rating (Class A Spread of Flame)
- CSI Eligible (CA-USA), FSEC (FL-USA), MCS (UK), CEC Listed (Australia), SII (Israel), InMetro (Brazil)<sup>1</sup>



#### MODULE WARRANTY<sup>2</sup>



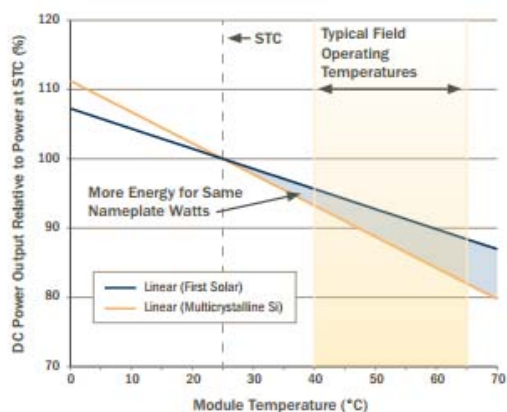
- 25-Year Linear Performance Warranty<sup>3</sup>
- 10-Year Limited Product Warranty

## FIRST SOLAR SERIES 4™ PV MODULE

MECHANICAL DESCRIPTION	
Length	1200mm
Width	600mm
Weight	12kg
Thickness	6.8mm
Area	0.72m <sup>2</sup>
Leadwire	2.5mm <sup>2</sup> , 610mm
Connectors	MC4 <sup>4</sup>
Bypass Diode	None
Cell Type	Thin-film CdTe semiconductor, 216 active cells
Frame Material	None
Front Glass	3.2mm heat strengthened Series 4A™ includes anti-reflective coating
Back Glass	3.2mm tempered
Encapsulation	Series 3 Black Laminate material with edge seal

MODULE NUMBERS AND RATINGS AT STC <sup>1,2</sup>							
NOMINAL VALUES		FS-492 FS-492A	FS-495 FS-495A	FS-497 FS-497A	FS-4100 FS-4100A	FS-4102 FS-4102A	FS-4105A
Nominal Power (± 5%)	P <sub>MPP</sub> (W)	92.5	95.0	97.5	100.0	102.5	105.0
Voltage at P <sub>MAX</sub>	V <sub>MPP</sub> (V)	67.0	67.9	68.7	69.4	70.0	70.4
Current at P <sub>MAX</sub>	I <sub>MPP</sub> (A)	1.38	1.40	1.42	1.44	1.47	1.49
Open Circuit Voltage	V <sub>OC</sub> (V)	86.0	86.5	87.0	87.6	88.0	88.2
Short Circuit Current	I <sub>SC</sub> (A)	1.54	1.55	1.55	1.57	1.57	1.58
Maximum System Voltage	V <sub>SYS</sub> (V)	1500 <sup>7</sup> / (1000 UL)					
Limiting Reverse Current	I <sub>R</sub> (A)	4.0					
Maximum Series Fuse	I <sub>CF</sub> (A)	4.0					
MODULE NUMBERS AND RATINGS AT 800W/m <sup>2</sup> , NOCT <sup>3</sup> 45°C, AM 1.5 <sup>4</sup>							
Nominal Power (± 5%)	P <sub>MPP</sub> (W)	69.7	71.6	73.5	75.4	77.3	79.1
Voltage at P <sub>MAX</sub>	V <sub>MPP</sub> (V)	62.8	63.4	63.9	65.0	65.5	65.7
Current at P <sub>MAX</sub>	I <sub>MPP</sub> (A)	1.11	1.13	1.15	1.16	1.18	1.20
Open Circuit Voltage	V <sub>OC</sub> (V)	81.2	81.7	82.1	82.7	83.1	83.3
Short Circuit Current	I <sub>SC</sub> (A)	1.24	1.25	1.25	1.27	1.27	1.27
TEMPERATURE CHARACTERISTICS							
Module Operating Temperature Range	(°C)	-40 to +85					
Temperature Coefficient of P <sub>MPP</sub>	T <sub>K</sub> (P <sub>MPP</sub> )	-0.29%/°C					
Temperature Coefficient of V <sub>OC</sub>	T <sub>K</sub> (V <sub>OC</sub> )	-0.28%/°C					
Temperature Coefficient of I <sub>SC</sub>	T <sub>K</sub> (I <sub>SC</sub> )	+0.04%/°C					

### SUPERIOR TEMPERATURE COEFFICIENT



### END-OF-LIFE RECYCLING

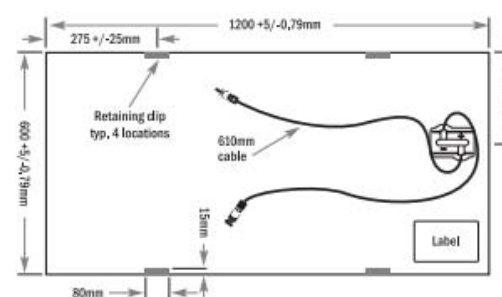
- Recycling services available through First Solar's industry-leading recycling program or customer-selected third party.

#### Disclaimer

The information included in this Module Datasheet is subject to change without notice and is provided for informational purposes only. No contractual rights are established or should be inferred because of user's reliance on the information contained in this Module Datasheet. Please refer to the appropriate Module User Guide and Module Product Specification document for more detailed technical information regarding module performance, installation and use.

The First Solar logo, First Solar™, and all products denoted with ® are registered trademarks, and those denoted with a ™ are trademarks of First Solar, Inc.

### MECHANICAL DRAWING



- InMetro Certification available on FS-495, FS-497, FS-4100, FS-4102, FS-495A, FS-497A, FS-4100A, FS-4102A
- Limited power output and product warranties subject to warranty terms and conditions.
- Ensures 97% rated power in first year, -0.7%/year through year 25.
- Multi-Contact MC4 (PV-KST4/PV-KBT4)
- Standard Test Conditions (STC) 1000W/m<sup>2</sup>, AM 1.5, 25°C
- All ratings ±10%, unless specified otherwise. Specifications are subject to change.
- Application Class A for 1000V (class II), Application Class B for 1500V (class II)
- Nominal Operating Cell Temperature: Module operation temperature at 800W/m<sup>2</sup> irradiance, 20°C air temperature, 1m/s wind speed.



# ReneSola

## Virtus II

### Virtus® II Module

250W, 255W, 260W



High Module Conversion Efficiencies



Easy Installation and Handling for Various Applications



Mechanical Load Capability of up to 5400 Pa



Conforms with IEC 61215:2005,  
IEC 61730:2004, UL 1703 PV Standards



ISO9001, OHSAS18001, ISO14001 Certified



Application Class A, Safety Class II, Fire Rating C



Also Applicable For Module With Black Frame

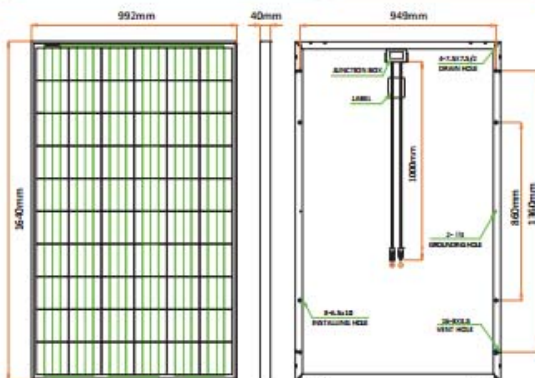


**10-year**  
material & workmanship

**25-year**  
linear power output

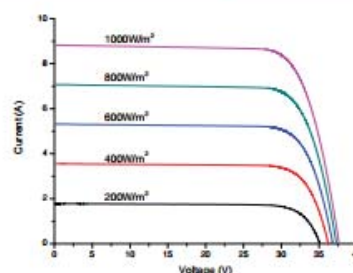


### Dimensions



**Drawing Only for Reference**

## I-V Curves



### Varied Irradiation Efficiencies

Irradiance	200 W/m <sup>2</sup>	400 W/m <sup>2</sup>	600 W/m <sup>2</sup>	800 W/m <sup>2</sup>	1000 W/m <sup>2</sup>
Efficiency	15.8%	16.2%	16.2%	16.1%	16.0%

## Electrical Characteristics STC

Electrical Characteristics STC	JC250M-24/Bb	JC255M-24/Bb	JC260M-24/Bb
Maximum Power (Pmax)	250 W	255 W	260 W
Power Tolerance	0 ~ +5W	0 ~ +5W	0 ~ +5W
Module Efficiency	15.4%	15.7%	16.0%
Maximum Power Current (Imp)	8.31 A	8.39 A	8.53 A
Maximum Power Voltage (Vmp)	30.1 V	30.4 V	30.5 V
Short Circuit Current (IsC)	8.83 A	8.86 A	8.95 A
Open Circuit Voltage (Voc)	37.4 V	37.5 V	37.6 V

Values at Standard Test Conditions STC (AM1.5, Irradiance 1000W/m<sup>2</sup>, Cell Temperature 25°C)

## Electrical Characteristics NOCT

Electrical Characteristics NOCT	JC250M-24/Bb	JC255M-24/Bb	JC260M-24/Bb
Maximum Power (P <sub>max</sub> )	185 W	189 W	193 W
Maximum Power Current (I <sub>mp</sub> )	6.57 A	6.63 A	6.74 A
Maximum Power Voltage (V <sub>mp</sub> )	28.2 V	28.5 V	28.6 V
Short Circuit Current (I <sub>sc</sub> )	7.12 A	7.20 A	7.27 A
Open Circuit Voltage (V <sub>oc</sub> )	35.0 V	35.1 V	35.2 V

Values at Normal Operating Cell Temperature, Irradiance of 800 W/m<sup>2</sup>, AM 1.5, ambient temperature 20°C, wind speed 1 m/s

### Mechanical Characteristics

Cell Type	Virtus II (Polycrystalline) 256 x 156 mm, 60 [6x10] pcs in series
Glass	High Transmission, Low Iron, Tempered Glass
Frame	Anodized Aluminum Alloy
Junction Box	IP65/IP67 Rated, With Bypass Diodes
Dimension	*1640 x 992 x 40 mm
Output Cable	4 mm <sup>2</sup> (EU)/12 AWG (US), 1000 mm
Weight	19 kg
Installation Hole Location	See Drawing Above

### Characteristics

Temperature Coefficient of Voc	-0.30%/°C
Temperature Coefficient of Isc	0.04%/°C
Temperature Coefficient of Pmax	-0.40%/°C
Nominal Operating Cell Temperature (NOCT)	45°C ±2°C

### Packing Information

Container	20' GP	40' GP	40' HQ
Pallets per Container	12	28	28
Pieces per Container	300	700	770

Rev. 104.X/105/2014.05 \*Contact Renewals for tolerance specification  
CAUTION: All rights reserved. Design and specification are subject to change without prior notice.

### Maximum Ratings

Operating Temperature	-40°C ~ +85°C
Maximum System Voltage	1000VDC (EU) / 600VDC (US)
Maximum Series Fuse Rating	20A (EU) / 20A (US)

## Appendix B



### Photovoltaic Geographical Information System

European Commission  
Joint Research Centre  
Ispra, Italy

### Incident global irradiation for the chosen location

Location: 30°9'38" South, 24°8'18" East, Elevation: 1211 m a.s.l.,

Optimal inclination angle is: 30 degrees

Annual irradiation deficit due to shadowing (horizontal): 0.0 %

Month	Hh	Hopt	DNI	lopt	D/G
Jan	7920	7140	8440	1	0.23
Feb	7130	7040	7700	14	0.24
Mar	6620	7410	7170	30	0.30
Apr	4940	6420	6590	45	0.24
May	3910	5820	6090	55	0.24
Jun	3480	5570	5980	60	0.24
Jul	3800	5920	6400	58	0.23
Aug	4730	6570	7100	50	0.21
Sep	6090	7260	7720	36	0.21
Oct	7320	7580	8140	20	0.24
Nov	8080	7470	8880	5	0.21
Dec	8290	7260	8990	-3	0.21
Year	6020	6790	7430	30	0.23

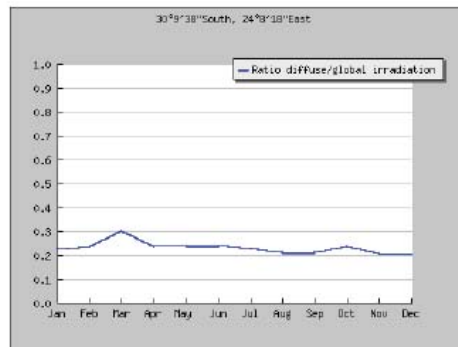
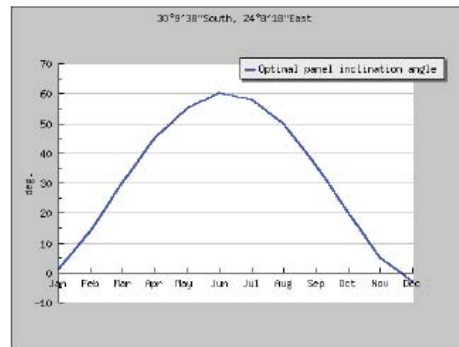
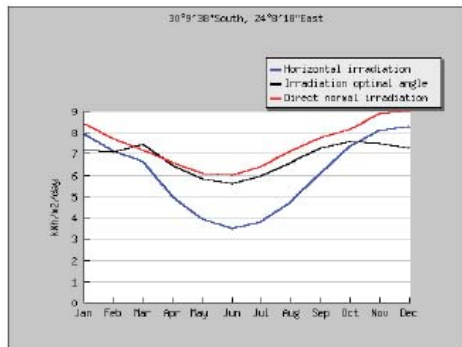
Hh: Irradiation on horizontal plane (Wh/m2/day)

Hopt: Irradiation on optimally inclined plane (Wh/m2/day)

DNI: Direct normal irradiation (Wh/m2/day)

lopt: Optimal inclination (deg.)

D/G: Ratio of diffuse to global irradiation (-)



PVGIS (c) European Communities, 2001-2012

Reproduction is authorised, provided the source is acknowledged.

<http://re.jrc.ec.europa.eu/pvgis/>

Disclaimer:

The European Commission maintains this website to enhance public access to information about its initiatives and European Union policies in general. However the Commission accepts no responsibility or liability whatsoever with regard to the information on this site.

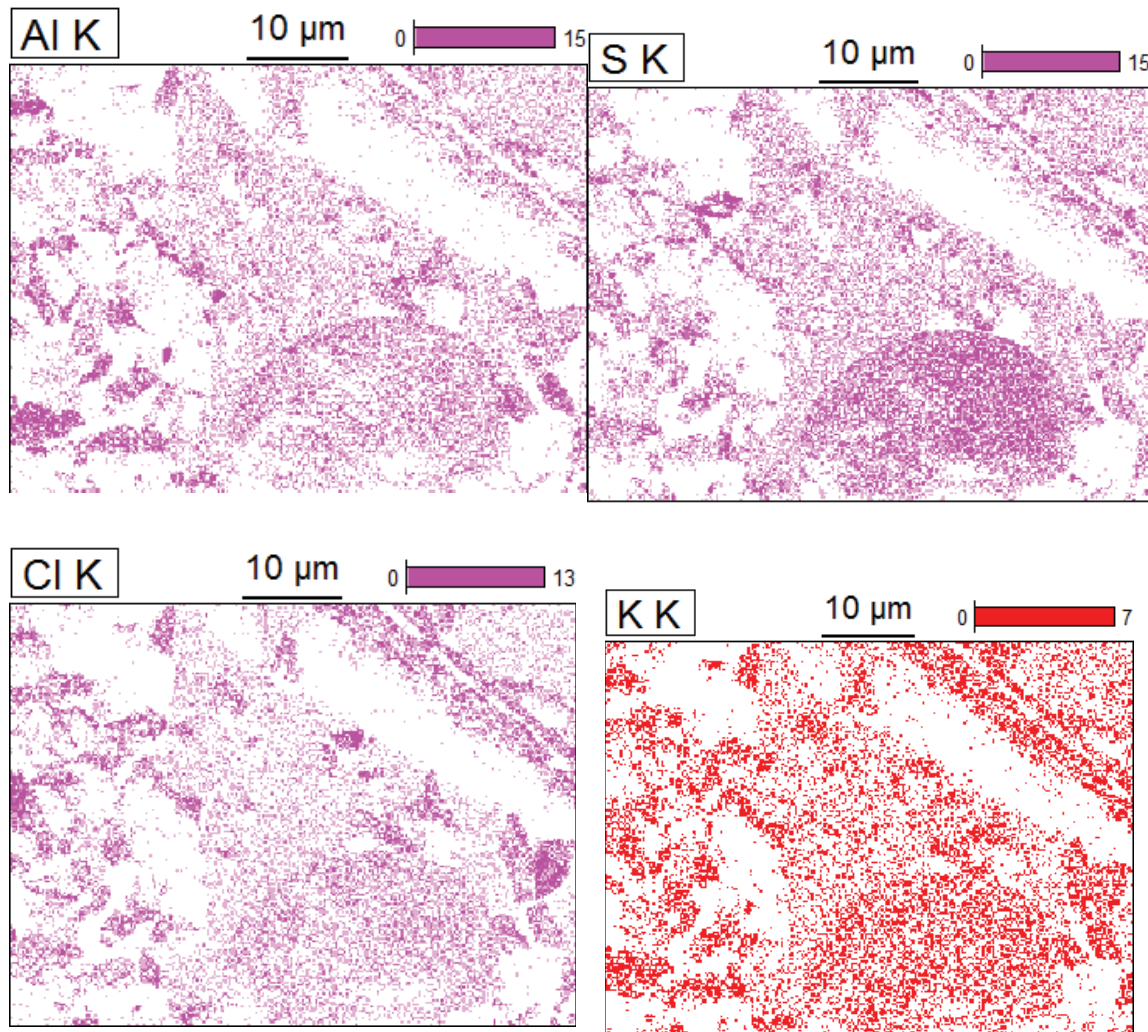
This information is:

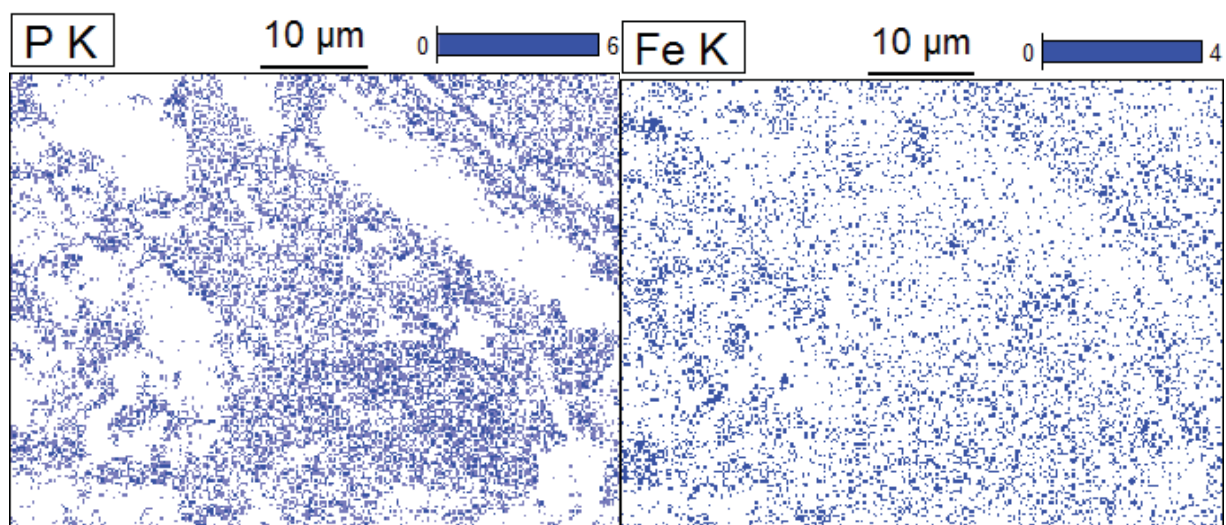
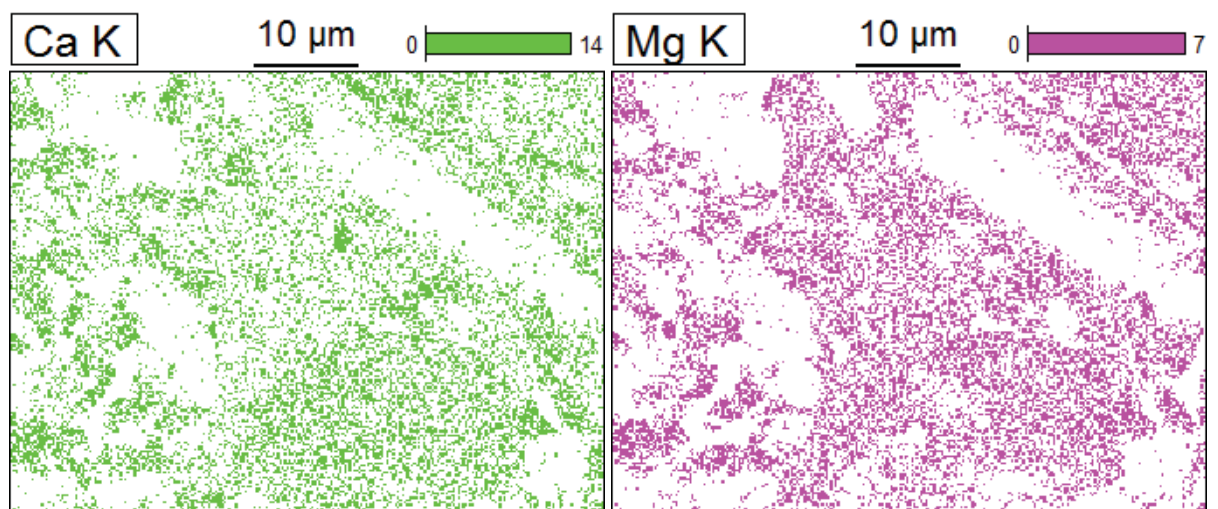
- of a general nature only and is not intended to address the specific circumstances of any particular individual or entity;
- not necessarily comprehensive, complete, accurate or up to date;
- not professional or legal advice (if you need specific advice, you should always consult a suitably qualified professional).

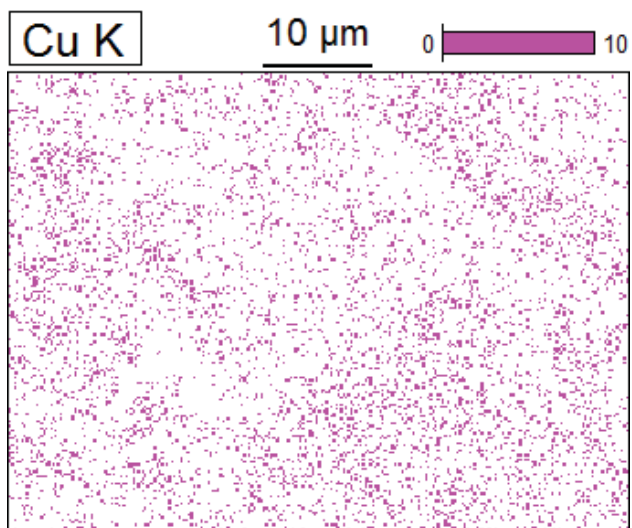
Some data or information on this site may have been created or structured in files or formats that are not error-free and we cannot guarantee that our service will not be interrupted or otherwise affected by such problems. The Commission accepts no responsibility with regard to such problems incurred as a result of using this site or any linked external sites.



## Appendix C











Norges miljø- og biovitenskapelig universitet  
Noregs miljø- og biovitenskapelige universitet  
Norwegian University of Life Sciences

Postboks 5003  
NO-1432 Ås  
Norway